Structural Behavior of Polymers from Monte Carlo Studies of Coarse-Grained Models

Der Fakultät für Physik und Geowissenschaften

der Universität Leipzig

eingereichte

D I S S E R T A T I O N

zur Erlangung des akademischen Grades

doctor rerum naturalium

(Dr. rer. nat.)

vorgelegt

von Dipl. Phys. Thomas Vogel

geboren am 19.10.1977 in Osterburg.

Leipzig, den 11.6.2009

Bibliographische Beschreibung:

Vogel, Thomas

Structural Behavior of Polymers from Monte Carlo Studies of Coarse-Grained Models

Universität Leipzig, Dissertation

136 S., 215 Lit., 61 Abb., 8 Tab.

Referat:

Polymere und Polymerwerkstoffe gehören zu den interessantesten Substanzen und Stoffen in der Wissenschaft und sind Gegenstand unzähliger experimenteller, theoretischer und rechnergestützter Studien in der Physik sowie der Biologie, Chemie und weiteren Fächern. Wie jeder andere Stoff auch, können Polymere in unterschiedlichen Zuständen abhängig von den Umgebungsbedingungen auftreten. Dazu gehören zum Beispiel der ausgedehnte, gasartige Zustand, der amorphe, geschmolzene Zustand und kristalline Zustände.

In dieser Arbeit werden neue Resultate zu verschiedenen Aspekten der Polymerforschung bezüglich dieser Aggregatzustände und Übergängen zwischen diesen vorgestellt, welche mit Hilfe von Monte Carlo Computersimulationen erhalten wurden. Im Detail werden der zweistufige Kollaps von zufälligen ausgestreckten Gitterpolymeren in den Grundzustand und strukturelle Übergänge von dicken Polymeren untersucht. Neue, hocheffiziente Algorithmen, die diese Untersuchungen überhaupt erst ermöglich, werden angewandt.

Bibliographic Information:

Abstract:

Polymers and polymeric materials are among the most interesting substances in science and subject of numberless studies in experimental, theoretical and computational physics, to say nothing of chemistry, biology and other relevant fields. As every substance, polymers can exist in different states depending on the external conditions. Amongst these are, for example, the swollen vaporlike state, the amorphous molten state and crystalline states.

In this work, new results on different aspects of polymer science regarding these aggregate states and structural transitions between them, which have been obtained by means of sophisticated Monte Carlo computer simulations, are presented. More precisely, the two-stage collapse from the random coil conformation to the ground state of lattice polymers and structural transition of tube polymers are studied. Recently developed, highly efficient algorithms, whose development made it possible in the first place to perform the presented studies are applied.

Contents

List of Figures

iii

List of Tables

Introduction

Polymers and polymeric materials are among the most interesting substances in science and subject of numberless studies in experimental, theoretical and computational physics, to say nothing of chemistry, biology and other relevant fields. As every substance, polymers can exist in different states depending on the external conditions. Amongst these are, for example, the swollen vaporlike state, the amorphous molten state and crystalline states [1–4]. In this work I present new results on different aspects of polymer science regarding these aggregate states and structural transitions between them, which have been obtained by means of sophisticated Monte Carlo computer simulations. More precisely, I study the two-stage collapse from the random coil conformation to the ground state of lattice polymers and structural transition of tube polymers. Recently developed, highly efficient algorithms, whose development made it possible in the first place to perform the presented studies are applied.

Definition of the Subject

Polymers are chemical compounds consisting of equal or similar molecules, forming a molecular chain. Polymers are therefore often called macromolecules as well. Two of the most important examples of polymers in our life are synthetic carbon-based homopolymers, such as polyethylene, and biopolymers, like proteins or DNA.

The first mentioned homopolymers consist of (a large number of) equal (simple) components. In the case of polyethylene, these components are ethene molecules simply consisting of two carbon and four hydrogen atoms. A short notation is hence:

$$\vdash H_2C - CH_2 \dashv_n .$$
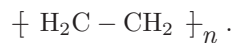
As synthetic homopolymers are the basis of macroscopic products (in daily life), it is in this context doubtlessly interesting to model and study polymer meshes, networks or dense polymer solutions.

Biopolymers consist, generally, of more complex and different molecules. In the case of proteins, these are the amino acids, in the case of DNA for example the so-called nucleotides. For proteins, it is widely assumed, that their primary structure, i.e., the sequence of amino acids, determines uniquely their three-dimensional native conformation and hence their biological function [5]. Unfortunately, the major question, how a protein exactly finds or folds

into its native state is still open, though extensively studied since decades. With the understanding of this process, one would be much closer to the solution of tasks like the cure of diseases based on misfolded proteins, the design of proteins for special purposes or the effect of mutations. DNA is of fundamental importance as it is the carrier of our genes. Beside this fact, its mechanical properties got recently in the focus of interest. They are studied, for example, by pulling the DNA off from a surface using optical or magnetic tweezers, zipping/unzipping or twisting experiments were carried out, entropic forces have been measured by pulling DNA through a grid of nanopores, etc [6–8]. Hence, in the case of biopolymers, the theoretical and computational interest is focused on the study of the behavior of single polymers (in solution), rather than polymer systems. Apart from these two "classical" or "generic" examples of polymers, organic macromolecules play (recently) an important role in electronics or optics. These fields make use of electric and optical properties or activity of certain polymers. Just think of solar cells, displays, optical filters or organic chips. In this regard, the behavior of polymers at surfaces is of particular importance.

Polymers can be experimentally studied using techniques like NMR, X-ray-, neutron- or visible light scattering or microscopy and much theoretical work has been done to describe the scaling of different properties of polymer chains in different (thermodynamical) phases [1, 2]. Anyhow, experimental techniques are, even though extremely sophisticated and leading to impressive particular results and insight, in different aspects restricted. Beside the fact, that they are, generally, very costly (in terms of time and money), they lead to results which are specific for the system under investigation. The measured structure data of a specific protein, for example, can be hardly generalized in order to draw conclusions for other systems. Furthermore, it is not trivial, to prepare and measure polymers and polymeric systems under arbitrary environmental conditions for verifying general theoretical predictions.

Here, computer simulations come into play as a third cornerstone of physics [9, 10]. Even though restricted to the study of polymer *models*, they are not restricted in a way described above. Results obtained by applying simplified, coarse-grained models [11] are valid for classes of polymers rather than for specific single systems. The simplicity of these models results from "integrating out" nonrelevant, microscopic degrees of freedom and replacing them by a few effective parameters. Atomic details, for example, do only play a secondary role for the collapse of large polymers or the formation of tertiary structures in proteins. Furthermore, as physical conditions of the system and the environment can be varied freely and rapidly, theories could be verified and statistical analyses could be carried out more easily in general. Anyhow, as computational power is still limited significantly regarding the complex problem, much effort has to be spent in developing highly sophisticated and efficient algorithms.

Detailed introductions in the field of computational polymer science and the specific models I used, as well as explanations of studies directly related to the present work are given at suitable locations later.

Structure of this Work

As mentioned at the beginning, in this work I study pseudo-phase transitions of finite size polymer systems with the main focus on the low-temperature regimes. As these systems are under high consideration in computational physics since decades, I give in Chap. 1 ("Rough Survey of Polymer Models and Computational Studies") a rough and not comprehensive overview of the work which has been done since the appearance of electronic computers. I will confine myself to the points which are directly related to the systems studied in this work and which are necessary to put them in the overall context of computational polymer physics.

As the sophisticated methods used in this work are essential for the studied problems, I present, explain and comment them in detail in Chap. 2 ("Methods"). In the first part of this chapter, I describe the development of efficient flat histogram chain growth methods, which are used for simulating lattice polymers at very low temperatures on the one hand and with a very high number of monomers on the other hand. In the second part I comment mainly on "standard" generalized ensemble algorithms used for ground-state searches and thermodynamical analyses in the whole temperature range of off-lattice models.

In Chapts. 3 ("Study of Lattice Models of Polymers") and 4 ("Tubelike Flexible Polymers") I present the main results of my studies. In Chap. 3 I consider lattice polymers and discuss the collapse from random coil conformations into frozen ground-state structures. Special attention is paid to the scaling of the transition temperatures for finite systems and the stability of the intermediate globular phase in the thermodynamic limit. Chapter 4 is dedicated to the tube polymer model. This model introduces an additional length scale, namely the three-dimensional extension of the monomer chain. I study there ground-state structures depending on the thickness of the polymer and present the full thermodynamical pseudo-phase diagrams for short polymers. Both chapters start with a separate introduction, where the work is motivated and related studies are presented and discussed. Furthermore, the respective models which I study are introduced in very detail. Short summaries are given at the end of both parts.

A comprehensive Summary of the main findings of my work and an outlook to potential further studies basing on the presented results is finally given at the end. In the appendices (A, "The HP-Transcription Problem" and B, "Non-Stochastic Minimization – Examples") two special, but secondary problems, which are related to some of the presented results, are discussed.

Chapter 1

Rough Survey
of Polymer Models
and Computational Studies

This section should give an overview of the development of polymer models and simulational techniques to treat them. Needless to say that the latter came up with the break through of electronic computers. But of course there was some science before. Earliest experimental investigations on polymers occurring in nature have already been made more than hundred years ago. Anyhow, it took a while, until the 30s of the last century, before the concept of polymers as giant molecules composed of covalent structures was widely accepted and became treated by means of statistical methods.

The first theoretical model introduced at that time for polymers has been the random walk (RW) in space [12].[1] In the following, much effort was spent in the development of theories, resulting in, amongst others, the path breaking and heavily cited works of Flory [1]. There, one can also find an elaborate historical introduction on the work done so far.

The Self-Avoiding (Random) Walk (SAW)

As said, the behavior of (long) polymer chains became a field of computational interest in the 50s of the last century. Probably the first investigations using "high-speed electronic digital computer"s were made by the Rosenbluths and Wall et al., published in the mid-50s [13–15]. They were studying a restricted random walk problem (the self-avoiding random walk on the

---

[1]It is interesting to note, that even the problem at that time was almost the same as today: "Die Winkelung und freie oder teilweise freie Drehbarkeit wird nämlich zur Folge haben, daß neben der annähernd vollständig gestreckten Form des Moleküls noch zahllose andere Formen möglich sind, [. . .] und deren Gestalt beliebig von der gestreckten Form abweicht. Wir fragen nach der Gestalt, die unter solchen Bedingungen im Mittel zu erwarten ist. Die Frage ist statistischer Art und soll nach einer statistischen Methode behandelt werden." [12]

Table 1.1: Some estimators of μ in the literature.

Year	Author(s)	Lattice			Reference
		$2D$ square	$3D$ cubic	$3D$ fcc	
1959	Fisher, Sykes	2.639(3)	4.69(2)	10.05(2)	[17]
1961	Fisher, Hiley	2.6390(5)	4.683(7)		[19]
1966	Fisher			10.036(6)	[20]
1972	Sykes et al.	2.6385(1)	4.6835(5)	10.035(1)	[23]
1983	Guttmann	2.6381^a	4.684^b	10.037^b	[24]
1987	Guttmann	$2.63815(1)^c$	$4.6839(2)^c$	$10.0364(6)^c$	[21]
1992	MacDonald et al.	2.63810(7)	4.68387(2)		[25]
1995	Douglas, Ishinabe	2.6385	4.6835	10.035^d	[26]
2000	MacDonald et al.		4.68404(9)		[27]

^{a} citing Sykes, Guttmann, Watts and Roberts, 1972 [23]

^{b} citing Guttmann, Ninham and Thompson, 1968

^{c} given as $x_c = 1/\mu$

^{d} citing Domb, 1969

simple cubic lattice), especially the scaling of mean dimensions like the average extension of these chains by means of Monte Carlo (MC) studies.

At the same time (or maybe a little later), rigorous numerical studies (exact calculation) were made, considering the problem of the total number of SAWs c_n.[2] It was found then the relation between the total number and the effective coordination number μ of the underlying lattice and the critical exponent[3] γ [2, 17–20];

$$c_n \sim \mu^n \, n^{\gamma-1} \, .$$

The estimators for these numbers μ and γ have already been very precise and have almost not changed since then. Nevertheless, the interest in evaluating these numbers has not went out up to now. Table 1.1 gives an historical overview of estimates for the value of μ. Since the 80s, the value of γ for $D = 2$ is known exactly to be $\gamma_{2D} = 43/32 = 1.34375$ (see, e.g. [21]). For three dimensions it is about $\gamma_{3D} \approx 7/6$ and still subject of investigations. Actual studies for example, deal also with the scaling behavior of SAW on special networks [22].

The Interacting Self-Avoiding Walk (ISAW)

The next step in the evolution of the simple polymer model was the introduction of attractive interactions,[4] allowing for the interplay of energetic and entropic effects. A straightforward

---

[2]The first attempts were already made in the 40s by Orr [16].

[3]γ was there sometimes called α.

[4]The first idea of the ISAW, to my best knowledge, was published already in the 40s [16], too.

implementation was the interacting self-avoiding walk (ISAW) on a regular lattice with an energy equals minus the number of contacts between monomers at neighboring lattice sites. This model was, for example, extensively studied by Grassberger et al. in the 1990s [28, 29] with the focus on the study of the so-called Θ-point. At this critical temperature, roughly spoken, monomer–monomer attraction and broadening due to configurational entropy cancel out each other, or, in other words, the excluded volume effect is exactly compensated by the monomer–monomer attraction.

Even though the (I)SAW as a polymer model is rather simple, restricted to a lattice and (apparently) outdated and exhaustively studied, it keeps under investigation up to now and is still used to study special polymer systems. See, e.g., [30–34]. Furthermore, depending on the special problem of interest, the model was adapted or extended in different ways. An interesting phenomenon that can be well investigated with variations of this model is, for example, the formation of intermediate states during protein unfolding by introducing stiffness to the model and applying a stretching force [35–37]. Further modifications were, for example, the mutually attracting SAWs (MASAWs) to study the unzipping of DNA [38] or the partially directed SAW (PDSAW) [39]. Some variants have been used (recently) to model the melting or denaturation of DNA [40, 41].

In this work, the model is used to study the freezing ("liquid–solid transition") and collapse ("Θ-transition") of polymers on the sc and fcc lattice. See Chap. 3, "Study of Lattice Models of Polymers", where a more detailed introduction to (I)SAWs is given, too.
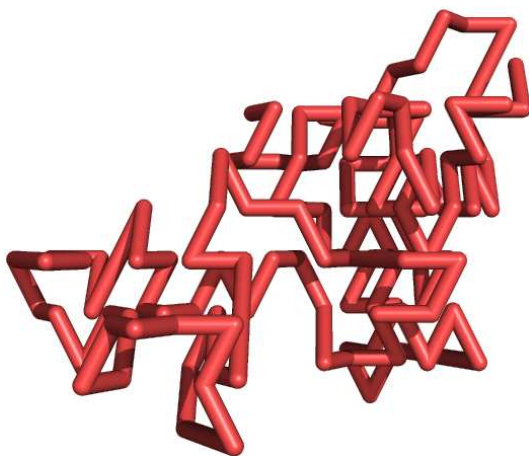
Figure 1.1: A self-avoiding walk on the fcc lattice. As an interacting self-avoiding walk, it has the energy $E = -285$ and represents a typical conformation in a poor solvent.

The HP Model

A main feature of biopolymers or proteins, a subclass of polymers in general, is the hydrophobicity of the side chains of the amino acids it is composed of. The first and simplest attempt to account for that in polymer models was just to introduce two types of monomers in the above mentioned ISAW, namely hydrophobic (H) and hydrophilic (polar, P) ones, by

K.A. Dill in the 80s [42, 43]. The two types of monomers differ only in their interaction among each other: Whilst hydrophobic monomers attract each other as in the case of the ISAW, there is no such interaction with polar monomers, which corresponds to the SAW model.[5]

Beside general studies on the effect of the monomer sequence (see, e. g., [44–47]), it was casually tried to mimic real proteins by translating the primary structure of the proteins into a HP-sequence, see, e.g., [48, 49]. Apart from the general dubiety regarding the translation of specific real proteins into HP proteins (see Appendix A ("The HP-Transcription Problem")), a variety of techniques have been developed to master the really difficult problem of understanding the low-temperature thermodynamics and finding ground- or native states generally. See, for example, [50–58] and [11, 59] and references therein.[6]
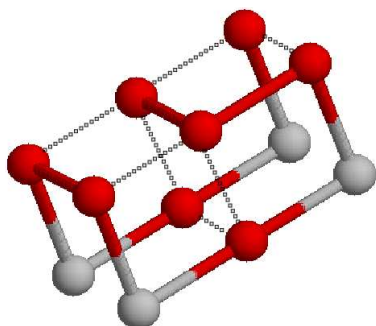
Figure 1.2: A HP protein consisting of twelve monomers on the sc lattice with energy $E = -7$. Hydrophobic monomers are *red*, polar ones *gray*. The contacts contributing to the energy, i.e., the H–H contacts, are marked by the *dotted lines*.

The Bond Fluctuation Model

Two properties which all models mentioned so far have in common is the restriction to an underlying lattice and the fixed bonds. In the Bond Fluctuation Model (BFM), the monomers are also restricted to a lattice but the bonds are not, they even are allowed to have different lengths. The model was introduced in the late 80s due to the fact, that "standard Monte Carlo algorithms" are not very efficient or even unable to simulate (branched) SAW problems [60, 61].

It was then occasionally used to study the Θ-transition of polymers [29, 62] and was recently still used to investigate the complete "[Unexpectedly normal] phase behavior of single homopolymer chains" [63].

---

[5]Hence, one may call this model the "Partially Interacting Self Avoiding Walk".

[6]Some of the methods work extremely well for lattice polymers in general (cp. Sec. 2.1, "Simulational Techniques on the Lattice"), i.e., they are not especially designed for HP proteins. Though, they have been applied initially to these systems.

The AB Model

The other way around, one could take away the lattice, but leave the bonds fixed. Using the idea of considering two types of monomers[7] and introducing a continuous potential including hard-core repulsion and van-der-Waals attraction (Lennard–Jones potential) depending on the interacting monomer types leads to the so-called AB model, introduced in two different forms by Stillinger et al. and Irbäck et al. in the 90s of the last century [64–66].

As for the preceding HP model, much effort was spent and sophisticated methods were applied to find ground states and reveal the thermodynamic behavior of specific monomer sequences [66–69]. A comparable bead-spring model was introduced by Iori, Marinari and Parisi in 1991 [70]. It allows in a similar way for the introduction of different types of monomers. The sequence dependence of this model was studied in later work by Irbäck and Schwarze [71].

For a detailed description of the AB model see Sec. 4.7 ("The Hydrophobic-Polar Tube Model"), where I extend the model to the AB tube model and present and discuss results of a specific, artificial AB sequence.
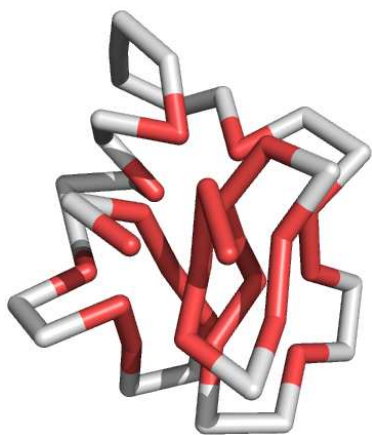
Figure 1.3: A low energy, collapsed configuration of an AB sequence consisting of 48 monomers. It was found in a simple Metropolis simulation with spherical updates. One observes the formation of a hydrophobic core (*red* monomers).

The FENE Bond Model

A further well studied off-lattice model, in which the polymer is a linelike, one-dimensional object made up of equal monomers connected by non-fixed bonds is the finite extendible nonlinear elastic (FENE) bond model for polymers.

It was originally introduced by H.R. Warner Jr. in the early 70s of the last century [72] as a useful model to study the "transition" between the rigid bond and the Hookean spring bond theory of polymers, both well studied at that time. Apart from this, it was expected, that a FENE bond is closer to real macromolecules as they have neither rigid bonds nor are infinitely extendible. The model was in the following years subject of further theoretical

---

[7]hydrophobic and polar ones like in the HP model, here called A and B

analysis and molecular dynamics (MD) computer simulations (see, e.g. [73, 74]), before it was extensively studied by means of Monte Carlo (MC) computer simulations since the 90s of the last century, see, e.g. [75] and references therein, or, for a recent work, [76, 77].
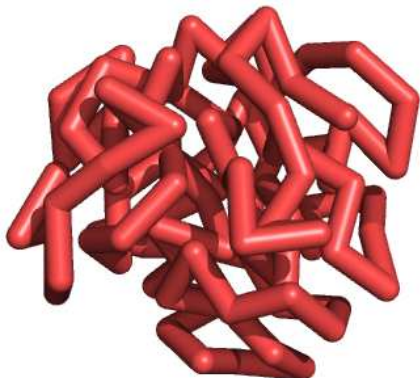
Figure 1.4: A homo100mer with finitely extendible non-elastic (FENE) bonds near the transition between the globular (liquid) and the crystallized (frozen) state.

Thick Polymer Models

All models so far considered the polymer as a one-dimensional (linelike) object. A possibility to account for the three-dimensional extension of polymers, due to steric constraints induced by amino acid side chains for example, without loosing the simplicity of a coarse-grained model is to model the polymer as a tube rather than a line. This idea was introduced about ten years ago by Banavar and Maritan et al. [78–80]. In a basic study they considered tubes with certain radii R_0 where the monomers interacts via a square well potential with interaction radius R_1. It was found, that different secondary structures may occur depending on R_0 and R_1 [81, 82].

In Chap. 4 ("Tubelike Flexible Polymers") I will present an elaborate and systematic study of native state conformations of thick polymers and I will unravel the complete thermodynamic behavior of short homopolymer tubes. I will also introduce the AB tube model, basing on a combination of the ideas of the AB- and the tube model. Comments on further previous studies on tube models can be found there (Sec. 4.1, "Related Studies, Alternative Approaches"), too.
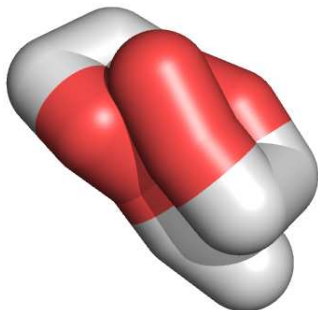
Figure 1.5: The putative ground state of an AB tube polymer with tube diameter equals 0.7 times the bond length.

Table 1.2: Summary of main features of polymer models.

Model	line-like	homo-polymer	stiff bonds	Interactions repulsive	attractive	restricted by lattice
RW	✓	✓	✓			
SAW	✓	✓	✓	(✓)		✓
ISAW	✓	✓	✓	(✓)	✓	✓
BFM	✓	✓		(✓)	✓	✓
HP	✓		✓	(✓)	✓	✓
AB	✓		✓	✓	✓	
Tube		✓	✓	✓	✓	
AB tube			✓	✓	✓	
FENE	✓	✓		✓	✓	

RW: Random Walk; SAW: Self-Avoiding Walk; ISAW: Interacting SAW; BFM: Bond Fluctuation Model; FENE: Model with Finite Extendible Nonlinear Elastic bonds; HP: Hydrophobic Polar model; AB: AB model; Tube: Tube model; AB tube: AB tube model;

Table 1.2 summarizes the main properties of the polymer models mentioned in this introduction so far. Figure 1.6 gives a sketchy overview of the coarse grained models used in this work.

Semiflexible Polymers – The Wormlike Chain

The majority of the coarse-grained models mentioned so far model flexible polymers. Anyhow, the stiffness of polymers is relevant when considering finite length systems. A model taking the stiffness of a linelike chain explicitly into account is the work-like chain model [83]. The characteristic length scale of such a polymer is called the persistence length l_p and depends of course on the bending stiffness. One speaks of semi-flexible polymers, if the persistence length is not much smaller than the system size L: $l_\mathrm{p} \lesssim L$. The case $l_\mathrm{p} \ll L$ corresponds to flexible polymers, if $l_\mathrm{p} \gg L$ we have stiff polymers and $l_\mathrm{p} \to \infty$ leads to rigid rods. Typical examples for the application of this model are studies of DNA [84], which is among the stiffest known polymers, having a persistence length of $\sim 50\,\mathrm{nm}$ [85]. The Hamiltonian of the model is, roughly spoken, the sum over the curvature of the chain, which can be rewritten for the discretized model into a sum over cosines of bending angles [86]. [8] Hence, the internal energy of the model is just the bending energy.

---

[8]Note, that in the AB model, similar terms occur. See [64–66] or Sec. 4.7, "The Hydrophobic-Polar Tube Model"
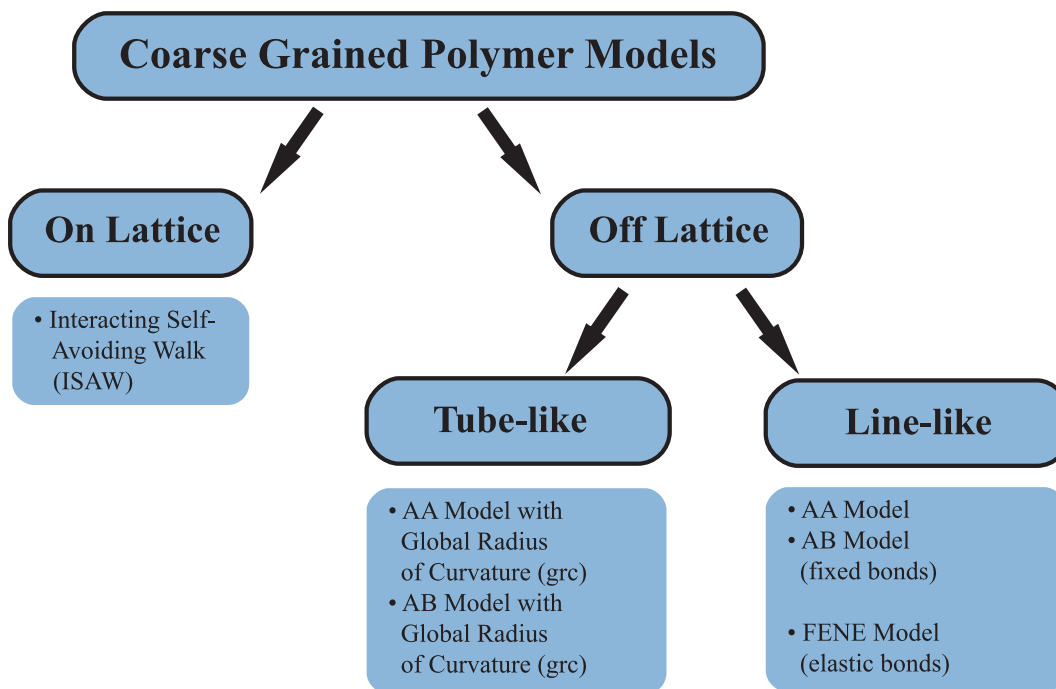
Figure 1.6: Sketch of the polymer models used in this work.

All Atom Models

Up to here we considered coarse grained models for polymers and only such models are used in this work. There exist of course atomic-level models with a variety of force fields, where all the atoms the polymers (mainly proteins) consist of, are included in the simulation. I will not go in detail as this field itself is very complex and, as said, not in the narrow focus of this work. I will instead just refer exemplarily to two nice works, where in the first, the native states of three small real proteins, including both, helical parts and sheets, could be reproduced with an all atom model [87]. In the second one, the spontaneous formations of so-called β-barrels, i.e., the aggregation of certain peptides to a fibril, consisting of six strands could be observed using a model of this class [88]. For further examples, including references to different force-fields, see, for example, [89–95].

Polymers at Surfaces

So far, just free polymers (in solutions) have been considered. A experimentally very relevant field of studies deals with the behavior of polymers under external constraints, i.e., polymers at surfaces or encased in geometrical objects like tubes.

Just to provide an introduction in the field, I would like to mention a few studies exemplarily. In these studies, variants of the above introduced models have been applied. In the

first study, Hegger and Grassberger estimated critical exponents of self-avoiding walks near an adsorbing surface [96]. Later, the thermodynamical behavior of lattice- and off-lattice polymers at attractive substrates has been investigated in dependence of the strength of the surface attraction [97, 98]. Finally, using the SAW model, Hsu et al. studied the behavior of polymers at membranes and the escape transition of a polymer which is confined in a nanotube [31, 33, 99].

It is worth to mention, that there is a certain connection between strongly attracted polymers and polymers in two dimensions. For off-lattice models, on finds for example identical ground-states conformations when simulating under these two conditions. Generally, one may say in a prosaic way, that polymers at surfaces are in a sense the link between 3D (weak attractions) and 2D polymers (strong attraction).

Simulational Techniques

There are generally two types of computer simulations, molecular dynamic (MD) simulations and Monte Carlo (MC) simulations. Whereas with MD simulations, the dynamics of a systems is emulated, in MC simulations a statistical ensemble is sampled in an arbitrary, randomized and method-dependent way, which does not reflect in general any "natural" dynamics. MD simulations proceed, very roughly, as follows: for a given system configuration, all forces, i.e., the gradient of the given potential, is calculated. Then, the equations of motion are solved for a little time step Δt. The conformation is then updated according to these calculations, the system time is increased by Δt and the procedure starts over. As I do not use MD in this work, I will not go into more detail or comment on the technical difficulties that may appear. With respect to the protein folding problem on may say though, that, at the moment(!), computationally accessible time scales are often far too short compared to the real time these processes need.

As for many problems, such as these in this work, the real dynamics is not important, MC simulations are the more useful alternative as it allows in principle for wide "jumps" in the configurational space. Hence, it is possible to explore a wide space of representative structures of different canonical ensembles in one simulation and therefore studies of thermodynamical or structural (pseudo)transitions will be feasible, for example. I will describe the MC methods I use in the separate Chap. 2 ("Methods") in all detail.

Chapter 2

Methods

In this chapter I will describe in more detail or comment all simulational methods, which have been used during this work and which are just shortly mentioned elsewhere. The methods used for the study of lattice polymers and of off-lattice systems follow different concepts. The first ones are described in Sec. 2.1 ("Simulational Techniques on the Lattice"), the latter ones subsequently in Sec. 2.2 ("Techniques for Off-Lattice Simulations").

2.1   Simulational Techniques on the Lattice

The generic model of lattice polymers is the self-avoiding walk. To study this model by means of computer simulations, there are mainly two different approaches. On the one hand, one may implement standard Markov chain Monte Carlo methods as described in Sec. 2.2 ("Techniques for Off-Lattice Simulations"). The conformational updates of existing chains may include semilocal changes of bond orientations as corner and end flips, crankshaft moves (see, for example, [100]) or more non-local updates such as the very popular pivot rotations [101, 102]. Although the application of these updates may result in very efficient simulations at high temperatures, i.e., for very dilute systems, they become inefficient in dense systems as most of the proposed moves will be rejected simply due to violations of the self-avoiding constraint.

This problem can be "solved", i.e, the efficiency of simulations in the dense phase can be improved drastically, by using chain-growth algorithms, where the chains are constructed during the simulation. The basic strategy is trivial: A new monomer is tried to be attached to the end of an already existing chain, taking into account the lattice constraints of course, until the total length is reached. [1] I will in the following describe step by step the set-up and optimization of such a method, which has been very successful already.

---

[1]Indeed, it may also happen, that all neighbors of the end of the chain are already occupied and, thus, the chain get trapped before the total length is reached.

2.1.1   The Rosenbluth Method

One can relatively easy assure oneself of the fact, that the probability of generating self-avoiding chains generally depends on the growth direction, as the number of free neighbors of a given lattice site, where a monomers can be placed, varies during the growth process. This is illustrated in Fig. 2.1, where a conformation with the respective (inverse) probabilities at each step is shown. To counterbalance this bias, so-called Rosenbluth weights are introduced [14]. These local weights at site n are nothing but the inverse probabilities of choosing a free neighbor, i.e., the number of free neighbors m_n of n. The total Rosenbluth weight of a chain of length N is just:

$$W_N \sim \prod_{n=1}^{N} m_n \,, \tag{2.1}$$
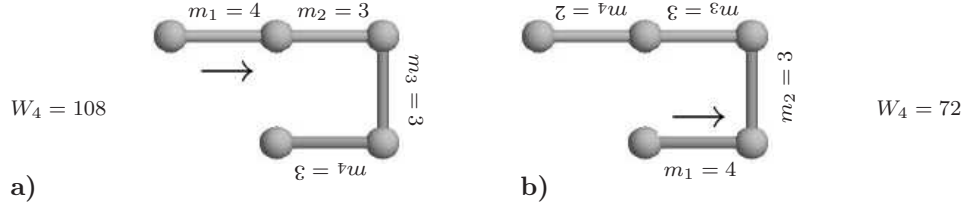
Figure 2.1: Example of a conformation on the two-dimensional square lattice grown from different directions. The conformation in **a** has the probability of 1/108 to be created, for the same conformation in **b** this probability is 1/72.

In order to simulate polymers at finite temperatures rather than simulating athermal self-avoiding walks, it is convenient to introduce thermal Rosenbluth weights including the Boltzmann factor. Hence, Eq. (2.1) is replaced by:

$$W_N \sim \prod_{n=1}^{N} m_n \, e^{-E_k/k_{\mathrm{B}} T} \,, \tag{2.2}$$

where $k = 1, \ldots, m_n$ is the number of the chosen free neighbor, E_k is the energy contribution from the new monomer placed there and k_{B} is the Boltzmann constant.[2]

2.1.2   Pruned Enriched Rosenbluth Method (PERM)

Using the above described Rosenbluth method, one creates a very broad distribution of the weights W_N. This is by far not optimal, as the error of sample means increase with the width of the W_N distribution. In the extreme case, a sample average is dominated by a single event

---

[2]Alternatively one might make the local weights independent of k by including the Boltzmann factor in the probability of choosing the direction for the next step [29].

with an extremely large weight. Furthermore, as a more technical aspect, much computer time is "wasted" simulating chains with very low weights. An essential improvement of the efficiency of the Rosenbluth method was hence achieved by the application of a population control, following the general idea of enriched samples of random walks [103]. On the one hand, the sample is enriched if the weights become large, reducing the weights of every single system appropriately, on the other hand it should be pruned, if weights become small.

In practice, this is done as follows [29]. One introduces for every chain length n a lower and an upper threshold value $W_n^{<,>}$ for the weights. If the actual weight W_n of a chain becomes larger than $W_n^>$, a copy of the chain is created and the weight is divided. Both, the original chain and the copy[3], get the weight $W_n/2$. If the weight W_n becomes lower than $W_n^<$, the chain is proposed to be terminated with a probability of $1/2$. If the chain survives, its weight will be doubled to maintain the overall weight of the sample[4].

In principle, the boundaries $W_n^{<,>}$ can be set arbitrarily and even changed during the simulation without making the algorithm incorrect. But of course depends the efficiency crucially on a good choice of them. In the optimal case, they are fixed such, that the sample size does not vary much for different n. A good strategy satisfying this request, is to initialize the boundaries with $W_n^< = 0$ and $W_n^> = \infty$, which corresponds indeed to a Rosenbluth run, and adapted them continuously whenever reaching the length n using the current estimate of the partition sum Z_n: $W_n^> = c^> Z_n$ and $W_n^< = c^< Z_n$, where $c^{<,>}$ are numbers of the order of unity and $c^>/c^< \approx 10$. Note that, since this method is a clever kind of simple sampling, the partition sum can be estimated as $Z_n \approx \sum_i W(\mathbf{X}_i)/S$, where the sum runs over all successfully generated polymer chains of length n in S growth starts.

Further refinements can be made by changing some details of the given procedure leading to the so-called nPERM ("new PERM") method [59]. Formerly, one copy of a chain was created, when its weight became large. Now, the number of copies k (including the "original" chain) should depend on the ratio of the actual weight and the upper threshold value:

$$k = \min\left\{ m_n, \frac{W_{n+1}}{W_{n+1}^>} \right\}, \qquad (2.3)$$

where $W_{n+1} = W_n + m_n$ is a predicted weight for the next step. As it is ensured, that there will not be more copies than free neighbor sites, all copies will furthermore be forced to grow in different directions, which avoids a possible loss of diversity. The weights are adapted accordingly be dividing by k. Although one can even care about the local growth directions of the copies (when there are less copies than free neighbors) leading to a kind of importance sampling, I choose them randomly and uniformly (simple sampling). The update of $W_n^{<,>}$

---

[3]In the simulation, there is of course no difference between the original chain and the copy.

[4]At the moment of pruning, the distribution is changed generally as some weight is (arbitrarily) removed or added. For a big number of terminated and surviving chains however, i.e., statistically, these effects cancel each other and the surviving chains collect the correct weights of the terminated chains.

in nPERM is made as follows:

$$W_n^> = C \frac{Z_n}{Z_0} \left(\frac{c_n}{c_0}\right)^2 , \qquad (2.4)$$

$$W_n^< = 0.2\, W_n^> . \qquad (2.5)$$

c_n counts the number of configurations of length n created so far and C is some number ≤ 1, which I set to $C = 1$.[5]

In this work, I use the nPERM method for the simulation of very large chains in the vicinity of the Θ point. For the more demanding study of the freezing regime I use generalized ensemble variants of PERM. Before describing them in detail, a general remark is in order. During the chain growth process, chains will all possible lengths $n \leq N$ are created by definition. Hence, on could in principle measure observables at every chain length within a single simulation of a system with length N. But, as these results are in general strongly correlated in an uncontrollable way, I always perform really independent simulations for different system sizes.

2.1.3 Multicanonical Version of PERM (mucaPERM)

A generalized ensemble variant of PERM, called mucaPERM, follows the idea of multicanonical sampling (see Sec. 2.2.3, "Multicanonical Generalized Ensemble Method") [55, 104]. The starting point is the same as for the "standard" multicanonical method. The statistical ensemble is changed by introducing an additional weight $W_n^{\mathrm{flat}}(E_n)$ in order to achieve a flat distribution in energy and hence enable the simulation to perform an (almost) random walk through the energy space:

$$Z_n \sim \sum_i W_n^{\mathrm{PERM}}(\mathbf{X}_{n,i})\, W_n^{\mathrm{flat}}(E_n(\mathbf{X}_{n,i}))[W_n^{\mathrm{flat}}(E_n(\mathbf{X}_{n,i}))]^{-1} , \qquad (2.6)$$

where the superscript in $W_n^{\mathrm{PERM}}(\mathbf{X}_{n,i})$ indicates, that this weight is the one used in the original PERM (see Eq. (2.2)). As the method is in fact independent of the actual chain length, Eq. (2.6) can be written in the product form, inserting also Eq. (2.2), as

$$Z_n \sim \sum_i [W_n^{\mathrm{flat}}(E_n(\mathbf{X}_{n,i}))]^{-1} \prod_{l=2} m_l\, \mathrm{e}^{-(E_l - E_{l-1})/k_{\mathrm{B}}T}\, \frac{W_l^{\mathrm{flat}}(E_l)}{W_{l-1}^{\mathrm{flat}}(E_{l-1})} . \qquad (2.7)$$

Choosing, for convenience, $\beta = 1/k_{\mathrm{B}}T = 0$, one can read off the combined weight given now to a chain:

$$W_n(\mathbf{X}_n) = \prod_{l=2} m_l\, \frac{W_l^{\mathrm{flat}}(E_l)}{W_{l-1}^{\mathrm{flat}}(E_{l-1})} . \qquad (2.8)$$

---

[5]By setting C much smaller, one could probably make the algorithm a little faster. The effect would be that, roughly spoken, the algorithm would correspond to an exact enumeration for short chains (leading to maximal diversity) and becomes stochastic only for longer chains [59].

This weight is used for pruning and enrichment of the sample in a completely analogous way to the one described for nPERM.

As in every variant of multicanonical simulations, the multicanonical weights W_n^{flat} are not known in advance, otherwise the problem would be solved trivially, as these weights are directly connected to the density of states. The proposed procedure of determining them is an iterative one, starting with $W_n^{\text{flat}}(E) = 1$ for all n. Then, in every iteration step, a certain number of chains are produced whose actual combined weights are added to a histogram $H_n(E)$. The new weights for the next iteration step are then obtained by $W_n^{\text{flat}}(E) \leftarrow W_n^{\text{flat}}(E)/H_n(E)$ and $H_n(E)$ and $W_n^{<,>}$ are reset to their starting values. The weights $W_n^{\text{flat}}(E)$ are obtained satisfactorily, when the histogram $H_n(E)$ becomes "flat".

2.1.4 Flat Histogram Version of PERM (flatPERM)

Alternatively, there is another strategy to optimize PERM than the ones described above. Prellberg and Krawczyk [105] propose a constant pruning and enrichment rather than just occasional changes depending on some threshold values, which are crucial for the efficiency furthermore. They consider the athermal estimator[6] $C_n^{\text{est}} = \langle W \rangle_n = S^{-1} \sum_i W_n^{(i)}$ (the "infinite temperature" partition function) with $W_n = \prod_{k=1}^n m_k$ (cp. Eq. 2.1). The actual sample should be enriched when $W_n > C_n^{\text{est}}$, whereas the number of copies and the corresponding correction of weights is calculated as in nPERM, otherwise it should be pruned with probability $1 - W_n/C_n^{\text{est}}$. Hence, the chain continues to grow with probability W_n/C_n^{est} and weight C_n^{est}. Particularly, pruning and enriching that way, the weights are set as closely as possible to C_n^{est}, what minimized fluctuations of them.

Keeping in mind, that PERM so far creates a roughly flat histogram in size n, it is now straightforward to design an algorithm performing a random walk in both, size and energy. In this sense, the algorithm can then be seen as a self-tuned flat (energy) histogram version of PERM. Therefore, in total analogy to the considerations above, one takes the microcanonical estimator $C_{n,m}^{\text{est}} = \langle W \rangle_{n,m} = S^{-1} \sum_i W_{n,m}^{(i)}$ (the "density of states"), where m corresponds to an energy, i.e., to the number of non-bonded nearest-neighbor contacts in the case of interacting self-avoiding walks. The pruning and enrichment rules are applied accordingly in the fashion described above. Figure 2.2 shows exemplarily the logarithm of $C_{n,m}^{\text{est}}$ depending on the system size n and the internal energy m for a simulation of lattice polymers up to length $N = 250$. One sees, that the numbers of configurations vary over hundreds of magnitudes. Averages of observables can be computed via

$$Q_{n,m}^{\text{est}} = \frac{\langle QW \rangle_{n,m}}{\langle W \rangle_{n,m}} = \frac{\sum_i Q_{n,m}^{(i)} W_{n,m}^{(i)}}{\sum_i W_{n,m}^{(i)}}, \qquad (2.9)$$

---

[6]The change to thermal ensembles is straightforward by multiplying the weights with the Boltzmann factor.
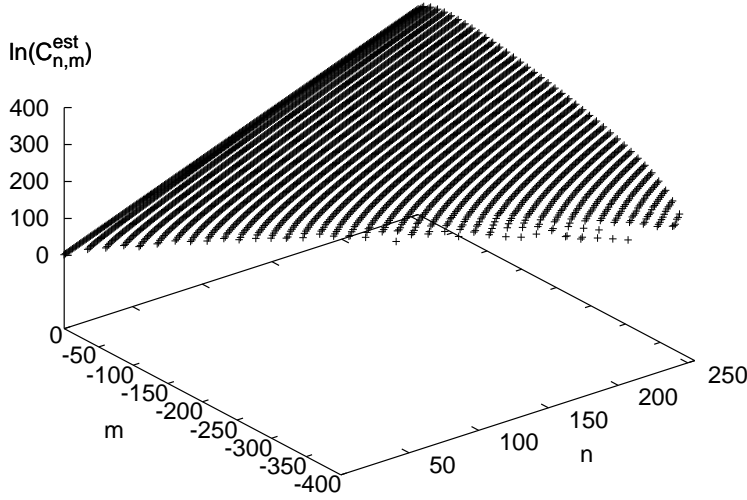
Figure 2.2: Logarithm of $C_{n,m}^{\mathrm{est}}$ obtained by a simulation of lattice polymers with lengths up to $N = 250$ using flatPERM.

expectation values in the canonical ensemble are then obtained by

$$Q_n^{\mathrm{est}}(\beta) = \frac{\sum_m Q_{n,m}^{\mathrm{est}} C_{n,m}^{\mathrm{est}} \, \mathrm{e}^{-\beta E_m}}{\sum_m C_{n,m}^{\mathrm{est}} \, \mathrm{e}^{-\beta E_m}} \, . \tag{2.10}$$

Both "flat histogram" variants of PERM described here, achieve in a sense the same aim and hence should work comparably well, especially considering the sampling of the low-temperature region. In both versions, the simulation performs a random walk in chain length and energy. In particular, one can use them for ground-state searches therefore. Interestingly, both approaches seem to base on different mechanisms. Whilst flatPERM uses "self-tuning" capabilities, in mucaPERM the simulated ensemble is changed "from the outside".

2.2 Techniques for Off-Lattice Simulations

For the off-lattice simulations of tubelike polymers, I used standard Markov chain Monte Carlo methods on the basis of acceptance or rejection of proposed local or global conformational updates of the systems, in difference to the methods I used for the lattice simulations. For updating conformations, I use the spherical update mechanism described in [68]: The new position of a monomer $i + 1$ should be located on a sphere with the radius of the (fix) bond length around monomer i. The following bonds are then just translated in order to preserve the chain structure.

In the following I will just give some remarks and comment on the methods which have been used in this work with the focus on the actual problems related to the studied problems,

rather than explaining them from scratch in all detail. I will not explain or repeat the basic concepts of Markov chain Monte Carlo simulations either. For both purposes, common textbooks [9, 10] are much more suitable.

2.2.1 Canonical Metropolis Simulations

The most fundamental Monte Carlo method to sample a canonical distribution is the by now so-called Metropolis simulation [106].

The method works as follows. For the system which is studied, a local update, i.e., a small change of local observables such as spatial positions of a particle in a many-particle system or the value of a single spin in a spin system, is proposed which leads to a change of the energy $\triangle E = E_{\mathrm{new}} - E_{\mathrm{old}}$ of the system defined by some Hamiltonian. If the energy E_{new} after the update is lower than before, the update will be automatically accepted, if not, the move is accepted just with certain probability. If the update is rejected, the former state is simply restored and counts as the new state. By using

$$p(E_{\mathrm{old}} \to E_{\mathrm{new}}) = \min \left\{ 1, \mathrm{e}^{-\beta \triangle E} \right\}$$

as the probability of accepting a local update, detailed balance is fulfilled and it is guaranteed, that the system converges, in principle and providing ergodic updates, to the correct canonical distribution at a fixed temperature. $\beta = 1/k_{\mathrm{B}}T$ is here the inverse temperature. The method fails in general at low temperatures and in the vicinity of phase transitions where transition states are highly suppressed. See, for example, [10].

On the other hand, the method can always be used, even if not very efficient in many cases, for cross checks of generalized ensemble simulations and for an easy generation of local observable distributions at high temperatures far from phase transitions. It is used in this work for just these purposes.

2.2.2 Parallel Tempering

On possibility to overcome the limitations of single Metropolis simulations and to study systems with complex energy landscapes is to simulate many systems in parallel at different temperatures $\beta_1 < \beta_2 < \ldots < \beta_m$ and interchange current configurations between the systems once in a while. By doing so, a system has the chance to travel through the temperature space and overcome, for example, high energetic barriers at low temperatures. This is exactly the idea of Parallel Tempering simulations [107, 108]. Each single system may be simulated using adequate update algorithms at fixed temperature. In the simplest case, the above described Metropolis algorithm can be applied. Then, after a determined number of updates within the single systems, conformation interchanges between the systems are attempted with the Metropolis like acceptance probability

$$p(\beta_1, E_1 \leftrightarrow \beta_2, E_2) = \min \left\{ 1, \mathrm{e}^{(\beta_2 - \beta_1)(E_2 - E_1)} \right\} .$$

The crucial point of these simulations is a good choice of the simulation temperatures β_i, or the distances between them respectively. Choosing to few temperatures, which are to far away from each other, leads to very small acceptance probabilities and thus to very large travelling or round-trip times, the time a system need to travel through the whole temperature space (and back). On the other hand, besides the fact that for each system a single processor is required, it is far from optimal to simulate at too much temperatures as well. Furthermore, it is not optimal, to distribute the simulation temperatures equally, think of systems with first-order transitions for example, and so on. Without going into detail, it should be noted that the mentioned problem is by far not trivial and still "open" and a big amount of strategies has been presented in the past years [109–112].

In this work, the parallel tempering method was applied just for cross-check simulation. The temperatures have been distributed without exhaustive optimization such that the exchange probability was roughly 50%. The obtained canonical histograms have been combined using the (multi)histogram reweighting technique [113, 114] in order to calculate the density of states. For a quick overview of applications of the Parallel Tempering methods in different disciplines, see [112].

2.2.3 Multicanonical Generalized Ensemble Method

The multicanonical method [115–117] is a way to obtain the statistics at all temperatures (or within a certain temperature interval) in a single simulation. Therefore the canonical ensemble is extended to a generalized, multicanonical ensemble by multiplying appropriate weight factors $W(E)$ to the Boltzmann weights such that the respective distribution P_{muca} becomes (in the optimal case) flat. This leads (in principle) to a random walk through the energy space during the simulation: $P_{\mathrm{muca}} = \mathrm{e}^{-\beta E} W(E) \overset{!}{\approx} \mathrm{const}$. The update probability during the simulation reads then:

$$p(E_{\mathrm{old}} \to E_{\mathrm{new}}) = \min\left\{1, \mathrm{e}^{-\beta(E_{\mathrm{new}}-E_{\mathrm{old}})}\frac{W(E_{\mathrm{old}})}{W(E_{\mathrm{new}})}\right\} .$$

The weight factors $W(E)$ are of course not known in advance and must be generated somehow. By the way, whatever the $W(E)$ are, canonical expectation values can be computed exactly by

$$\langle \mathcal{O} \rangle_{\mathrm{can}} = \frac{\langle \mathcal{O}\, W^{-1} \rangle_{\mathrm{muca}}}{\langle W^{-1} \rangle_{\mathrm{muca}}},$$

hence, multicanonical simulations are always "safe". Indeed, the performance of the simulation depends crucially on a good determination of $W(E)$ in order to make the multicanonical distribution "flat". This determination can be done for example iteratively [118], starting with $W(E) = \mathrm{const}$ and updating then, in most naive manner, via $W(E)_{\mathrm{new}} = W(E)/H(E)$, where $H(E)$ is a histogram obtained during the actual iteration. A further possibility is to work directly with estimators for the density of states, obtained by Wang–Landau iterations (see the following subsection), instead of iterating the multicanonical weights. This may

be more efficient and easier to implement, but makes no difference in principle. See for a detailed discussion also [114] and references therein.

It should be mentioned, that the method is not especially designed for flat histograms in energy space. In principle, it works with weights depending on arbitrary observables $W(\{Q_i\})$. Hence, there exist various variants of the idea which have been applied to an huge number of different systems. See again [114] for a first impression. In particular, the multicanonical idea was successfully used for the study different polymer models, which lead for example to the development of a multicanonical chain-growth algorithm [55, 58, 68, 97, 104]. See also Sec. 2.1.3 ("Multicanonical Version of PERM (mucaPERM)").

2.2.4 Random Walk Algorithm by Wang and Landau

The main idea of the method proposed by Wang and Landau [119] is similar to the one of the multicanonical sampling – to perform a random work in a certain energy range during the simulation and hence sample the density of states $g(E)$ within this range directly. The estimate for $g(E)$ is initialized arbitrarily and then, whenever visiting a state with energy E, continuously modified by multiplying its value corresponding to this energy level by some number $f_i > 1$: $g(E) \rightarrow g(E) f_i$. This number f_i itself should be modified (using a function monotonically decreasing to 1) once in a while until satisfying some stop criterion. The acceptance probability for a proposed update is:

$$p(E_{\text{old}} \rightarrow E_{\text{new}}) = \min\left\{1, \frac{g(E_{\text{old}})}{g(E_{\text{new}})}\right\} .$$

As suggested by the word choice, there are a lot of technical parameters, which has to be fixed in practice and at least the efficiency of the implementation may depend on the setting of these parameters. The maybe most controversial issue is the choice of the criterion, when to update $f_i \rightarrow f_{i+1}$. Wang and Landau propose to carry a histogram $H(E)$ of the visited states and to update f whenever this histogram becomes "flat". Furthermore, they use the square-root function to update then f_i: $f_{i+1} = \sqrt{f_i}$, whereas this choice seems to be arbitrary to some extent. Anyway, both, decreasing f_i to fast or to slow, may lead to more or less strong slowing down of the convergence of the simulation, not to mention the choice of the initial value f_0.

Shortly later, another strategy based on a mathematical analysis was presented by Zhou and Bhatt [120] in order to obtain a fast convergence. They suggest an update of f_i, when an energy level E has been reached at least $n(f_i)$ times, whereas $n(f_i) = 1/\sqrt{\ln f_i}$. Furthermore, f_0 should be chosen "large" ($f_0 = e^4$) and reduced in "large" steps, for example by dividing $\ln f$ by 10. Anyhow, the algorithm violates, strictly speaking, detailed balance as the ensemble is constantly changed during the simulation, even though the condition is in practice "asymptotically" fulfilled by converging $f \rightarrow 1$. A statistically correct method can be obtained by setting $f = 1$ at the end for a final simulation run, which is essentially

the same as carrying out a multicanonical simulation with weight factors obtained by the Wang–Landau iteration [114, 120, 121].

However, the Wang–Landau method has been successfully applied, even in its originally proposed version and with a direct use of the obtained estimate of the density of states for extracting canonical observables, for a huge number of different problems in the most varied fields, as for (simple) lattice models [122, 123], in quantum Monte Carlo simulations [124], for peptide and protein folding [125, 126], and in particular also for simulations of polymeric systems [127, 128].[7]

But, at this point, a further crucial point of the method concerning the simulation range should be addressed. Besides the fact, that special care has to be taken anyhow, when sampling within a bounded energy range [129], the energy range must not be changed during a simulation either. This means in particular, that one has to search (or reasonably estimate) in advance native- or ground states of the simulated system, which are in principle not known, to determine a reasonable energy range for reliable studies of the thermodynamics at low temperatures. By studying FENE polymers for example, I found that the carelessly chosen lower simulational bound of $E_<(N) = -4N$ (N is the system size) in [130, 131][8], "motivated" by an appropriate bound for a completely different system [128], led to wrong interpretations of the low temperature behavior of these systems (see also [76]). This finding, in particular, has been independently reconfirmed in the meantime [133, 134]. Hence, Wang–Landau simulations in this work are always preceded by adequate ground-state searches.

2.2.5   Energy Landscape Paving

Such a ground-state search can be done for example using the energy landscape paving (ELP) method [135]. The main idea is to travel at low temperatures through the energy landscape and overcome energy barriers to not to get stuck in local energy minima by filling up the energies of the visited states constantly. The idea behind is in a sense the same as in the methods described before: To change the sampled distribution in some favorable way. Anyhow, the philosophy is slightly different. Whilst with the former methods, the thermo-dynamical behavior can be studied by sampling "at all temperatures at once", ELP runs at low temperatures. Whenever visiting a state with energy E, the Boltzmann factor is changed by increasing, in the simplest case, a number that is added to E: $\mathrm{e}^{-\beta E} \rightarrow \mathrm{e}^{-\beta(E+H(E))}$.[9] Obviously, this procedure violates detailed balance, hence it is not appropriate for the sampling of thermodynamic distributions. For a ground-state search, this fact causes no problem

---

[7]I will not give here a in some way comprehensive list of publications. The given references are more or less arbitrarily chosen examples.

[8]With a naive and by no means optimized ground state search, I could find quickly conformations with $E < -480$ for $N = 100$. The current bound for the ground-state conformation found so far by extensive simulations is $E = -515.638$ [132].

[9]Generally, the histogram may depend on any "order parameter" and an arbitrary function of it is added to the energy: $\mathrm{e}^{-\beta E} \rightarrow \mathrm{e}^{-\beta(E+f(H(q)))}$.

of course. The method was hence successfully applied for finding global energy minima of different proteins elsewhere [68, 135–138].

2.2.6 Conjugate Gradient Optimization

The conjugate gradient (CG) optimization [139] is, in contrast to all other methods describes so far, a deterministic procedure which can not overcome energetic barriers by definition. It rather finds the minimum of the valley of a energy landscape a conformation already resides in by following a deterministic trajectory. The naive idea, also called "steepest descent" method, is, starting from a point $\vec{x}_i$ in the phase space, to move to the point $\vec{x}_{i+1}$ by minimizing along the direction of the gradient $\vec{g}_i = -\nabla f(\vec{x}_i)$, and so on until the gradient vanishes after a certain number of iteration steps and the minimum is hence found. This idea is improved by calculating the minimization direction $\vec{h}_i$ with some "memory" of the last one:

$$\vec{h}_{i+1} = \vec{g}_{i+1} + \gamma_i \vec{h}_i \,,$$

where

$$\gamma_i = \frac{\vec{g}_{i+1} \cdot \vec{g}_{i+1}}{\vec{g}_i \cdot \vec{g}_i} \,.$$

Note that finding the minimum along $\vec{h}_{i+1}$ is a search in one direction, a problem for which a variety of efficient algorithms exist [139].

The method is hence a candidate for refining optimization results obtained by stochastic methods. As it will not worsen the results by definition it can always be applied risklessly on top of stochastic global energy minimization. Examples of successful applications lowering energies of different systems significantly are given in Appendix B ("Non-Stochastic Minimization – Examples").

Chapter 3

Study of Lattice Models
of Polymers

It is well known, that polymers or polymer solutions appear in different states depending on external parameters like temperature or solvent quality [2, 30, 63]. Thus, a single polymer in solvent can experience conformational transitions between different structural phases. Anyhow, the analysis of these transitions is not trivial, as I will show in this chapter.

At hight temperatures (or in good solvents) dissolved or random coil structures dominate. Approaching the critical point at the Θ temperature or the solvent medium becomes sufficiently poor, respectively, the polymer collapses and globular conformations are formed. At the Θ point, the influence of volume exclusion causing an effective repulsion is exactly compensated by the attractive monomer-monomer interaction. The polymer conformation then takes the so-called random flight conformation, i.e., behaves like a Gaussian random chain [1]. Below the Θ point, i.e., at low temperatures or in poor solvent, the polymer enters the globular phase. Globules are very compact conformations with little internal structure, i.e., the globular phase is still entropy-dominated. Therefore, a further transition towards low-degenerate energetic states is expected to happen: the freezing or crystallization of the polymer. [1] Since this transition can be considered as a liquid–solid phase separation process, it is expected to be of first order, in contrast to the Θ transition, which exhibits characteristics of a second-order phase transition [140–142].

In principle, there is no longer any difficulty to investigate the collapse transition for finite systems up to very long chains by means of computer simulations. Well working techniques to deal with the problem are chain growth algorithms considered below and in detail described in Sec. 2.1 (“Simulational Techniques on the Lattice”). Anyhow, the problem of the infinite-length Θ transition is still unsolved. The complexity of this problem appears

---

[1] This transition is elsewhere called ground-state–globule [55], liquid–solid [127] or melting transition [130]. These term are used as synonyms in this work.

in the quantitative description of these processes. From the analysis of the corresponding field theory [2] it is known that for the Θ transition the upper critical dimension is $d_{\mathrm{c}} = 3$, i.e., multiplicative and additive logarithmic corrections to the Gaussian scaling are expected and, indeed, predicted by field theory [143–146]. However, until now neither experiments nor computer simulations could convincingly provide evidence for these logarithmic corrections. This not only regards analyses of different single-polymer models [28, 29, 100, 127, 128, 130, 131, 147], but also the related problem of critical mixing and unmixing in polymer solutions [62, 148–151].

In a remarkable recent study of a bond-fluctuation polymer model (Sec. 3.2, "Preliminary Remarks, Related Studies"), it was shown that collapse and freezing transition can fall together in the thermodynamic limit [127]. That this surprising phenomenon is, however, not general, but depends on the intramolecular interaction range, was found a little later by the same group [63, 128]. For an off-lattice bead-spring polymer with finitely extensible nonlinear elastic (FENE) bond potential and intra-monomer Lennard-Jones interaction, for example, it could be shown that both transitions remain well separated in the limit of infinitely long chains [76, 77]. [2]

In this chapter, motivated by above mentioned recent publications, I investigate the structural transitions of interacting self-avoiding walks (Sec. 3.1, "Model and Methods"), the simplest model for polymers, restricted to simple cubic (sc) and face-centered cubic (fcc) lattices. The focus lies primarily on the freezing transition (Sec. 3.3, "The Freezing-Transition Regime"), where comparatively little is known as most of the analytical and computational studies in the past were devoted to the controversially discussed collapse transition; see, e.g., [28, 29, 62, 149, 150, 152–158]. A precise statistical analysis of the conformational space relevant in this low-temperature transition regime is difficult [3] as it is widely dominated by highly compact low-energy conformations which are entropically suppressed. Most promising for these studies appear sophisticated chain-growth methods based on Rosenbluth sampling [14] combined with improved pruning-enrichment strategies [29, 59, 159] which, in their original formulation, are particularly useful for the sampling in the Θ regime. To top the work off, I will revisit the Θ regime in Sec. 3.4 ("The Θ-Transition Revisited") and present results for the scaling of the collapse transition temperature in comparison with various approaches known from literature. Eventually, the chapter is concluded by a summary of the findings in Sec. 3.5 ("Summary").

---

[2]The same conclusion was drawn in [130, 131], but the interpretation of the data there was not reliable. See Sec. 2.2.4 ("Random Walk Algorithm by Wang and Landau") for more details.

[3]See for example [100, 147], where the low-temperature region could not be sampled using local update moves in standard Monte Carlo schemes.

3.1 Model and Methods

The model I use here is the interacting self-avoiding walk (ISAW), the simplest model of lattice polymers. In this model, the polymer chain is a walk on a lattice, which is not allowed to cross itself, i.e., a lattice site can only be occupied by a single monomer. In order to mimic the poor solvent behavior in the energetic regime nearest-neighbor contacts of nonadjacent monomers reduce the energy. Thus, the most compact conformations, i.e., the conformations with the maximal number of nearest-neighbor contacts, possess the lowest energy. Formally, the total energy of a conformation $\mathbf{X} = (\mathbf{x}_1, \mathbf{x}_2, \ldots, \mathbf{x}_n)$ of a chain with n beads is simply given as

$$E(\mathbf{X}) = -\varepsilon_0 m(\mathbf{X}), \tag{3.1}$$

where ε_0 is an unimportant energy scale (which is set $\varepsilon_0 \equiv 1$ in the following) and $m(\mathbf{X})$ is the number of nearest-neighbor contacts between nonbonded monomers.

The total number of self-avoiding walks of length $n-1$ scales (for large m) as [2]

$$C_n \sim \mu^{n-1}(n-1)^{\gamma-1}, \tag{3.2}$$

where μ is the effective coordination number[4] of the respective lattice and γ a universal, i.e., lattice independent, exponent. For the sc lattice, the effective coordination number is $\mu_{\mathrm{sc}} \approx 4.684$ and in the fcc case $\mu_{\mathrm{fcc}} \approx 10.036$ and γ has in three dimensions the value $\gamma \simeq 7/6 \approx 1.16$ [2, 25, 27, 56, 160–163]. See also Chap. 1 ("The Self-Avoiding (Random) Walk", pp. 5), for further introductory remarks.

A further important quantity is the maximal number of contacts in a self-avoiding walk $m_{\mathrm{max}}(n)$ for a given length $n-1$ of the walk. Particularly, in the case of interacting self-avoiding walks, this number is directly connected with the ground-state energy, see Eq. (3.1). In the limit $n \to \infty$ and for a lattice coordination number z,

$$m_{\mathrm{max}}(n) \overset{n\to\infty}{\sim} \frac{zn - 2n}{2} = an, \tag{3.3}$$

with $a = (z-2)/2$. For the hypercubic lattice holds $a = d-1$, where d is the spatial dimension. In the asymptotic estimate above, surface sites have been neglected, whose number scales as $n^{(d-1)/d}$. Taking them into account, one can approximate (an upper bound) for the maximal number of contacts in a self-avoiding walk on a hypercubic lattice as [26]:

$$m_{\mathrm{max}}(n) \approx \mathrm{int}(an - b^{(d-1)/d} + c), \tag{3.4}$$

where $a = d-1$, $b = d(n+1)$, $c = d$ and $\mathrm{int}(x)$ just gives the integer value of x.[5] In

---

[4]For the random walk, the *effective* coordination number would be simply equal to the *real* coordination number of the underlying lattice. The effective coordination number for self-avoiding random walks is always lower due to occupied and hence forbidden lattice sites.

[5]$c = d$ corresponds to the value given in [26]. Taking in mind, that c accounts for the additional contacts due to the missing bonds at the ends of the chain, I would suggest c to be $c = 2$. This, by the way, fits also better to my Monte Carlo data, see Fig. 3.2.

particular, for the three-dimensional cubic lattice Eq. (3.4) would read:

$$m_{\max}(n) \approx \text{int}\left(2n - 3(n+1)^{2/3} + c\right). \tag{3.5}$$

Due to the exponential growth of the number of conformations given in Eq. (3.2), the investigation of all conformational transitions a homopolymer of a given length can experience requires numerical methods being capable of estimating the density of states for all possible energies with high accuracy. For that purpose, rather than applying standard Markov chain Monte Carlo methods with conformational updates, I used the alternative concept of chain growth. Depending on the lattice constraints, a new monomer is tried to be attached to an end of the already existing chain until the total length or a "dead end" is reached, i.e., the chain end is trapped.

As a first attempt, already in the 50s of the last century, the so-called Rosenbluth Method was introduced [14], a chain growth algorithm balancing the conformational bias induced by the growing process. For the investigation of the Θ-point, an enhanced version, the Pruned Enriched Rosenbluth Method (PERM) [29] is used. This method turned out to be very powerful for simulating very long chains in the Θ region. It combines the original Rosenbluth method with the "Go with the winners" strategy, i.e., it introduces some kind of population control. Unfortunately, it fails when simulating at low temperatures, i.e., it is unsuitable for the analysis of the freezing transition. Therefore, I apply in the simulations in that region generalized contact-density variants [104, 105] of PERM, which have proven to be very successful in the low-energy sampling of protein-like heteropolymers [55, 104] and the adsorption of polymers and peptides to solid substrates [164, 165]. The precision of these algorithms when applied to lattice polymers as in the present study, is manifested by unraveling even finite-length effects induced by symmetries of the underlying lattice.

To get an idea of manageable system sizes, Fig. 3.1 visualizes conformations of different orders of magnitude in size. Whilst the low-temperature region can be sampled reliably with the flat histogram methods up to lengths of $n \approx 100$ (left picture in Fig. 3.1), polymers at the Θ point can be simulated with flat histogram simulations up to lengths of $n \sim \mathcal{O}(10^3)$ (middle) and using canonical nPERM runs chains with lengths up to $n \approx 30\,000$ (right picture) have been treated. For a detailed description of all mentioned methods, see Sec. 2.1 ("Simulational Techniques on the Lattice").

3.2   Preliminary Remarks, Related Studies

As mentioned above, there are some works dealing with the phase behavior of single polymer chains, in particular with the freezing and collapse transition. Some years ago, it was found by F. Rampf et al. studying the bond fluctuation model [166], that both transitions coincide for a special choice of the interaction range λ_1 in the thermodynamic limit $n \to \infty$, where n is the number of monomers the polymer chain consists of [127]. In other words, for very
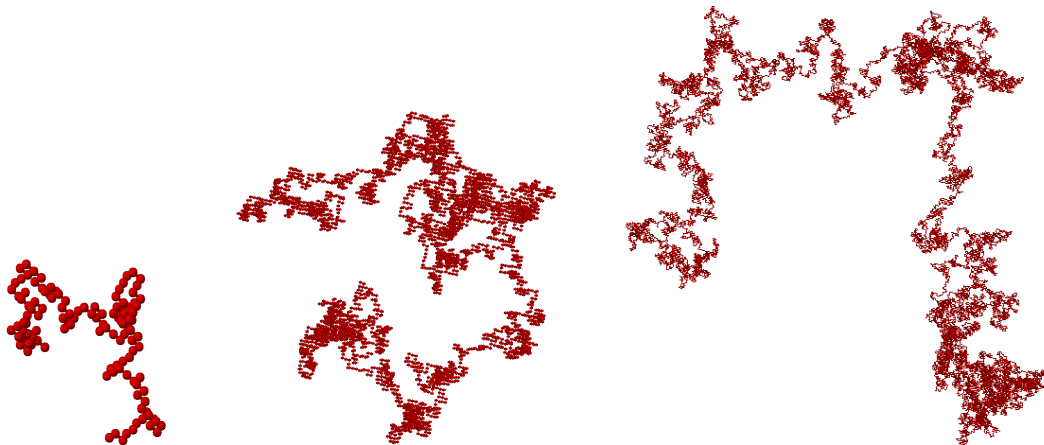
Figure 3.1: Polymer conformations with different sizes n on the sc lattice. Left: $n = 125$, $E = -22$. Middle: $n = 4000$, $E = -1551$. Right: $n = 32\,000$, $E = -13\,671$.

large chain lengths, there is a direct transition from the coil phase to the frozen phase when decreasing the temperature of the system, the globular or liquid phase is entered only by finite chains. Interestingly, it was later found [63], that both transitions remain well separated, just by increasing the interaction range to λ_2.

The effect of the stability of liquid phases was extensively discussed in the context of particle systems with repulsive and attractive pairwise interactions. See, for example, [167] and references therein. The crucial point is, roughly spoken, the range of the attractive interaction. A dimensionless measure for this range was introduced as $R = \lambda/\sigma - 1$, where σ and λ are the parameters in a square-well potential for hard spheres, for example: [6]

$$V(r) = \begin{cases} \infty & r \leq \sigma \,, \\ -\epsilon & 1 < r \leq \lambda \,, \\ 0 & \lambda < r \,. \end{cases}$$

In experimental approaches, the critical value R_{c}, separating stable from metastable liquid phases, was found to be $R_{\mathrm{c}} \approx 0.25$, see [30, 63] and references therein. Below this value, i.e., for attractive interaction with short ranges, the liquid or globule phase is metastable.

The bond-fluctuation model is a lattice model of polymers, where the monomers occupy a unit cell of the lattice and the bonds are allowed to vary in length between λ_{min} and λ_{max}. The interaction between the monomers is described by a square well potential with an attraction interval $[0, \lambda]$. It is argued, that this model is the lattice equivalent to a tethered-hard-spheres chain [63] and R can be calculated. By setting $\sigma = \lambda_{\mathrm{min}} = 2$ and $\lambda = \lambda_1 = \sqrt{6}$, $R_1 = 0.225$. For $\lambda = \lambda_2 = \sqrt{10}$, R becomes larger than R_{c}: $R_2 = 0.58$. The result concerning the disappearance or continuance of the globular phase in the thermodynamic limit are in fact in qualitative agreement with the described theory.

---

[6]I follow here the notation from [63], where $\lambda \leftarrow \lambda\sigma$ compared to [167].

A further recent study dealing with that problem studied flexible off-lattice polymers with finitely extendible bonds (FENE polymer) [76, 77]. The monomers interact via (a truncated) 12-6 Lennard-Jones potential. It was shown, that Θ-transition and freezing remain well separated in the thermodynamic limit as well. Anyhow, the application of the above described concept, i.e., the calculation of effective interaction ranges, is not that trivial [167], but it was shown, that the $2n$-n Lennard-Jones potential can be considered to cause long-range interaction for the case of $n = 6$ [168].

In the case of the lattice model, I study here, the potential could be written as:

$$V(r) = \begin{cases} \infty & r < 1\,, \\ -1 & 1 = r\,, \\ \infty & 1 < r\,. \end{cases}$$

Hence, $R = \lambda/\sigma - 1 = 0$, which is trivially below any positive threshold value. In particular, it is also lower than *another* threshold value $R_{c'} \approx 0.015$ known from colloidal systems, for which different solid phases can coexist [169] and which I have neglectd in the discussion so far. Even though the liquid phase would not be stable in the thermodynamic limit, following the colloid interpretation, a further stable solid phase would thus emerge.

In general, since the range of interactions seems to play a crucial, quantitative role, it is an interesting, still widely open question to what extent the colloidal picture in the compact crystalline and globular phases is systematically modified for polymers with different nonbonded interaction ranges, where steric constraints (through covalent bonds) are a priori not negligible.

3.3   The Freezing-Transition Regime

3.3.1   Results for the sc lattice

In order to study the freezing transition, i.e., the low-temperature regime of the system, the used algorithm must necessarily be able to find the ground states of the system. Fortunately, there are quite good estimates for the maximum number of contacts in self-avoiding walks, remember Eq. (3.4). Thus, a first test is to check the ground states obtained during the simulation against the predicted bound. As described in Sec. 2.1.4 ("Flat Histogram Version of PERM (flatPERM)"), I calculate during the simulation $C_{n,m}^{\text{est}}$, the estimator for the density of states. I hence plot for every length n the maximal number m for which $C_{n,m}^{\text{est}} > 0$ and compare with Eq. (3.5) with $c = 2$. The result is shown in Fig. 3.2. It can be seen, that the energies of the ground states (found during a single simulation) for all chain lengths agree very well, besides periodic local fluctuation which will be explained later, with the prediction. Note in particular, that Eq. (3.5) holds exactly for compact cubic ground-state conformations (see below) at, for example, $n = 36$, 64 or $n = 125$. The other way around,
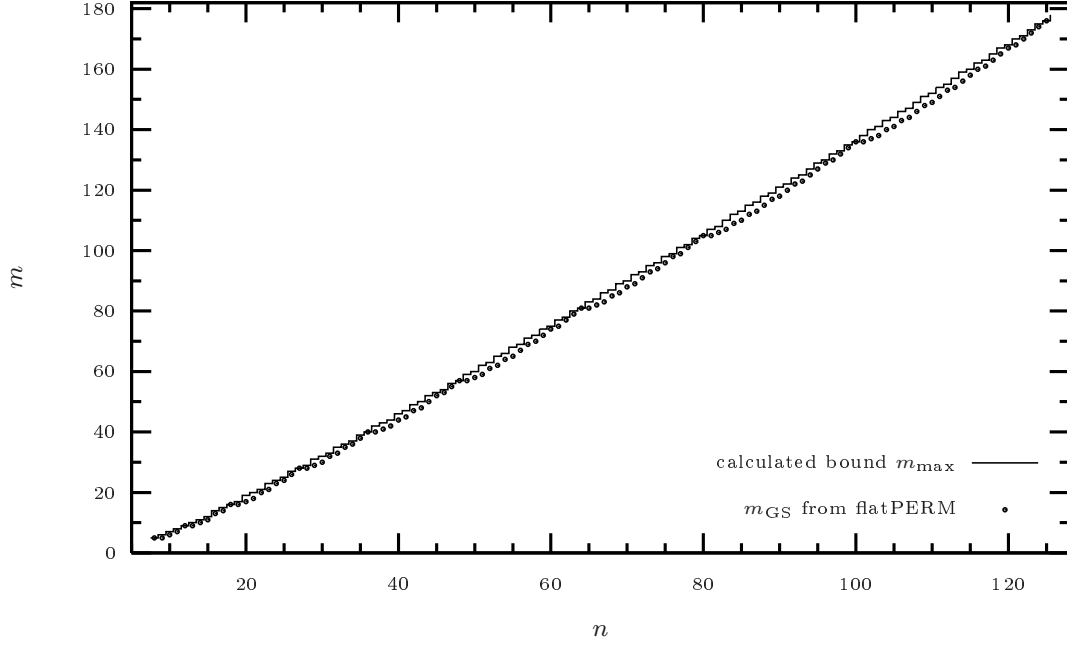
Figure 3.2: The maximal number of contacts in a self-avoiding walk of length n calculated using Eq. (3.5) with $c = 2$ (solid steps) and the number of contacts in ground states obtained in a single flatPERM run (dots).

the shown Monte Carlo results confirms the scaling approximation for large n,[7] an open task explicitly mentioned by the authors of [26].

For investigating structural transitions of the polymer models, I calculate the specific heat and analyze its peak structure. It is expected that even for polymers of finite length, peaks of fluctuating quantities signalize conformational activity. For more detailed analyses energy histograms will be considered as well in the subsequent discussion.

Figure 3.3 shows typical examples of specific heats for very short chains on the sc lattice and documents the difficulty of identifying the phase structure of flexible homopolymers. The 27-mer exhibits only a single dominating peak – which is actually only an sc lattice effect. The reason is that the ground states are cubic ($3 \times 3 \times 3$) and the energy gap towards the first excited states is $\Delta E = 2$.[8] Actually, also the most pronounced peaks for $N = 48$ ($4 \times 4 \times 3$) and $N = 64$ ($4 \times 4 \times 4$) are due to the excitation of perfectly cuboid and cubic ground states, respectively. The first significant onset of the collapse transition is seen for the 48-mer close to $T \approx 1.4$. A clear discrimination between the excitation and the melting transition is

---

[7]The simulation was done for $N = 256$ and ground-state contacts are in agreement with the approximation for $n \lesssim 250$. As I do not consider in the following lengths $n \gtrsim 125$ either and for reasons of visibility, the respective data are not shown in Fig. 3.2.

[8]This gap is an artifact of the simple-cubic lattice. See below for a intuitive explanation.
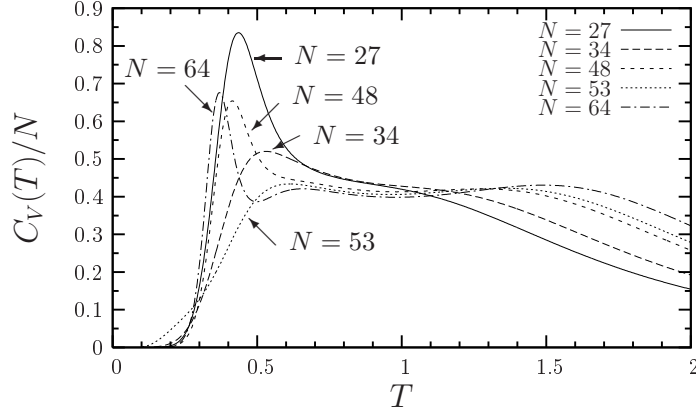
Figure 3.3: Examples of specific-heat curves (per monomer) for a few exemplified short homopolymers on the sc lattice. Absolute errors (not shown) are smaller than 0.03 in the vicinity of the low-temperature peaks and smaller than 10^{-5} in the onset of the Θ-transition region near $T \approx 1.5$.

(a)   (b)

$E = -79$ $E = -60$

(c)

$E = 0$
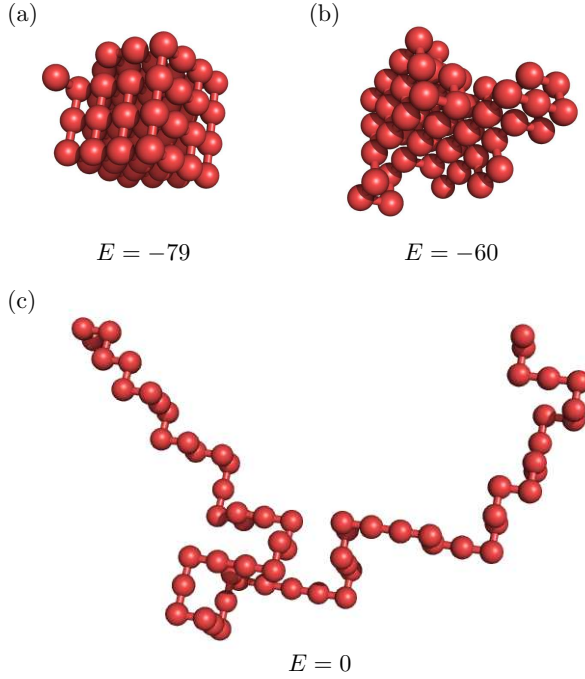
Figure 3.4: Representative conformations of a 64-mer in the different pseudophases: (a) Excitation from the perfect $4 \times 4 \times 4$ cubic ground state (not shown, $E = -81$) to the first excited crystal state, (b) transition towards globular states, and (c) dissolution into random-coil conformations.
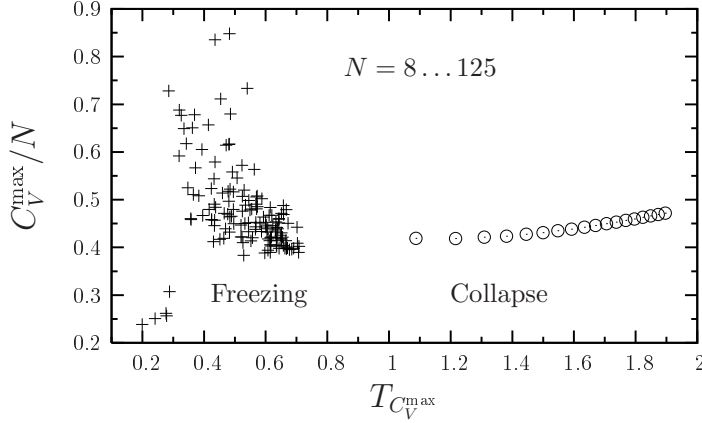
Figure 3.5: Map of specific-heat maxima for several chain lengths taken from the interval $N \in [8, 125]$. Circles ($\odot$) symbolize the peaks (if any) identified as signals of the collapse ($T_{C_V^{\max}} > 1$). The low-temperature peaks (+) belong to the excitation/freezing transitions ($T_{C_V^{\max}} < 0.8$). The group of points in the lower left corner corresponds to polymers with N_{c+1} monomers, where N_c denotes the "magic" lengths allowing for cubic or cuboid ground-state conformations (see Fig. 3.6 and text).

virtually impossible. In these examples, solely for $N = 64$ three separate peaks are present. The pictures in Fig. 3.4 show representative conformations in the different pseudophases of the 64-mer. Due to the energy gap, the excitations of the cubic ground state with energy $E = -81$ (not shown) to conformations with $E = -79$ (Fig. 3.4 a) result in a pseudotransition which is represented by the first specific-heat peak in Fig. 3.3. The second less-pronounced peak around $T \approx 0.6$–0.7 signalizes the melting into globular structures, whereas at still higher temperatures $T \approx 1.5$ the well-known collapse peak indicates the dissolution into the random-coil phase.

Anyhow, this first view did not show any regularity regarding the low-temperature peak(s). In particular, one could not observe any uniform scaling behavior of the specific heat peaks depending on the chain length as it was found in other studies, for example, in [127]. Hence, a more systematic approach simulating all system sizes is required. Therefore, I plot in Fig. 3.5 the peak values of all polymers with lengths $N = 8, \ldots, 125$. What one sees are three regions. A sparsely populated one at very low temperatures with little peak heights, a further with peak temperature $0.3 < T < 1$ and the Θ-peak region at $T > 1$. Not surprisingly, the peaks belonging to the excitation and freezing transitions (+) appear to be irregularly "scattered" in the low-temperature interval $0 < T_{C_V^{\max}} < 0.8$. The first trend one notices in that region is that with increasing peak temperature, the relative height of the peak decreases. And, assuming (for the same region) that even if the lower peaks would correspond to larger chain lengths, what is not generally true as has been showen exemplarily
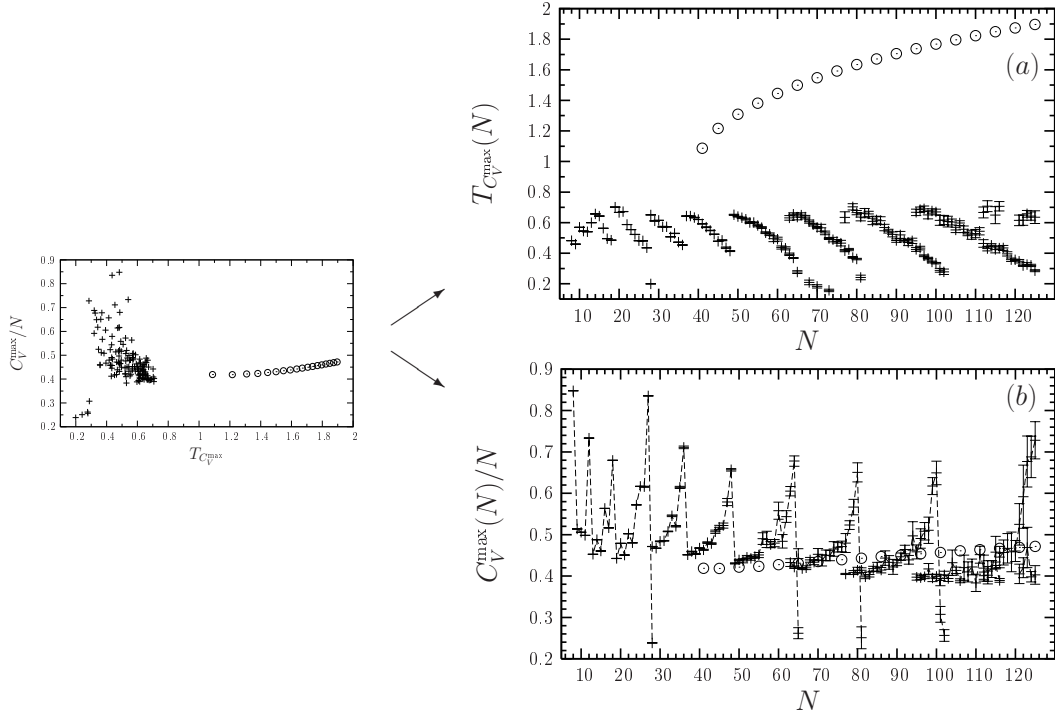
Figure 3.6:   (a) Collapse ($\odot$) and crystallization/excitation ($+$) peak temperatures of the specific heat for all chain lengths in the interval $N \in [8, 125]$, (b) values of the specific-heat maxima in the same interval. Error bars for the collapse transition data (not shown) are much smaller than the symbol size. Θ peaks appear starting from $N = 41$. For the sake of clarity, not all intermediate Θ data points are shown (only for $N = 41, 45, 50, \ldots$). The left plot is that one shown in Fig. 3.5.

in Fig. 3.3, the peak temperature would increase slower than the peak temperature for the Θ-peak. As expected, the Θ-peak itself behaves very smooth, i.e. it grows homogeneously in both directions, temperature und peak height.

Looking at the specific-heat peaks depending on chain length, as shown in Fig. 3.6, more systematics are revealed. There, the peak temperatures and the peak heights, respectively, as functions of the number of monomers are plotted. The Θ-peak line emerges around $N = 40$ as an almost straight, slowly increasing line. At mentioned chain lengths, the Θ-peak becomes the first time a real maximum of the function. At shorter chains, it exists only as a shoulder (cp. Fig. 3.3).

The freezing-transition temperatures show a sawtooth-like behavior which is clearly a lattice effect. At the lowest peak temperatures (and highest peak amplitudes), one finds chains with very compact ground state conformations which are arranged as cubes or compact cuboids, respectively, e.g. $N = 27$ ($3 \times 3 \times 3$-cube), $N = 36$ ($3 \times 3 \times 4$-cuboid), $N = 48$

($3 \times 4 \times 4$-cuboid) and so on, until $N = 100$ ($4 \times 5 \times 5$-cuboid) and $N = 125$ ($5 \times 5 \times 5$-cube). I will denote these special lengths in the following by N_c. Chains with these lengths have a very pronounced freezing-transition peak (see Fig. 3.6 b). Furthermore, they have an energy gap of $\Delta E = 2$ between the ground state and the first excited state. For the sc-lattice, this can easily be explained. Consider a cuboid conformation with a chain end located in one of the corners. It forms two energetic contacts with the nearest neighbors. Performing a local rotation of the bond the chain end is connected with, these two contacts are lost and none new is formed. In the specific heat curves, this effect causes the emergence of a second peak for $N_c \geq 64$. Here, the crystallization and the transition into the (very compact) ground state, are two distinguishable processes. At $N = 48$ this behavior is already conjecturable because of a shoulder in the specific heat curve. Figure 3.7 a shows again the specific heats for the chains $N = 48$, 64, and for $N = 80$ for illustration.

On the other hand, at the other side of the "teeth", the respective chains with one more monomer ($N_c + 1$) reside. Here, the formerly pronounced low-temperature peak at
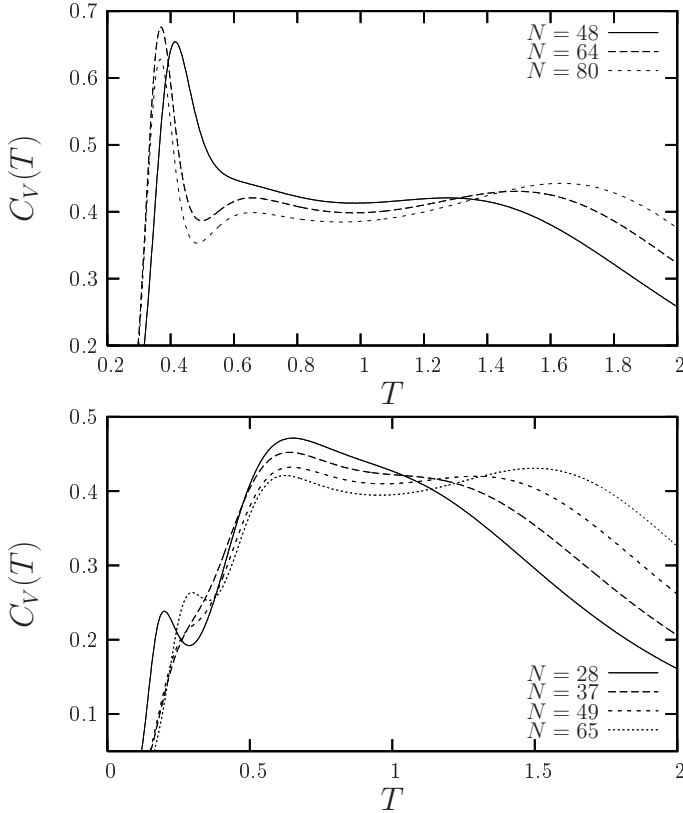
Figure 3.7: Examples of specific heats of polymers with compact ground states ($N_c = 48$, 64, and 80) (a) and of polymers with $N_c + 1$ (b). Error bars are again not shown but are sufficiently small.

N_c becomes very weak or just a shoulder at the "foot" of the second peak, respectively, while the second peak itself now dominates the situation. The energy gap between the ground state and the first exited one for these chains is (as usual) $\Delta E = 1$ (take a monomer from a corner, place it next to the single remaining monomer at the surface). Figure 3.7 b shows the respective heat capacities. It is worth noting that the mentioned behavior can already/still be seen arising or disappearing, respectively, at lengths $N_c - n$ and $N_c + n$ with $n = 1, 2, 3$ (no data plotted).

What we have seen until here is, that there exists a clear low-temperature freezing collapse below the Θ-point, which is strongly influenced by lattice restrictions. It "moves" with increasing chain length to lower temperatures ($T_{C_V^{max}}(N) \approx 0.4$) and higher amplitudes and jumps for chains with very compact ground states back to a value of $T_{C_V^{max}}(N) \approx 0.6$ and a smaller amplitude. Around these jumps the peak splits into two more or less pronounced ones. The temperature interval, in which the first peak "moves", does not change depending on chain length, while the Θ-peak, as commonly known and explicitly visible, does. Additionally, the amplitude of the first peak tends to decrease with increasing chain length. For large chain lengths, it even becomes smaller than the Θ-transition amplitude. The Θ-transition then dominates the thermodynamic behavior. This is different from what has been observed recently in similar studies of the bond-fluctuation model with short-range interaction [127], where the crystallization and collapse transition points converge towards the Θ-transition temperature and coincide in the thermodynamic limit.

As a technical remark: I am presenting results here for chains with lengths $N \leq 125$. For chains longer than $N \approx 125$ it is extremely difficult or almost impossible to sample the low-temperature region with satisfying accuracy, even with the very sophisticated methods used. This is due to three effects, accompanying and amplifying each other. On the one hand, the freezing-transition peak decreases and becomes dominated by collapse-transition signal, on the other hand the computation time grows anyway with increasing system size. Generally, the low-energy states are increasingly suppressed in the density of states. By contrast, the Θ-region, as I will show later, can be sampled very well and accurate up to chain lengths of order $N \sim 10^4$ with flat histogram simulations gaining the complete density of state of that region and up to order of $N \sim 10^5$ with canonical simulations at discrete temperatures.

Let us now look at the transitions in a little more detail. Exemplified for chains of lengths $N = N_{c-1}, N_c$, and N_{c+1} with $N_c = 36, 64$, specific heats and densities of states are shown in Fig. 3.8, which exhibit the length-dependent characteristic properties discussed above. While in Fig. 3.8 a for chain lengths around $N = 36$ only some low-temperature activity is visible and the collapse transition is vaguely indicated by a broad shoulder, the transition characteristics are better resolved for $N = 64$ shown once more in Fig. 3.8 c. As mentioned, the most pronounced low-temperature peak of the specific heat of the 64-mer is the excitation peak, the second peak belongs to the freezing transition, and the third, still very shallow peak
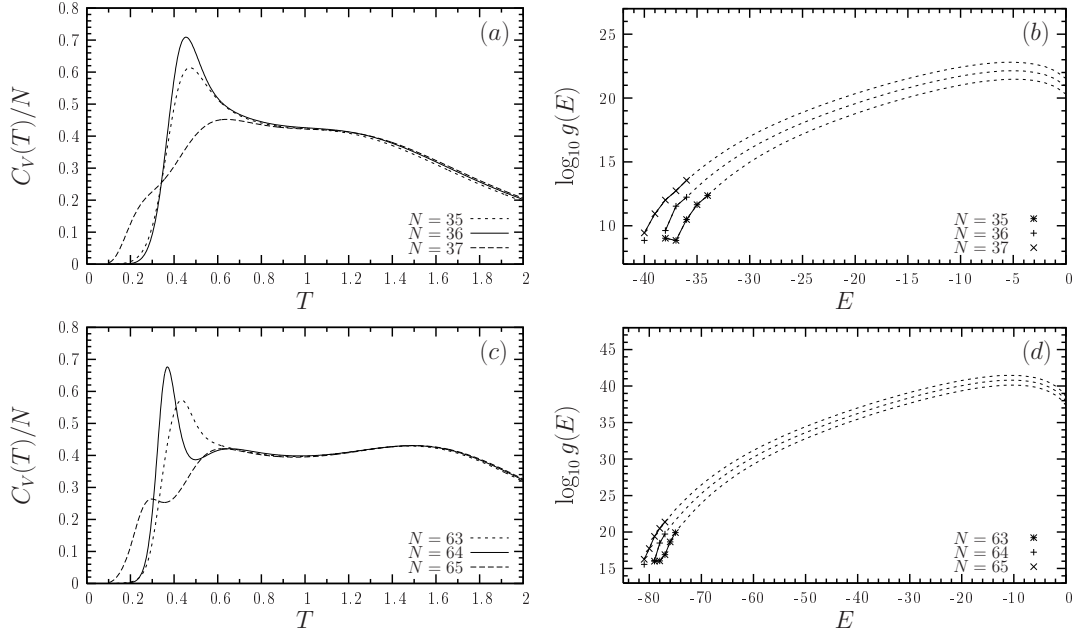
Figure 3.8: Examples of specific heats for polymers with (a) $N_c = 4 \times 3 \times 3 = 36$ and $N_c \pm 1$ and (c) $N_c = 4 \times 4 \times 4 = 64$ and $N_c \pm 1$ monomers. In (b) and (d), the respective densities of states are shown (lines are only guides to the eye). Symbols $*$, $+$ and $\times$ emphasize the lowest-energy states. Note the energy gaps between the ground and the first excited states in the compact cases $N_c = 36, 64$ and the dip for $N = 35, 63$.

signals the collapse transition. The low-temperature behaviors of the 63-mer and the 65-mer are quite different: While the low-temperature peak of the 63-mer close to $T \approx 0.4$ is due to excitation as is indicated by the $E = -79$ "dip" in the density of states in Fig. 3.8 d (similar to the 35-mer in Fig. 3.8 b at $E = -38$), the relevant peak for the 65-mer is the freezing peak close to $T \approx 0.6$. In this case, the excitation is of much less relevance (although it is still reflected by a small peak near $T \approx 0.3$). This is a consequence of the missing convex lowest-energy dip in the density of states (or microcanonical entropy). The convex monotony is a signal of a strong first-order phase separation [170, 171]. This is confirmed by analyzing the canonical energy distributions for the examples $N = N_{c-1}, N_c$, and N_{c+1} with $N_c = 36, 64$ shown in Fig. 3.9 for temperatures close to the respective excitation and freezing transitions. For $N_{c-1} = 35, 63$ (Fig. 3.9 a), the pronounced excitation transition is expressed by the respective double peaks with the strong gap in between, which are for the polymers with chain lengths $N_c = 36, 64$ (Fig. 3.9 b) due to the energy gap between ground state and first excited state. This induces the first-order-like character of this pseudotransition. The energy distributions for various temperatures shown in Fig. 3.9 c for the case $N = N_{c+1} = 65$ do not exhibit, on the other hand, pronounced double-peaked shapes. The excitation transition at
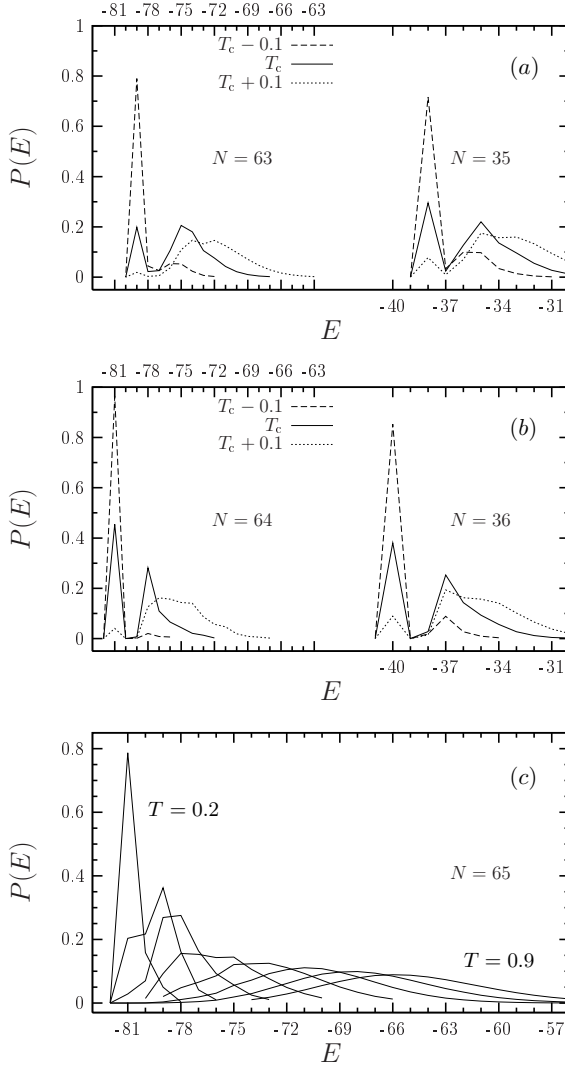
Figure 3.9: Energy distributions $P(E)$ at low temperatures for sc lattice polymers with (a) $N = N_{c-1} = 35$ and 63, (b) $N = N_c = 36$ and 64 monomers. In (c), $P(E)$ is shown for the chain with length $N = N_{c+1} = 65$ for several temperatures $T = 0.2, 0.3, \ldots, 0.9$. The distributions for $N = 37$ (not shown) are similar. Note that lines are only guides to the eyes.

extremely low energies is still weakly present as a small shoulder in the distribution at the corresponding temperature. The freezing transition is associated with slightly larger energies (and temperature) and visible in the distribution with a weak tendency to a double-peaked shape.

Finally, for an idea, how typical conformations at different temperatures or energies look like, see Fig. 3.10. There, conformations of the $N = 49$-mer are shown, beginning with the ground state, followed by conformations near the transition temperatures and ending with a stretched conformation far beyond the Θ-point. Compare with Fig. 3.7 b to evaluate, in which regions that conformations typically dominates. Figure 3.11 illustrates analogously the visually not that interesting and surprising freezing transition. I show the ground state, two states near the transition peak (first and second excited state; the corresponding mean
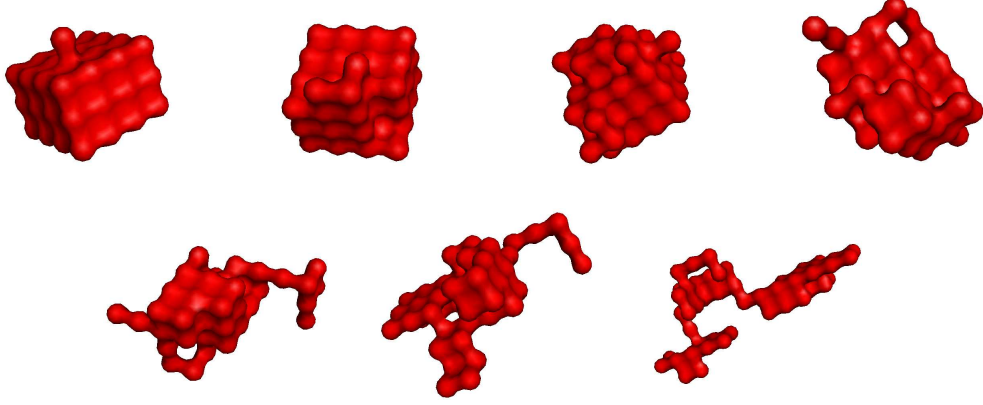
Figure 3.10: Typical conformations for the $N = 49$-mer. Top: Ground State ($E = -57$, $T \to 0$); ($E = -55$, $T \approx 0.37$); ($E = -50$, $T \approx T_{c_1} = 0.6475$); ($E = -43$, $T \approx 1$) (in the valley between the peaks). Bottom: ($E = -37$, $T \approx T_{c_2} = 1.2925$); ($E = -31$, $T \approx 1.6$); ($E = -20$, $T \approx 2.4$).
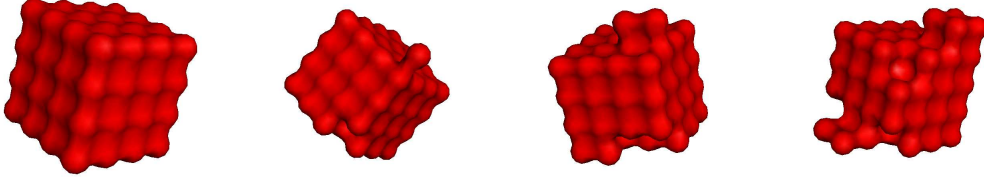
Figure 3.11: Typical conformations around the freezing transition for the homopolymer with $N_c = 64$. From left: Ground State ($E = -81$, $T \to 0$); ($E = -79$, $T \approx 0.36$); ($E = -78$, $T \approx 0.38$), the transition lies at $T_{c_1} = 0.37$; ($E = -75$, $T \approx 0.47$) (in the valley to the next peak).

energy value at the transition temperature lies almost exactly between these energies) and a typical conformation shortly after the transition. Compare with Figs. 3.8 b and d and 3.9 b.

3.3.2   Polymers on the fcc Lattice

The general behavior of polymers on the fcc lattice is comparable to what was found for the
sc polymers. The main difference is that excitations play only a minor role, and the freezing
transition dominates the conformational behavior of the fcc polymers at low temperatures.
Nonetheless, finite-length effects are still apparent as can be seen in the chain-length depen-
dence of the peak temperatures and peak values of the specific heats plotted in Fig. 3.12 a
and b, respectively. Figure 3.12 a shows that the locations of the freezing and collapse tran-
sitions clearly deviate with increasing chain lengths and one hence can conclude that also
for fcc polymers there is no obvious indication that freezing and collapse could fall together
in the thermodynamic limit.
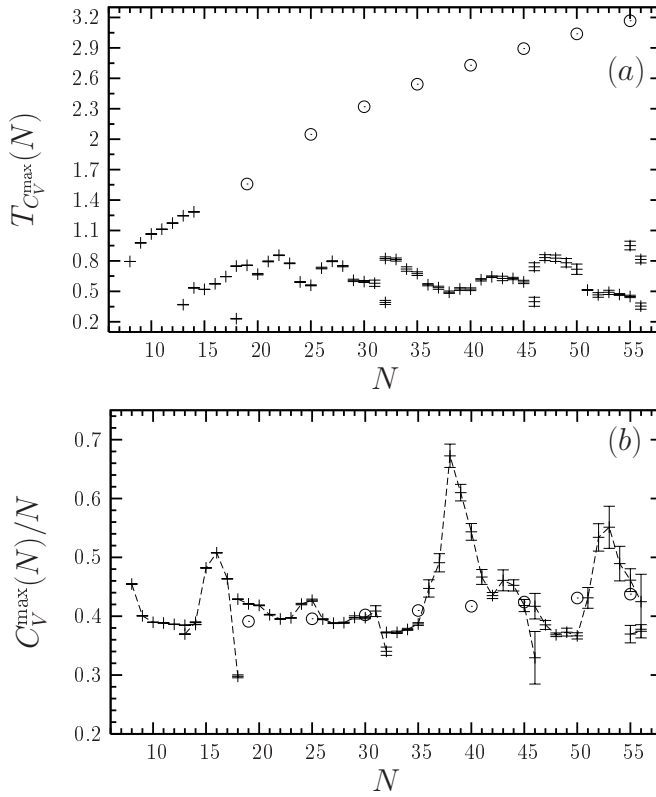
Figure 3.12: Peak temperatures (a) and peak values (b) of the specific heat for all chain
lengths $N = 8, \ldots, 56$ of polymers on the fcc lattice. Circles ($\odot$) symbolize the collapse
peaks and low-temperature peaks (+) signalize the excitation/freezing transitions. The
error bars for the collapse transition are typically much smaller than the symbol size. Only
for the freezing transition of longer chains, the statistical uncertainties are a little bit larger
and visible in the plots. Θ peaks appear starting from $N = 19$. For clarity, Θ data points
are only shown for $N = 19, 25, 30, \ldots$.

(a)   (b)   (c)

$N = 13$ $N = 18$ $N = 19$
$E_0 = -24$ $E_0 = -39$ $E_0 = -42$

(d)   (e)

$N = 27$ $N = 30$
$E_0 = -67$ $E_0 = -77$
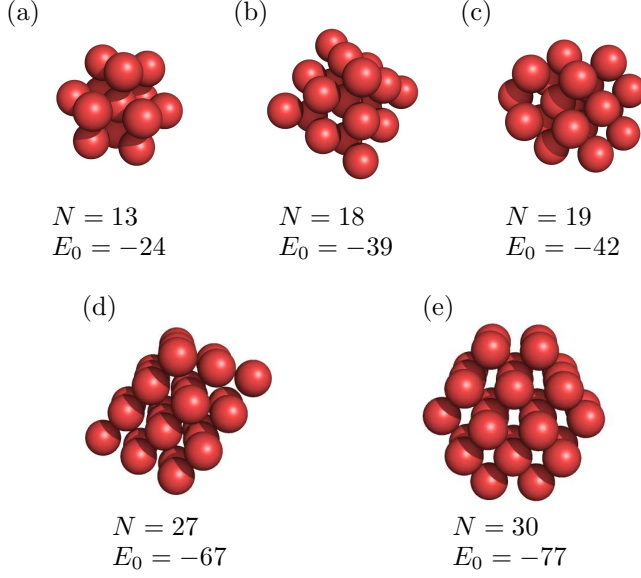
Figure 3.13: Ground-state conformations and energies of the 13- (a), 18- (b), 19- (c), 27- (d), and 30-mer (e) on the fcc lattice (bonds not shown).

Similar to the sc polymers, the finite-length effects at very low temperatures are apparently caused by the usual compromise between maximum compactness, i.e., maximum number of energetic (nearest-neighbor) contacts, and steric constraints of the underlying rigid lattice. The effects are smaller than in the case of the sc lattice, as there are no obvious "magic" topologies in the fcc case. Ground-state conformations for a few small polymers on the fcc lattice are shown in Fig. 3.13. The general tendency is that the lowest-energy conformations consist of layers possessing triangular pattern. This is not surprising, as these conformations are tightly packed which ensures a maximum number of nearest-neighbor contacts and, therefore, lowest conformational energy. An obvious example is the ground-state conformation of the 13-mer as shown in Fig. 3.13(a) which corresponds to the intuitive guess for the most closely packed structure on an fcc lattice: a monomer with its 12 nearest neighbors ("3–7–3" layer structure). A simple contact counting yields 36 nearest-neighbor contacts which, by subtracting the $N - 1 = 12$ covalent (nonenergetic) bonds, is equivalent to an energy $E = -24$. However, this lowest-energy conformation is degenerate. There is another conformation (not shown) consisting of only two "layers", one containing 6 (a triangle) and the other 7 (a hexagon) monomers ("6–7" structure), with the same number of contacts.

A special case is the 18-mer, which exhibits an additional peak in the specific heat at very low temperatures (see Fig. 3.12 a). As Fig. 3.13 b shows, its ground state is formed by a complete triangle with 6 monomers, a hexagon in the intermediate layer with 7 monomers, and an incomplete triangle (possessing a "hole" at a corner) with 5 monomers ("6–7–5"

structure). Although this imperfection seems to destroy all rotational symmetries, it is compensated by an additional symmetry: Exchanging any of the triangle corners with the hole does not change the conformation at all. In other words, neglecting this defect, the conformation would look equal independent from the position of the observer. Similar observations can presumably also be made for the 32-, 46-, and 55-mers, also showing the split from one peak in the specific heat into two, but for these larger ground-state conformations it does not make much sense to go into such intricate details, as the anomalies are much less pronounced anyway, compared to the case of the sc lattice. However, the naive expectation resulting from the observations made for the 18-mer ground state, that the 19-mer, which can form a perfect shape without any "holes" ("6–7–6" structure), is a prototype of peculiar behavior is wrong. This is due to the existence of degenerate less symmetric ground-state conformations, as the exemplified conformation shown in Fig. 3.13 c. The described geometric peculiarities are, however, only properties of very short chains. One of the largest of the "small" chains that still possesses a non-spherical ground state, is the 27-mer with the ground-state conformation shown in Fig. 3.13 d. For larger systems, the relative importance of the interior monomers will increase, because of the larger number of possible contacts. This requires the number of surface monomers to be as small as possible which results in compact, sphere-like shapes. A representative example is the 30-mer shown in Fig. 3.13 e.

To get another view on the peak behavior of the "larger" systems, Fig. 3.14 finally presents the specific heat curves for the 27- and 30-mer. One sees furthermore, that the errors are under good control, but they grow rapidly with increasing system size (not shown). For chain lengths $N \gtrsim 50$, the errors become almost as large, i.e. greater than 0.1 in absolute numbers, as the specific heat value itself for low temperatures.
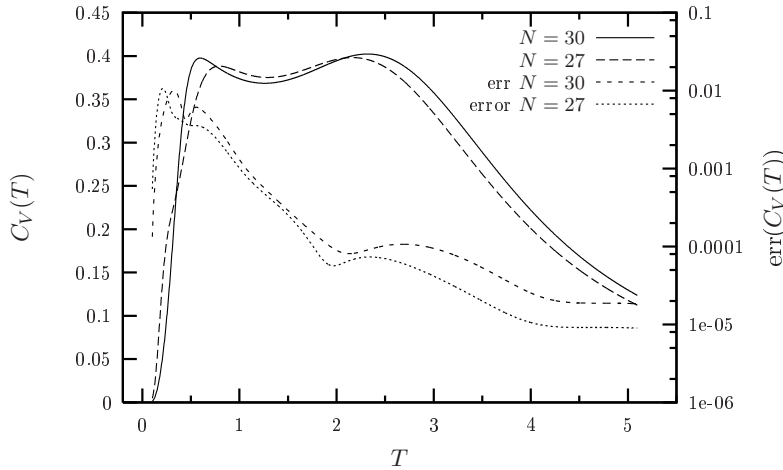
Figure 3.14: Examples of heat capacities for the polymers with $N = 27$ and 30 on the fcc lattice. Error bars lies between 0.01 for low temperatures and 10^{-4} at the Θ-peak.

3.4   The Θ-Transition Revisited

The scaling behavior of several quantities at and close to the Θ point in three dimensions has been the subject of a large number of field-theoretic and computational studies [28, 29, 62, 149, 150, 152–158]. Nonetheless, the somewhat annoying result is that the nature of this phase transition is not yet completely understood. The associated field theory has an upper critical dimension $d_c = 3$, but the predicted logarithmic corrections [143–145] could not yet be clearly confirmed from the numerical data produced so far. In this work, I mainly focus on the critical temperature T_Θ for polymers on the sc and on the fcc lattice. The sc value of T_Θ has already been precisely estimated in several studies, but only a few values are known for the fcc case. Some previous estimates in the literature are given in Table 3.1.

As the main interest here is devoted to the expected difference of the collapse and freezing temperatures, I will focus here on the scaling behavior of the finite-size deviation of the maximum specific-heat temperature of a finite-length polymer from the Θ temperature, $T_c(N) - T_\Theta$, as it has also been studied for the bond-fluctuation model [127, 128] or for polymer solution models [62, 148, 150]. As a first impression, Fig. 3.15 shows data obtained by my simulations for the finite size collapse temperature $T_c(N)$ versus the chain length N for large polymers. The uncorrected leading-order expression of the scaling reads:

$$T_c(N) - T_\Theta \sim \frac{1}{\sqrt{N}} \,. \tag{3.6}$$

lattice type	T_Θ	model	Ref.	(year)
sc	$3.64 \ldots 4.13\,^a$	single chain	[152]	(1973)
	3.713 ± 0.007	single chain	[153]	(1984)
	$3.650 \pm 0.08\,^b$	single chain	[155]	(1990)
	3.716 ± 0.007	single chain	[28]	(1995)
	$3.60 \pm 0.05\,^{c,e}$	single chain	[147]	(1996)
	$3.62 \pm 0.08\,^{d,e}$	single chain	[100]	(1996)
	3.717 ± 0.003	single chain	[29]	(1997)
	3.71 ± 0.01	polymer solution	[150]	(1998)
fcc	$8.06 \ldots 9.43$	single chain	[152]	(1973)
	8.20 ± 0.02	single chain	[154, 156]	(1988/96)
	8.264	lattice theory	[157]	(1998)

[a] Given in terms of reduced interactions strength $\Phi_\Theta \sim 1/T_\Theta$

[b] Given as $K_t \sim 1/T_t = 0.274 \pm 0.006$

[c] Given as $\beta_\Theta \sim 1/T_\Theta = 0.2779 \pm 0.0041$

[d] Given as $\beta_\Theta \sim 1/T_\Theta = 0.276 \pm 0.006$

[e] Fit to Eq. (3.6) ignoring corrections

Table 3.1: T_Θ values on the sc and fcc lattice from literature.
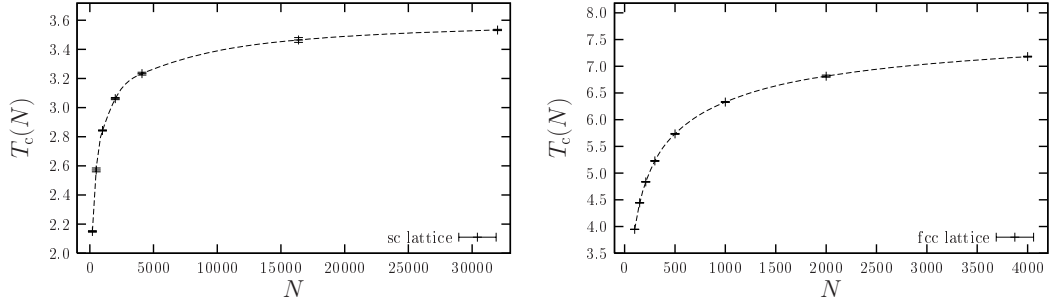
Figure 3.15: collapse temperature $T_c(N)$ versus chain length N. Left: For the sc-lattice, right: for the fcc-lattice. Dotted lines are cubic splines and plotted just to guide the eye. The upper bounds of the plots correspond to the respective infinite Θ-temperature (as estimated below). One notes, that even these large chains are still "far away" from the infinite length limit. Error bars are plotted but may not be visible.

It is valid for $d < 3$ [141], but approximately correct for $N \rightarrow \infty$ in $d = 3$. In the case of polymer solutions, Flory–Huggins mean-field theory [1] suggests the corrected scaling to be

$$\frac{1}{T_{\text{crit}}(N)} - \frac{1}{T_\Theta} \sim \frac{1}{\sqrt{N}} + \frac{1}{2N}, \tag{3.7}$$

where $T_{\text{crit}}(N)$ is the critical temperature of a solution of chains of finite length N and $T_\Theta = \lim_{N\rightarrow\infty} T_{\text{crit}}(N)$ is the collapse transition temperature. In this case, field theory [28, 145] predicts a multiplicative logarithmic correction of the form $T_{\text{crit}}(N) - T_\Theta \sim N^{-1/2}[\ln N]^{-3/11}$.

Logarithmic corrections to the mean-field theory of single chains are known, for example, for the finite-chain Boyle temperature $T_B(N)$, where the second virial coefficient vanishes. The scaling of the deviation of $T_B(N)$ from T_Θ reads [28]:

$$T_B(N) - T_\Theta \sim \frac{1}{\sqrt{N}(\ln N)^{7/11}}. \tag{3.8}$$

The authors of [130] claim that, for their data obtained from simulations with the FENE bond potential, this expression can also be used as a fit ansatz for $T_c(N) - T_\Theta$. However, also the mean-field-motivated fit without explicit logarithmic corrections,

$$T_c(N) - T_\Theta = \frac{a_1}{\sqrt{N}} + \frac{a_2}{N}, \tag{3.9}$$

has been found to be consistent with the off-lattice data [130], and also with the results obtained applying the bond-fluctuation model of single chains with up to 512 mono-

mers [127, 128]. Up to corrections of order $N^{-3/2}$, Eq. (3.9) is equivalent to

$$\frac{1}{T_c(N)} - \frac{1}{T_\Theta} = \frac{\tilde{a}_1}{\sqrt{N}} + \frac{\tilde{a}_2}{N}, \tag{3.10}$$

which was found to be consistent with numerical data obtained in grand-canonical analyses of lattice homopolymers and the bond-fluctuation model [62, 148, 150].

As said, the situation remains diffuse as there is still no striking evidence for the predicted logarithmic corrections (i.e., for the field-theoretical tricritical interpretation of the Θ point) from experimental or numerical data. Using the data from independent long-chain nPERMss [59, 159] chain-growth simulations (sc: $N_{\max} = 32\,000$, fcc: $N_{\max} = 4\,000$) in the vicinity of the collapse transition, I have performed a scaling analysis of the N-dependent collapse transition temperatures $T_c(N)$, identified as the collapse peak temperatures of the individual specific-heat curves, and estimated from it the $N \to \infty$ limit T_Θ. For the single-chain system, field theory [28, 145] predicts the specific heat to scale at the Θ point like $C_V(T = T_\Theta)/N \sim (\ln N)^{3/11}$. Short-chain simulations [155] did not reveal a logarithmic behavior at all, whereas for long chains a scaling closer to $\ln N$ was read off [29]. The situation is similar for structural quantities such as the end-to-end distance and the gyration radius.

Figure 3.16 shows the data points of the inverse collapse temperature T_c^{-1} from the simulations on the sc (left scale) and on the fcc lattice (right scale), plotted against $N^{-1/2}$ (same data as in Fig. 3.15). Error bars for the individual data points in Fig. 3.16 were obtained by jackknife error estimation [172, 173] from several independent simulation runs. Also shown are respective fits according to the ansatz (3.10). Optimal fit parameters using
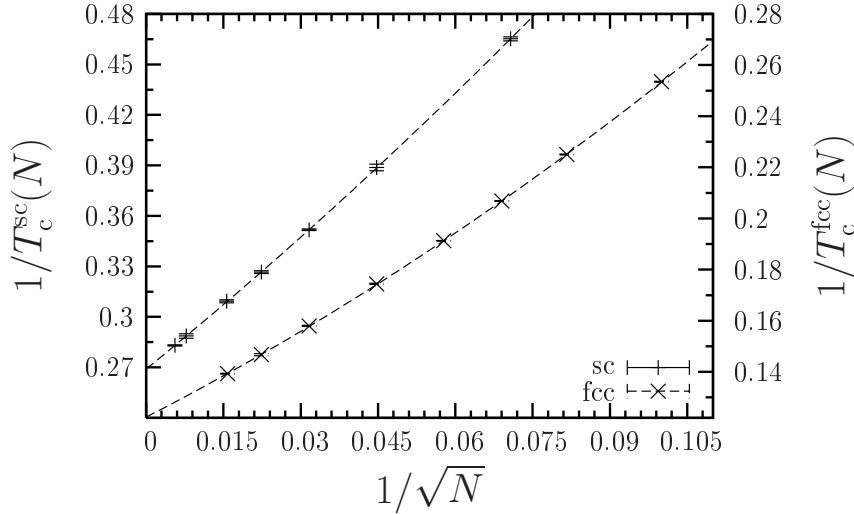
Figure 3.16: Inverse collapse temperatures for several chain lengths on sc ($N \leq 32\,000$) and fcc lattices ($N \leq 4\,000$) (same data as in Fig. 3.15). Dashed lines are fits according to Eq. (3.10).

the data in the intervals $200 \leq N \leq 32\,000$ (sc) and $100 \leq N \leq 4\,000$ (fcc) were found to be

$$T_{\Theta}^{\mathrm{sc}} = 3.717 \pm 0.007\,,$$

$\tilde{a}_1 \approx 2.5$, and $\tilde{a}_2 \approx 8.0$ (sc) and

$$T_{\Theta}^{\mathrm{fcc}} = 8.18 \pm 0.02\,, \tag{3.11}$$

$\tilde{a}_1 \approx 1.0$, and $\tilde{a}_2 \approx 5.5$ (fcc). In addition, I investigated also other fit functions motivated by field theory and mean-field-like approaches, corresponding to Eqs. (3.7)–(3.10), each of which also with different fit ranges. These results are listed in Tables 3.2 and 3.3, respectively. In order to decide which of the fits is consistent with my data, the χ^2 test is used. Depending

sc-lattice	T_{Θ}	a, resp. a_1, a_2	N	χ^2/d.o.f.	d.o.f
$T_c(N) - T_{\Theta} = \frac{a}{\sqrt{N}}$					
	3.6671 ± 0.0051	-26.0	$500 - 32\,000$	12.7	4
	3.6741 ± 0.0053	-26.5	$1000 - 32\,000$	6.61	3
	3.6898 ± 0.0065	-28.3	$2000 - 32\,000$	1.39	2
$T_c(N) - T_{\Theta} = \frac{a}{\sqrt{N}} (\ln N)^{7/11}$					
	3.7353 ± 0.0056	-8.24	$500 - 32\,000$	0.57	4
	3.7370 ± 0.0057	-8.27	$1000 - 32\,000$	0.21	3
	3.7398 ± 0.0072	-8.36	$2000 - 32\,000$	0.10	2
$T_c(N) - T_{\Theta} = \frac{a}{\sqrt{N} (\ln N)^{7/11}}$					
	3.6164 ± 0.0048	-83.0	$500 - 32\,000$	39.5	4
	3.6287 ± 0.0049	-86.0	$1000 - 32\,000$	20.7	3
	3.6531 ± 0.0059	-97.6	$2000 - 32\,000$	4.14	2
$\frac{1}{T_c(N)} - \frac{1}{T_{\Theta}} = a \left(\frac{1}{\sqrt{N}} + \frac{1}{2N} \right)$					
	3.7255 ± 0.0060	2.6	$500 - 32\,000$	0.28	4
	3.7245 ± 0.0061	2.6	$1000 - 32\,000$	0.11	3
	3.7221 ± 0.0076	2.6	$2000 - 32\,000$	0.03	2
$\frac{1}{T_c(N)} - \frac{1}{T_{\Theta}} = \frac{a_1}{\sqrt{N}} + \frac{a_2}{2N}$					
	3.7173 ± 0.0071	$2.5, 8.0$	$200 - 32\,000$	0.05	4
	3.7173 ± 0.0104	$2.5, 8.0$	$500 - 32\,000$	0.07	3
	3.7194 ± 0.0131	$2.5, 6.3$	$1000 - 32\,000$	0.07	2
$T_c(N) - T_{\Theta} = \frac{a_1}{\sqrt{N}} + \frac{a_2}{N}$					
	3.7030 ± 0.0059	$-32, 135$	$200 - 32\,000$	0.53	4
	3.7090 ± 0.0078	$-32, 161$	$500 - 32\,000$	0.25	3
	3.7140 ± 0.0104	$-33, 186$	$1000 - 32\,000$	0.12	2

Table 3.2: Values of T_{Θ} on the sc lattice from different fits and their χ^2 tests with several degrees of freedom d_{f}.

fcc-lattice	T_Θ	a, resp. a_1, a_2	N	$\chi^2/$d.o.f.	d.o.f
$T_c(N) - T_\Theta = \frac{a}{\sqrt{N}}$					
	7.2673 ± 0.0052	-34.1	$100 - 4000$	1000	6
	7.5760 ± 0.0070	-39.4	$150 - 4000$	418	5
	7.7101 ± 0.0080	-42.0	$210 - 4000$	213	4
	7.8445 ± 0.0096	-45.5	$300 - 4000$	67.8	3
	7.9561 ± 0.0013	-50.0	$500 - 4000$	13.6	2
$T_c(N) - T_\Theta = \frac{a}{\sqrt{N}} (\ln N)^{7/11}$					
	7.9218 ± 0.0064	-15.2	$100 - 4000$	200	6
	8.0757 ± 0.0083	-16.1	$150 - 4000$	69.2	5
	8.1356 ± 0.0093	-16.5	$210 - 4000$	32.7	4
	8.1953 ± 0.0110	-17.0	$300 - 4000$	9.45	3
	8.2468 ± 0.0149	-17.6	$500 - 4000$	1.00	2
$T_c(N) - T_\Theta = \frac{a}{\sqrt{N} (\ln N)^{7/11}}$					
	6.8260 ± 0.0045	-79.5	$100 - 4000$	2000	6
	7.2258 ± 0.0062	-99.3	$150 - 4000$	1000	5
	7.4166 ± 0.0072	-110.2	$210 - 4000$	500	4
	7.6051 ± 0.0087	-125.7	$300 - 4000$	164	3
	7.7544 ± 0.0011	-146.3	$500 - 4000$	38.1	2
$\frac{1}{T_c(N)} - \frac{1}{T_\Theta} = a \left(\frac{1}{\sqrt{N}} + \frac{1}{2N} \right)$					
	8.5434 ± 0.0110	1.27	$100 - 4000$	111	6
	8.4208 ± 0.0120	1.23	$150 - 4000$	29.6	5
	8.3821 ± 0.0125	1.22	$210 - 4000$	13.5	4
	8.3369 ± 0.0141	1.20	$300 - 4000$	3.00	3
	8.3048 ± 0.0187	1.18	$500 - 4000$	1.15	2
$\frac{1}{T_c(N)} - \frac{1}{T_\Theta} = \frac{a_1}{\sqrt{N}} + \frac{a_2}{2N}$					
	8.1778 ± 0.0169	$1.04, 5.49$	$100 - 4000$	0.81	5
	8.1987 ± 0.0211	$1.06, 5.04$	$150 - 4000$	0.32	4
	8.2107 ± 0.0259	$1.07, 4.75$	$210 - 4000$	0.21	3
	8.2288 ± 0.0386	$1.09, 4.18$	$300 - 4000$	0.11	2
$T_c(N) - T_\Theta = \frac{a_1}{\sqrt{N}} + \frac{a_2}{N}$					
	8.0374 ± 0.0110	$-58.9, 360$	$100 - 4000$	13.1	5
	8.0876 ± 0.0133	$-61.5, 414$	$150 - 4000$	4.71	4
	8.1219 ± 0.0163	$-63.5, 461$	$210 - 4000$	1.81	3
	8.1640 ± 0.0244	$-66.5, 541$	$300 - 4000$	0.04	2

Table 3.3: Values of T_Θ on the fcc lattice using the same methodology as in Table 3.2 for the sc lattice.

on the sizes of the data sets entering into the analyses and the number of fit parameters, there are 2 to 6 degrees of freedom d_f. I make the typical assumption that deviations of the fit from the used data set are significant, if $\chi^2 > \chi^2_{d_f;0.05}$, i.e., if χ^2 lies in the 5% tail of the $p_{d_f}(\chi^2)$ distribution of χ^2 values. In this case, with 95% probability the correlation between data and fit function are not random. The thresholds for the different degrees of freedom lie between $\chi^2_{2;0.05}/d_f = 3.0$ and $\chi^2_{6;0.05}/d_f = 2.1$. The calculated χ^2 values associated with the data sets and the fit functions used are also listed in Tables 3.2 and 3.3.

From the results in Table 3.2 for the polymers on the sc lattice, one finds that the two-parameter mean-field-like fits (3.9) and (3.10) as well as the single-parameter fit according to (3.7) are consistent with my data. The estimated sc Θ temperatures from these good fits are in perfect agreement with the most reliable estimates from literature. Surprisingly poor, on the other hand, is the goodness of the fit against the logarithmic scaling (3.8). Even more astonishing is, however, the good coincidence with a logarithmic fit of the "wrong" form $N^{-1/2}(\ln N)^{7/11}$ with the data. Summarizing these results, if logarithmic corrections as predicted by tricritical field theory are present at all, even chain lengths $N = 32\,000$ on an sc lattice are too small to observe deviations from the mean-field picture. At least, the goodness of the logarithmic fit with the "wrong" exponent $+7/11$ could lead to the speculative conclusion that for $N \leq 32\,000$ multiplicative and additive logarithmic corrections to scaling are hidden in the fit parameters of the "mean-field-like fits". The subleading additive corrections are expected to be of the form $\ln(\ln N)/\ln^2 N$.[9] They thus not only disappear very slowly – they are also found to be even of the same size as the leading scaling behavior, which makes it extremely unlikely to observe the logarithmic corrections in computational studies at all [146].

The corresponding fcc results are listed in Table 3.3. In this case, only the fit function (3.10) (and its goodness) is independent of the data sets used and, therefore, consistent with the data obtained for all chain lengths. However, considering the noticeable improvement of the goodness for the fits to Eqs. (3.9) and (3.7) and the "wrong" $N^{-1/2}(\ln N)^{7/11}$ form by excluding the very short chains from the data sets leads to the conclusion, that even chains with $N = 4\,000$ monomers on the fcc lattice are also too short to find evidence for the logarithmic corrections to mean-field scaling. The best estimates for the fcc Θ temperature agree nicely with other results presented earlier [154, 156].

3.5 Summary

In this part of the work, I studied homopolymers on the simple cubic (sc) and the face centered cubic (fcc) lattice. In particular, I studied conformational transitions of these systems, namely the collapse (or coil–globule transition) at the so-called Θ-temperature

---

[9]Similar additive logarithmic scaling is also known, for example, from studies of the two-dimensional XY spin model [174].

and the freezing transition at very low temperatures, i.e., well below the Θ-temperature. A question of particular interest deals with the coincidence of these transitions or, in other words, with the instability of intermediate phases, in the thermodynamic limit, as found for colloidal and polymeric systems with short range interaction [63, 127, 167].

Before studying the thermodynamic behavior of the polymer systems, I showed in a preceding test that the used chain-growth algorithms are in practice able to find ground states of the system up to relatively large system sizes ($N \lesssim 250$), which is essential for the aimed studies but by itself a quite hard task that should not be underestimated [26]. Looking then at the low temperature peaks in the specific heat, considering them as indicators of structural activity, the first thing one notes on the sc lattice is, that there seems to be no regularity at all. It becomes then clear, that the general behavior of the finite size freezing temperature is strongly superposed by a systematic pattern due to lattice effects. Due to the high precision of my simulations, it was possible to unravel and to explain this pattern. It turned out, that the freezing temperature fluctuates between almost fix boundaries in a periodic manner. In particular, I found "magic" lengths [10] where the ground states fit into compact cuboid shapes. For these lengths, there exists an energy gap between the ground state and the first exited one, causing a first-order like pseudotransition. For polymers on the fcc lattice, the situation becomes more complex. Nevertheless, polymers behave similar on both lattices with respect to the general behavior of the freezing transition.

To determine the deviations of the finite size collapse transition temperature from the infinite length Θ temperature, I simulated polymers with lengths up to $N = 4000$ monomers for the fcc lattice and $N = 32\,000$ monomers for the sc lattice, respectively. This deviation scales in the leading order as $T_{\mathrm{c}}(N) - T_{\Theta} \sim 1/\sqrt{N}$ with the system size N. As I simulate in the upper critical dimension $d_{\mathrm{c}} = 3$, there should be corrections to this scaling. Hence, I fitted my data against various fit functions motivated by field theory and mean-field-like approaches. It turned out that even these apparently large systems are still to short to uniquely identify some type of correction. Anyhow, my estimates for the infinite length Θ temperature agree very well with the most precise estimates from the literature and confirm, to my best knowledge, the only experimental value existing so far for the fcc lattice.

Concerning the question of the stability of intermediate phases, it can be concluded from my results, that both transitions, the collapse and the freezing remain well separated also in the extrapolation towards the thermodynamic limit. This can be explained by a further stable "solid" pseudophase due to the very short attractive interaction in the model. For publications of parts of this chapter, see [30, 175].

---

[10]This notation is indeed borrowed from field of particle clusters, where it indicates particle numbers, for which compact (icosahedral) conformations can be formed [76].

Chapter 4

Tubelike Flexible Polymers

In the previous part of my work I concentrated on the global structure formation, i.e., on the collapse and crystallization for comparatively large polymers using a very simple lattice model. A further fundamental issue in polymer research is resolving the underlying secondary structure segments as the functionality of these macromolecules, e.g., biopolymers, strongly depends on the formation of stable ground-state conformations with specific substructures. Experimentally, the identification of these substructures is performed, for example, using single-molecule microscopy techniques, X-ray analyses of polymer crystals, or NMR for polymers in solution, methods which identify structural details of *specific* molecules. As these techniques are, unfortunately, relatively costly and can hardly be generalized in a systematic manner, the structural behavior of polymers and its modeling got into the focus of computer simulations, too.

One central question is of course, what degree of abstraction (coarse-graining) is reasonable, preserving the highest possible generality, to treat certain features of real (bio)polymers or, the other way around, what features one can reliably study with a certain degree of abstraction. As shown before, one may, for example, understand the well-known coil-globule transition by studying simplest one-dimensional models, but neither are these models, nor simple off-lattice generalizations of them, appropriate to develop a classification scheme of distinct secondary structures. In other words, questions about the formation of secondary structures of proteins will generally not be answered satisfactorily. Of course, there are studies on the formation of secondary structures using linelike models. I will refer to and comment them shortly in the first section of this chapter (4.1, "Related Studies, Alternative Approaches") and give also short comments on other recent, related studies. Certainly, the other extreme would be to tackle the problem using all-atom simulations, which indeed led to a huge amount of amazing results so far [87, 93, 94], but, anyhow, suffers from the same lack of generalizability as mentioned experimental techniques as these simulations deal with specific molecules.
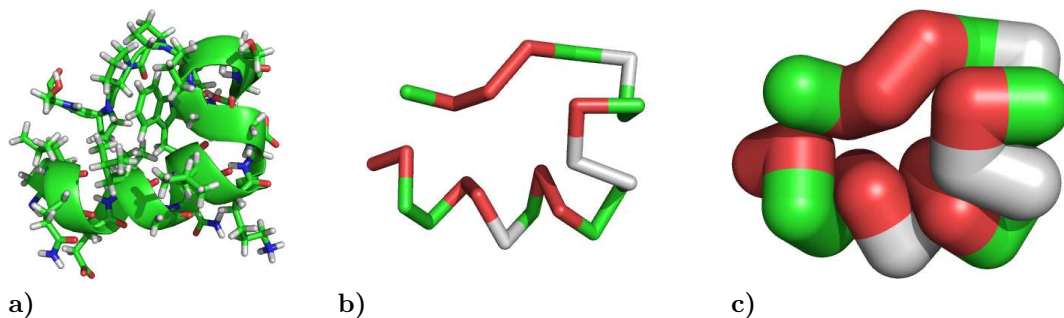
Figure 4.1: Visulaization of the macromolecule with Protein Data Bank (PDB) code 1RIJ [176] in three different models. **a** All-atom representation with usual secondary structure marking. **b** Representation of the backbone (i.e., the C_α atoms) in a linelike AB model. **c** Same as before, but in the tube model.

I will therefore try to approach this problem in this part of my work using some kind of, in a sense, "intermediate" model, which I introduce in Sec. 4.2.1 ("Model and Simulational Methods"). It is derived from a line-like model but steric influences, for example of monomeric side-chains in real biopolymers, will be effectively introduced by a geometric thickness constraint, which enlarge the "line" to a "tube" without taking into account further microscopical details [78, 80, 177]. (See Fig. 4.1 for visualisation of the mentioned models exemplified by an experimentally obtained conformation of a real macromolecule.) I implement that thickness constraint using the concept of the global radius of curvature of a curve (4.2.2, "The Global Radius of Curvature"), an elegant mathematical ansatz arisen in the context of knot theory, which is proven to provide a concise characterization of the thickness of a curve [178]. Section 4.2.3 ("The Tube Thickness") dedicates to that relation to the thickness of the polymer tube.

In Sec. 4.3 ("Motivation and Overview") the usage of the tube model will be motivated in more detail and an abstract of the study presented in this chapter is given. I will then in Sec. 4.4 ("Ground State Analysis, $\sigma = 1$") concentrate in very detail on the ground states of the model depending on the thickness constraint at fixed interaction parameters. Based on that, I will emphasize in Sec. 4.5 ("Deeper Analysis and Remarks") special topics of ground-state formation, like the crystallization on regular lattices or the appearance of biological relevant structures varying the interaction parameter. After considering the behavior of the model at temperature $T \to 0$, i.e., the behavior of ground states, in Sec. 4.6 ("Thermodynamic Behavior of Tubelike Homopolymers") the complete phase diagram for short polymers at finite temperatures depending on their thickness will be revealed. The classification of polymer conformations, including biologically relevant structures like the α-helix or β-sheets, which are solely controlled by the intrinsic thickness parameter, becomes then evident. Finally, I will show in Sec. 4.7 ("The Hydrophobic-Polar Tube Model"), by

way of example, results for a prominent and, without thickness contraint, extensively studied heteropolymer and discuss, how the introduction of different types of monomers interacting by different potentials, may influence the general structural behavior of tubelike polymer models. See also [179–181].

4.1 Related Studies, Alternative Approaches

I mentioned in the above introduction, that simple linelike models with pairwise interactions are not appropriate to study secondary-structure formation. It is generally true, that modeling volume exclusion by means of pure pairwise interaction potentials without taking into account further details is not sufficient for that purpose (see, for example, [79]).

But of course are there interesting studies on this topic. Aside from early attempts to study helix formation with simple lattice models, resulting in the definition of the so called "lattice helices" of different types [182], off-lattice models have been used which were, however, to some extent dedicated or less general. Some time ago, for example, it has been shown by Noguchi and Yoshikawa, that introducing a bending potential to the single linelike homopolymer chain, i.e., considering stiff polymer chains, can lead to the formation of toroidal structures, i.e., helices, in the crystalline or "frozen" conformational phase [183]. In the same year, Kemp and Chen reported in a very interesting letter on the formation of very stable helical conformations in a wormlike polymer chain with pairwise volume exclusion. They found different helical phases at different temperatures, including perfect helical ground states. Anyhow, the authors themselves point out that only a strong directional, anisotropic pairwise interaction with fixed bond angles of $\pi/3$ led to these impressive results and, besides further variable parameters in the potential, that this directional interaction, which is, for example, caused by hydrogen bonds, is obviously essential [184]. Considering, for example, also the work by Rapaport [185] on helix formation using torsional potentials including information on the helical ground state, it becomes clear, that helices can be stabilized rather easily with suitable potentials, as stated also by Sabeur et al. [186]. In their dynamical study, helical structures appear as, relatively stable, intermediate conformations during the collapse process of an also linelike model with pairwise interaction between beads connected by harmonic springs. It should be noted, that the so far mentioned studies dealt "just" with helix formation, other biological important secondary structures, like sheets, do not seem to occur as relevant conformations in these models.

Helical tubes have been in the focus of recent works by Snir and Kamien, especially the computation of compact shapes of helices, complementing the original ideas of Maritan et al. [187–189]. A main result in these works is the computation of an optimal pitch to radius ratio c^* for most compact α-helices, which I will use as a reference structure later. Another interesting statement there, which will be confirmed by my work, is that the helix is only optimal in the sense of minimized excluded volume, up to a certain tube length. At longer

tube lengths, the helix gives way to more complex tube conformations [189]. Introducing then a bending rigidity, Snir and Kamien study also the competition between elongated tubes and helices. With a comparable ansatz, using a hard-sphere solvent and calculating the solvation free energy F_{sol}, Hansen-Goos et al. confirm and extend the results of the above mentioned study. Depending on the solvent properties, they present for example regions of different protein structures which minimize F_{sol} [190].

In a fundamental work by Banavar and Maritan [81, 82] considering a square-well potential for the interaction between monomers, it was shown, that different secondary structures may generally emerge by varying tube thickness and interaction radius (see also Sec. 1, "Thick Polymer Models"). A possibility for stabilizing or facilitating the formation of secondary structures is, as briefly mentioned already above, indeed the consideration of hydrogen bonds, i.e., a further attracting interaction, between specific monomers or the integration of further interactions. This was succesfully done for example in work by Hoang et al., Auer et al. or Wolff et al. [191–193], where different classes of secondary structure types could be assigned to different interaction strengths, relative to the hydrogen bond strength. Note, that in the last both works, the cylindrical tube model is applied, where the tube is approximated by real cylinders around the covalent bonds between the C_α monomers and spheres at the position of them [194]. This is different in nature from the model I use here, as cooperative behavior does not play a role and the consideration of hydrogen bonds is therefore necessary for the generation of secondary structures [79, 179].

4.2   Technical Details

4.2.1   Model and Simulational Methods

As said, what I simulate in this part of my work is a model for flexible polymer (initially *homo*polymer) chains consisting of a certain number of (equal) monomers, modeled as off-lattice, pointlike particles. The bond length between consecutive monomers along the chain is fixed to unit length. The whole object is then coated by a tube with certain thickness. See for a visualisation for example Fig. 4.1 c.

Every monomer interacts pairwisely with every other monomer in the chain, except for the neighbouring ones along the chain. The interaction potential consists of an attractive van-der-Waals-like force and strong repulsive forces at short distances. In other words, I use the Lennard-Jones potential for the pairwise interaction between two monomers i and j:

$$V_{\mathrm{LJ}}(r_{ij}) = 4\epsilon \left(\left(\frac{\sigma}{r_{ij}} \right)^{12} - \left(\frac{\sigma}{r_{ij}} \right)^{6} \right) , \qquad (4.1)$$

with $\epsilon = 1$. Note that $V_{\mathrm{LJ}}(\sigma) = 0$ and $\sigma = 2^{-1/6}\, r_{ij}^{\mathrm{opt}}$, where r_{ij}^{opt} is the minimum position of the potential. The thickness of the tube is implemented considering a three body potential resulting in cooperative effects capturing the steric constraint imposed by the tube [79]. This

concept will be described in detail in the following Sects. 4.2.2 ("The Global Radius of Curvature") and 4.2.3 ("The Tube Thickness").

I study the model by means of advanced Monte Carlo computer simulations and numerical methods. For ground-state problems (Secs. 4.4, "Ground State Analysis, $\sigma = 1$" and 4.5, "Deeper Analysis and Remarks"), one may use for example the multicanonical method [115, 116, 121], the efficient random walk algorithm introduced by Wang and Landau ("Wang–Landau algorithm") [119], parallel tempering [107, 108] simulations or the energy-landscape paving procedure [135]. All these methods guarantee, if appropriately applied, that one does not stick in local energy minima, possibly "far away" from the ground state. Furthermore, for the purpose of ground-state search, they work, in principle, nearly equally well as one does not have, for example, to care about the quality of the sampling of the whole configuration space. In fact, the performance of the simulation depends mainly on the simulational parameters used, like temperature sets or energetic bin sizes, and, if necessary, updating procedures of them. Additionally, I use standard deterministic conjugate gradient methods to refine stochastically obtained results [139].

For the methodologically more challenging task of studying the thermodynamic behavior (Sects. 4.6, "Thermodynamic Behavior of Tubelike Homopolymers" and 4.7, "The Hydrophobic-Polar Tube Model"), I use generalized-ensemble methods [115, 116, 119] to estimate the density of states. I employ the recursive method of Wang and Landau [119] within a reasonable, predetermined energetic interval, with the control parameter f initialized and subsequently decreased to $f - 1 < 10^{-7}$ as described in [120]. Since detailed balance is violated, as described in Sec. 2.2.4 ("Random Walk Algorithm by Wang and Landau"), I then freeze the weights and perform multicanonical production runs for validation.[1]

Furthermore, I checked my results for reliability also against data [195] obtained by parallel tempering simulations [107, 108, 112] for selected parameter sets, as well as against data [196] from a multicanonical study presented in [68]. For such a comparison, see Fig. 4.29 (p. 93). The simulations of different polymer lengths and thickness constraint values were carried out separately to avoid correlations and statistical imbalances. For a general description of the mentioned methods I refer to Sec. 2.2 ("Techniques for Off-Lattice Simulations").

4.2.2   The Global Radius of Curvature

To implement the self-avoiding tube, I use the concept of the global radius of curvature. The radius of curvature of three points, i.e., the radius of the circumcircle of three monomers i, j and k located at positions $\mathbf{x}_i$, $\mathbf{x}_j$ and $\mathbf{x}_k$, can be calculated as

$$r_c(\mathbf{x}_i, \mathbf{x}_j, \mathbf{x}_k) = \frac{r_{ij}\, r_{ik}\, r_{jk}}{4A_\triangle(\mathbf{x}_i, \mathbf{x}_j, \mathbf{x}_k)}\,, \tag{4.2}$$

---

[1]Actually, this was done for a reasonable number of simulations. As the preliminary estimates for the density of states obtained by the Wang–Landau method were quite good, the final production run was not carried out for every parameter set.
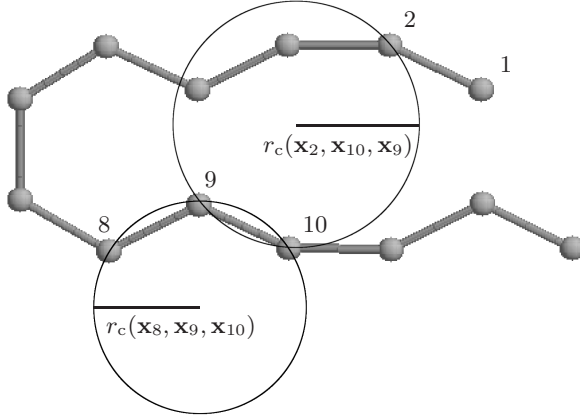
Figure 4.2: Two examples of circumcircles around three monomers and the corresponding radii of curvature. The small circle corresponds to the radius of curvature of three consecutive monomers, i.e., to the local radius of curvature r_{lc} of the monomers $(i, i+1, i+2) = (8, 9, 10)$. The bigger circle corresponds to the radius of curvature r_{c} of the monomers $(i, j, k) = (2, 10, 9)$.

where $A_\Delta(\mathbf{x}_i, \mathbf{x}_j, \mathbf{x}_k)$ is the area of the triangle corresponding to the three points and r_{xy} denotes the distance between two points. Figure 4.2 shows for illustration two of such circumradii in a specific polymer conformation. Note, that the value of the radius depends on three monomers, which causes a three point interaction between monomers, in contrast to a two-point interaction one may use in hard sphere models to incorporate volume exclusion effects.

An interesting subclass of radii of curvature in this connection are local radii of curvature $r_{\text{lc}}(\mathbf{x}_i, \mathbf{x}_{(i+1)}, \mathbf{x}_{(i+2)})$, i.e., the radii of curvature of three consecutive monomers. An example can be found in Fig. 4.2 as well. Local radii of curvature are indeed related to the bending angles ϑ between two consecutive bonds connecting these three monomers: $\vartheta = 1/r_{\text{lc}} + \mathcal{O}(r_{\text{lc}}^{-2})$ for small ϑ. Besides this relation, local radii are of interest for technical reasons (see below), they can help, for example, to determine the most compact exact helix conformation using them to build an order parameter for the transition between, in its main direction, elongated helices and compressed and, in the perpendicular direction, widened ones. For more details, see the discussion in Sec. 4.4.2 ("Preliminary Remarks, Overview") or [187, 189].

The global radius of curvature is then defined as the minimal radius of all circumcircles r_{c} of any three monomers in the chain:

$$r_{\text{gc}}(\mathbf{X}) := \min\{r_{\text{c}}(\mathbf{x}_i, \mathbf{x}_j, \mathbf{x}_k), \, \forall \, 1 \leq i < j < k \leq N\}. \tag{4.3}$$

As a technical remark: Really calculating all radii of curvature explicitly to obtain the global radius of curvature of a given conformations is obviously needless and would be very expensive in terms of computing time as the number of radii grows with the third power of the monomer number ($\mathcal{O}(N^3)$). Excluding a huge number of a priori too large radii with much less effort, using previously calculated local radii as estimates or bounds for the global radius of curvature, sorting then segments of the triangles with respect to one coordinate and finally eliminating evidently to large segments, the calculation can be done, in practice almost always, nearly in $\mathcal{O}(n \log n)$ steps (eventually plus some marginal higher order terms) [177].
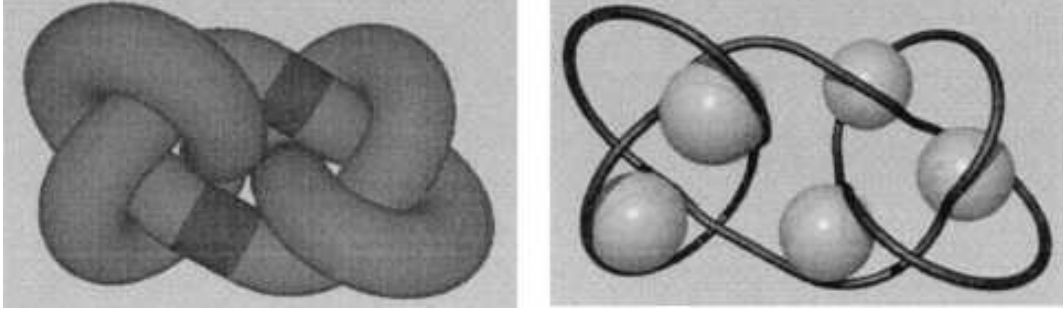
Figure 4.3: Illustration of the relation between the thickness of a curve and the global radius of curvature. *Left*: The tube interpretation. The radius of the tube is the global radius of curvature of the curve. *Right*: The sphere interpretation. The radius of the spheres equals also the global radius of curvature. Picture from [178]. Copyright (1999) National Academy of Sciences, U.S.A.

4.2.3 The Tube Thickness

Figure 4.3 illustrates the relation between the above introduced concept and the generic thickness of a tube. At the left side, the curve is shown with a smooth, non-intersecting tube of constant radius centered on the it, the natural idea of a tubelike curve. The right subfigure shows the same curve with spheres of the same radius intersecting the curve at at least three point (shown is a continuous curve, but the concept can be applied to discrete curves as well [178]). Bigger spheres, provided a rigid curve and hard speres, could not be placed at these positions, spheres with a radius less than the tube radius would not intersect the curve at three or more points. It has been shown, that both radii, the tube radius and the radius of the shown spheres are equal to the global radius of curvature, i.e., that the global radius of curvature is proven to be a concise characterization of the thickness of a curve [178].

Hence, given a polymer conformation $\mathbf{X} = (\mathbf{x}_1, \ldots, \mathbf{x}_N)$ with N monomers, I define as its "natural thickness" (diameter) $d(\mathbf{X})$ twice the global radius of curvature $r_{\mathrm{gc}}(\mathbf{X})$,

$$d(\mathbf{X}) = 2r_{\mathrm{gc}}(\mathbf{X}) \,. \tag{4.4}$$

The other way around, considering a tube conformation $\mathbf{X}^*$ with some diameter $d(\mathbf{X}^*)$, one can of course find conformations $\mathbf{X}$ with $2r_{\mathrm{gc}}(\mathbf{X}) > d(\mathbf{X}^*)$ or even $2r_{\mathrm{gc}}(\mathbf{X}) \gg d(\mathbf{X}^*)$ by deforming $\mathbf{X}^*$. It is, in a sense, natural, that all these conformations should account for the partition sum of tube $\mathbf{X}^*$, i.e., when simulating tube models, the conformational space should be restricted by some constraint on the global radius of curvature, which I will call ρ from here on, such that all tube conformations with $d(\mathbf{X}^*) < 2\rho$ are not allowed. Applied to discrete homopolymers on can say that, given a such a thickness constraint ρ, one can construct an excluded volume depending on ρ around two monomers, which is "forbidden" for

any other monomer. A polymer conformation then complies with the thickness constraint if any other monomer resides outside these circles. This view is nicely illustrated and amplified in [177]. Since the energy of the polymer is given by $E(\mathbf{X}) = \sum_{i,j>i+1} V_{\mathrm{LJ}}(r_{ij})$, the partition function reads in this case:

$$Z_\rho = \int \mathcal{D}X \Theta(r_{\mathrm{gc}}(\mathbf{X}) - \rho) \, \mathrm{e}^{-\beta \, E(\mathbf{X})} \,, \tag{4.5}$$

where $\Theta(z)$ is the Heaviside step-function and $\beta = (k_{\mathrm{B}}T)^{-1}$ is the inverse thermal energy. The constraint ρ will be used as the thickness parameter in all simulations done in this work, the Boltzmann constant k_{B} is set to $k_{\mathrm{B}} = 1$.

Please note that the model may behave different by setting $d = 2\rho$, i.e. by using the natural thickness as the simulation parameter. A conformation then only contributes to the partition sum, iff it actually has the natural thickness ρ. $\Theta(r_{\mathrm{gc}}(\mathbf{X}) - \rho)$ is in that case replaced by $\delta(r_{\mathrm{gc}}(\mathbf{X}) - \rho)$ in the partition function [177].

4.3   Motivation and Overview

What precisely motivates one to simulate homopolymer models with a geometric constraint "thickness" at all and especially in the way described above?

Even if the most polymer models are general models for classes of polymers, what one should always keep in mind is the most prominent subclass of polymers, namely biopolymers or proteins. Definitely, polymers in biology are not thin strings. Amino acids, and thus proteins do have side chains, which could not overlap and hence induce steric contraints. It might be therefore useful, to introduce some constraint that could mimic this three dimensional volume exclusion in a cooperative manner. The tube model using the concept of the global radius of curvature is indeed appropriate, whilst pure pairwise volume exclusion is not, as indicated in Sec. 4.1 ("Related Studies, Alternative Approaches") and in detail discussed in [79]. Furthermore, and this is the main reason, it has been adumbrated, that just introducing the thickness of a curve could lead to secondary structure formation [78, 81].

A comprehensive study of the influence of the tube thickness over the whole parameter range on ground-state formation as well as for the thermodynamic behavior is still missing, to the best of my knowledge, and will therefore be the subject of this chapter.[2] As some kind of abstract, I will here give an outlook on the main results I present in the following, exemplified by the polymer with $N = 9$ monomers.

---

[2]By the way, as a technical remark, the introduction of a geometric constraint might implicate some technical advantages for finding minimal energy conformations or resolving thermodynamic properties by providing a tool to restrict the conformational space of one-dimensional models, which is in general highly beneficial in broad histogram simulations. See also the corresponding remark in Sec. 4.7 ("The Hydrophobic-Polar Tube Model").
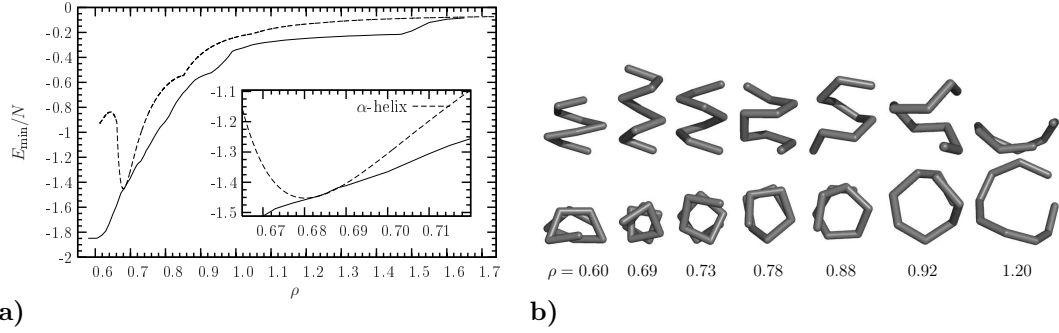
Figure 4.4: **a** Ground-state energy per monomer $E_{\min}/N$ of tubelike polymers with nine monomers as a function of the global radius of curvature constraint ρ (*solid line*). For comparison, also the energy curve of the perfect α-helix is plotted (*dashed line*). The *inset* shows that for a small interval around $\rho \approx 0.686$, the ground-state structure is perfectly α-helical. **b** Side and top views of putative ground-state conformations for various exemplified values of ρ. For the purpose of clarity, the conformations are not shown with their proper thickness.

Figure 4.4 shows the energy of ground-state conformations of tubelike polymers as a function of the thickness parameter ρ. Also shown are visualizations of selected conformations for particular values of ρ. The ground-state energy per monomer for the linelike 9mer, i.e., the polymer which is not influenced by the thickness at all ($0 \leq \rho \lesssim 0.6$) is $E_{\min}/N = -1.85$. Increasing the thickness slightly such that the thickness constraint becomes important and starts to affect the structure formation, the first interesting structure formation, namely the helix formation can be observed. Furthermore, optimal space-filling helical symmetry [187, 188] is reached when approaching $\rho_\alpha \approx 0.68$ (see inset of Fig. 4.4), where the ground-state conformation takes the perfect α-helical shape. In that conformation, all torsional angles are identical (near $41.6°$) and also all local radii are constant; the number of monomers per winding is 3.6. Note that for proteins, where the effective distance between two C^α atoms is about $3.8\,\text{Å}$, ρ_α in the units used here corresponds indeed to a pitch of about $5.4\,\text{Å}$ as known from α-helices of proteins. Thus, as a first observation on will see, that an α-helix is a natural geometric shape for tubelike polymers. For larger values of ρ, helices unwind, i.e., the pitch gets larger and the number of monomers per winding increases. In the interval $\rho_\alpha \leq \rho \lesssim 0.92$, fluctuation peaks of the derivative $\triangle E_{\min}/\triangle \rho$ indicate that there are also stable helical conformations in the vicinity of $\rho \approx 0.73$ (winding number ≈ 4.5) and $\rho \approx 0.78$ (winding number ≈ 5.0). Near $\rho \approx 0.92$, the final helical state has been reached. The thickness has increased in such a way that the most compact conformation is a helix with a single winding. After that, a topological change occurs and the ground-state conformations are getting flatter. The helix finally opens up and planar conformations with similarities to β-hairpins become dominant. Of coure, the system size plays some role,
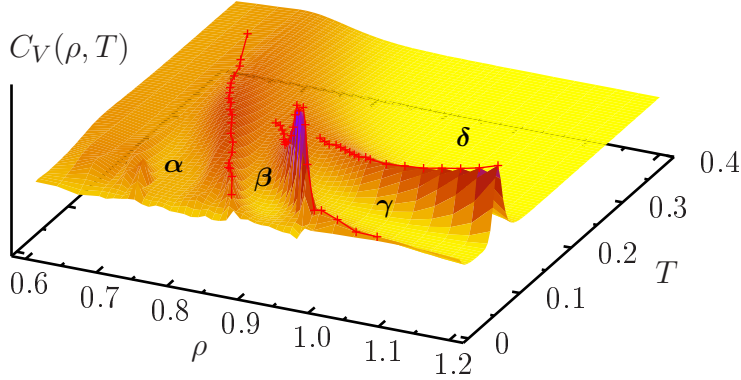
Figure 4.5: Structural pseudophase diagram of thermodynamically relevant tube polymer conformations as a function of the thickness constraint ρ and temperature T for polymers with $N = 9$ monomers. The height of the peaks corresponds to the value of the specific heat. Helical or helix-like conformations dominate in region α, sheets in region β, rings in region γ, and stiff rods in pseudophase δ. The general structure of the phase diagram will remain unchanged also for longer polymers.

even if the dominant behavior will be the same for all (short) chains. For some reason, the 9mer shows the most pronounced helical behavior, whereas one will see the formation of flat sheetlike structures more clearly for other system sizes. For thickness values $\rho \approx N/2\pi$, ground-state conformations are almost perfect circles with radius ρ.

After the preparatory study of ground-state properties, the thermodynamic behavior of the tube polymers will be discussed in the following. Based on the peak structure of the specific heat $C_V(\rho, T) = (\langle E^2 \rangle_\rho - \langle E \rangle_\rho^2)/T^2$ as a function of temperature T and thickness constraint ρ, the structure of the conformational ρ-T pseudophase diagram is identified. Figure 4.5 shows this specific-heat landscape for the $N = 9$ homopolymer as obtained from the densities of states for given thickness constraint ρ. The peaks or ridges of the profile indicate conformational activity and thus represent transitions between different conformational pseudophases. Guided by the analyses of the ground-state properties, one identifies four principal pseudophases which will be called α, β, γ and δ. In region α, helical conformations are the most relevant structures. In particular, as shown, the α-helix resides in this pseudophase. Characteristic for the transition from pseudophase α to β is the unwinding of the helical structures which become more planar. Thus, region β is dominated by simple sheetlike structures. For very short chains, the only sheetlike class of conformations is the hairpin. For longer chains, one also finds more complex sheets. A characteristic property of the hairpins is that these are still stabilized by monomer contacts. These break with larger thickness and higher temperature. Entering pseudophase γ, the dominating structures possess ringlike shapes. Finally, region δ is the phase of random coils, which are getting stiffer
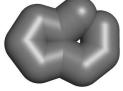
phase	type	views of representative example
α	helix	
β	sheet	
γ	ring	
δ	rod	

Table 4.1: Exemplified conformations being thermodynamically relevant in the respective pseudophases shown in Fig. 4.5, visualized in different representations.

for large thickness and eventually resembling rods. Representative polymer conformations dominating the pseudophases in the regions α to δ are depicted in Table 4.1 in different representations. In the following sections, I will present these results in more detail and also explain the methodology and care about selected problems of special interest.

4.4 Ground State Analysis, $\boldsymbol{\sigma = 1}$

4.4.1 Nomenclature and Methodology

I will characterize and/or identify conformations of course by their total energy $E(\mathbf{X})$, but naturally also by geometrical properties like end to end distance r_{end} or radius of gyration r_{gyr}. However, as this turns out to be not sufficient to distinguish between different conformations satisfactorily, I also take into account local radii of curvature $r_{\text{lc},i} := r_{\text{c}}(\mathbf{x}_i, \mathbf{x}_{i+1}, \mathbf{x}_{i+2})$, which are related to the bending angles between two bonds ϑ via $\vartheta = 1/r_{\text{lc}} + \mathcal{O}(r_{\text{lc}}^{-2})$ for small ϑ, as well as torsion angles $\phi \in (-\pi, \pi]$.

One speaks of a κ_0-conformation, if the chain has a constant local curvature at all monomer positions, i.e., if $r_{\text{lc},i} = r_{\text{lc},j}, \forall i, j$. Analogously, a structure with constant torsion angles is called a τ_0-conformation [197]. For example, a prominent structure with both, κ_0- and τ_0-property, is the perfect α-helix. A conformation is called "closed" if the distance between both ends of the chain, i.e., r_{end}, resides in the close vicinity of the Lennard-Jones minimum, whereas a "symmetric" structure exhibits a symmetry of the torsion angles with respect to the center of the chain (see the following subsection for a detailed description and

remarks). Nice examples for "closed" κ_0 conformations, namely twisted circles of constant curvature (in German, so-called "windschiefe Kreise" [198]), are discussed in [197]. Finally, in "flat" conformations, the backbone has an almost two-dimensional planar structure, where all torsion angles converge to 0, i.e., $\sum_i \phi_{\pi/2}^{(i)} \to 0$, where

$$\phi_{\pi/2} := \min(|\phi|, \pi - |\phi|) \,. \tag{4.6}$$

4.4.2   Preliminary Remarks, Overview

For the comprising study of the ground states of the model, I first set the Lennard-Jones parameter to $\sigma = 1$.[3] In this case, the "natural thickness" of a flexible LJ polymer *without* thickness constraint, $r_{\mathrm{gc}}^{\min}$, i.e., the global radius of curvature of the ground state of that system (cp. Sec. 4.2.3, "The Tube Thickness"), is roughly half the interaction length $r_{ij}^{\min}/2 = 2^{-5/6} \approx 0.56$, which thus sets a reasonable bound for the thickness constraint. Below this value, the thickness constraint does neither influence the ground-state properties nor the thermodynamic behavior at all. See, in this context, Fig. 4.29 (p. 93), where the thermodynamic behavior of an examplified polymer sequence at $\rho = 0.0$ and $\rho = 0.6$ is directly compared. Thus, in the following, only tube polymers with $\rho > r_{\mathrm{gc}}^{\min}$ are considered. Actually, due to the discrete nature of the bead-stick polymer model, I measure a "natural thickness" $\gtrsim 0.59$ for all polymers considered. Data for $\rho < 0.6$ is therefore not shown in the plots in this section. As mentioned before, I carried out simulations for different thickness constraints separately. The bin size of the simulations is $\Delta\rho \leq 0.01$ in the most interesting regions. Specific regions, for example the α-helices, have been studied with bin sizes $\Delta\rho = 0.0005$. Figure 4.6 displays the different thickness values for which ground-state search and thermodynamic analyses have been performed. Overall, more than threehundred ground-state searches and more than thousand flat histogram simulations[4] have been carried out. This number of simulations was necessary to get reliable statistics and to obtain the high coverage of the thickness space, particularly in the low-temperature regime, which is essential for the high-precision results I present.

I compare some of my results with observables for the spacefilling, perfect, most compact (all synonymously used here) α-helix. This helix is defined as the helix $(x, y, z) = (r \sin \phi, r \cos \phi, p\phi/2\pi)$ with a pitch p such that the surface of the tube has a self-contact at the cylinder with radius r and the radius r is minimal under the thickness constraint. In other words, the optimally packed, i.e., spacefilling, helix corresponds to the transition between the two qualitatively different regimes of $p/r > c^*$ and $p/r \ll 1$ [187]. The local radius of curvature can be used to distiguish them. While in the firstmentioned regime, the global radius of curvature is always equal to the local radii, it is stricly lower than the local radii in the latter. The computation of this helix is non-trivial, as the critical ratio c^*

---

[3]I will make this parameter variable for selected problems later.

[4]For every thickness value several independent simulations were done to get reasonable averages and to estimate the standard statistical error.
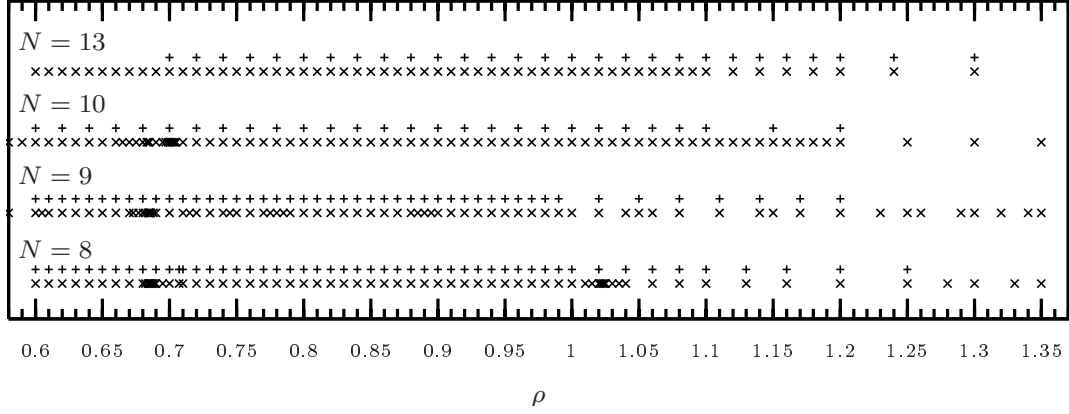
Figure 4.6: Thickness values at which simulations have been performed for different tube lengths. ×-signs mark values for ground-state searches, +-signs mark positions where the thermodynamic behavior was determined by flat histogram sampling. A few simulations have been performed at $\rho > 1.35$, but are not shown.

depends on the discretization level and ranges from $c^* \approx 2$ for $\rho \approx 0.7$ to $c^* = 2.512$ for the continuous case, which is equivalent to $\rho \to \infty$. An interesting and detailed discussion of compact helix formation and the critical ratio c^*, leading of course to the same result, can be found also in [189].

Figure 4.7 shows the energies of the ground states for various chain lengths in dependence of ρ. Additionally, the energy of the corresponding calculated space-filling α-helix described above is shown in comparison. In Fig. 4.8 the corresponding derivatives $dE/d\rho$ are plotted, in order to emphasize regions of structural activity. In these regions, where the derivative exhibits peaks, noticeable qualitative conformational transitions occur.

To describe and understand the different classes of ground-state conformations, I present in Figs. 4.9 and 4.10 significant structures and plot in Fig. 4.11 the corresponding contact maps, in which a contact is counted, if the distance between two monomers $r_{ij} < r_{ij}^{\min} + \epsilon$. I set, to some extent indiscriminately, $\epsilon \approx 0.2$ but, of course, the contact maps do not depend on minor variations of ϵ. Furthermore, due to the small size of the systems, the contact maps do not become more meaningful by scaling ϵ with the thickness in some way, instead of keeping ϵ constant. In addition, in Figs. 4.12 and 4.13 end-to-end distances and mean torsional angles are shown, and Fig. 4.14 shows the fluctuations of local radii of curvature and the torsional angles, which I use as a measure for the κ_0 and τ_0 property, whereas the existence of these properties corrensponds to vanishing fluctuations. Based on this data, one can classify the generic ground-state behavior by introducing three general regions: thin, intermediate, and thick tubes, which will be discussed in detail in the following subsections.

Finally, in Fig. 4.15 torsional symmetry values $\tau_{s\mp}$ of the ground-state conformations are plotted. Conformations are called symmetric, i.e, have symmetric torsional angles along the
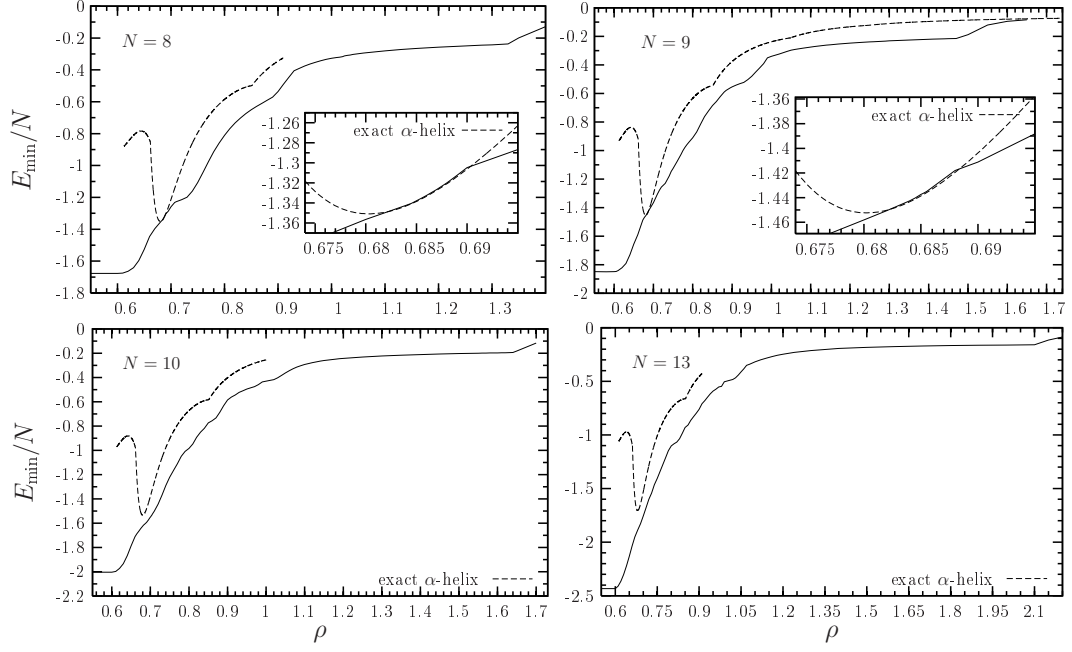
Figure 4.7: Energies of ground states depending on the thickness constraint ρ. *Dashed lines show for comparison the energy for exact α-helices.*
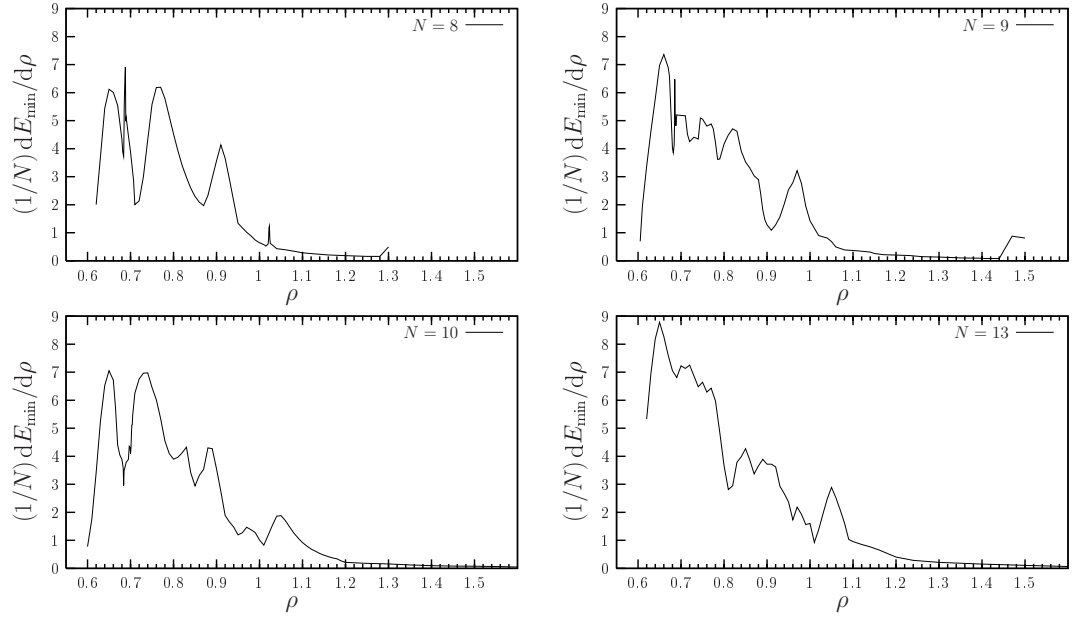
Figure 4.8: Numerical derivatives of the energies in Fig. 4.7 with respect to ρ.

$N = 8$

$\rho = 0.60$ 0.685   0.72   0.73   0.91   0.94   1.023   1.10

$N = 9$

$\rho = 0.60$ 0.6855   0.73   0.78   0.88   0.92   1.20

$N = 10$

$\rho = 0.699$ 0.76   0.83   0.87   1.10   1.12   1.25

$N = 13$

$\rho = 0.68$ 0.73   0.74   0.75   0.80   0.97   1.02   1.60
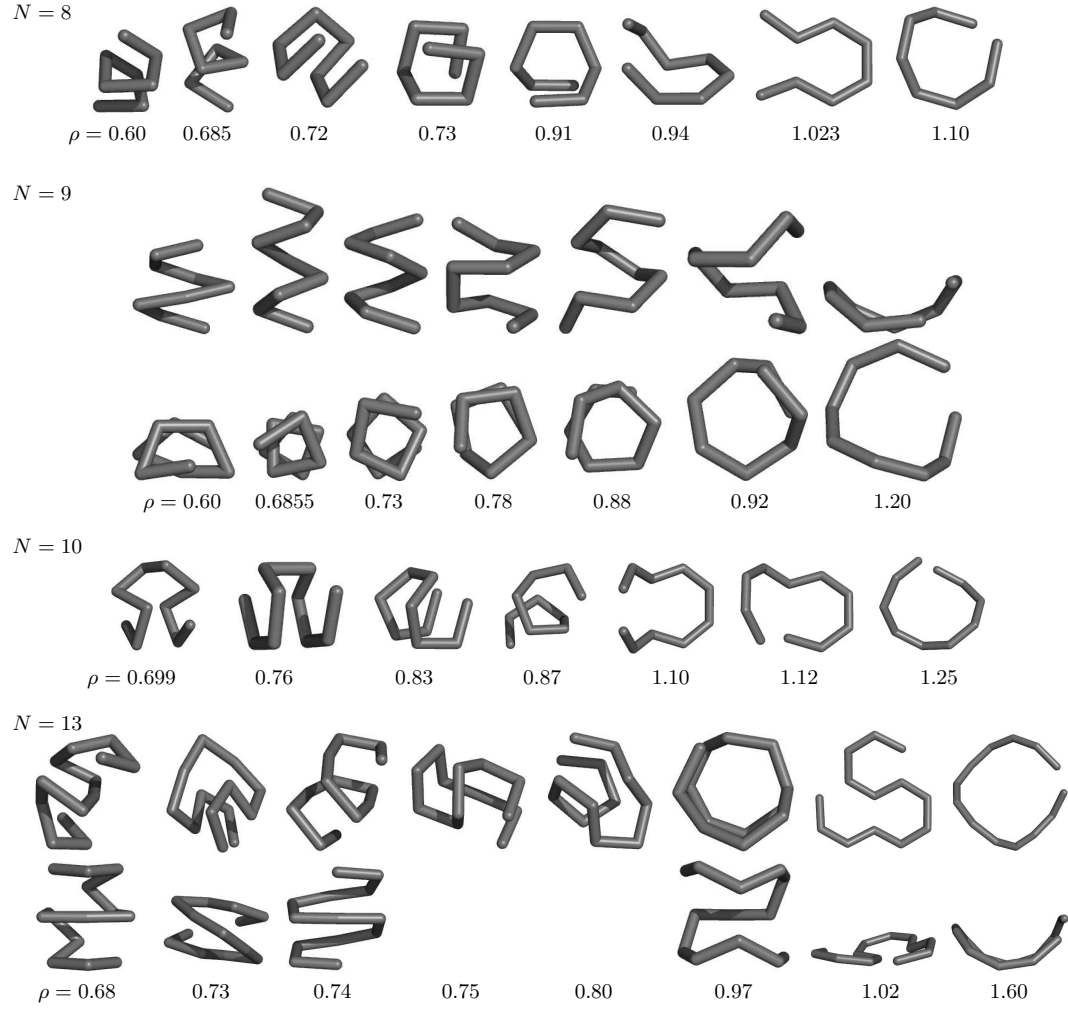
Figure 4.9: Ground-state conformations for selected thickness parameters ρ for $N = 8$, 9, 10 and 13 (from *top* to *bottom*). The second rows for $N = 9$ and $N = 13$ show alternative views of the same configurations. For reasons of better visibility, the thickness is not shown in the proper scale. See Fig. 4.10 for an example of an appropriate visualization.
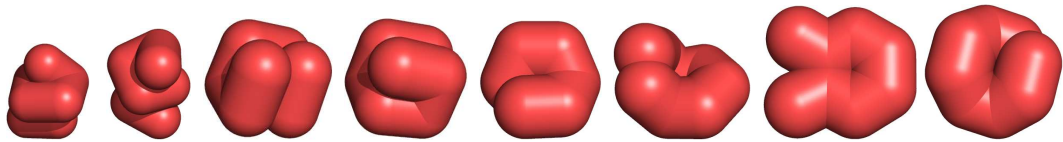
Figure 4.10: The same ground states as in Fig. 4.9 for $N = 8$ shown with appropriate thickness, to give a better idea of the "real" systems.
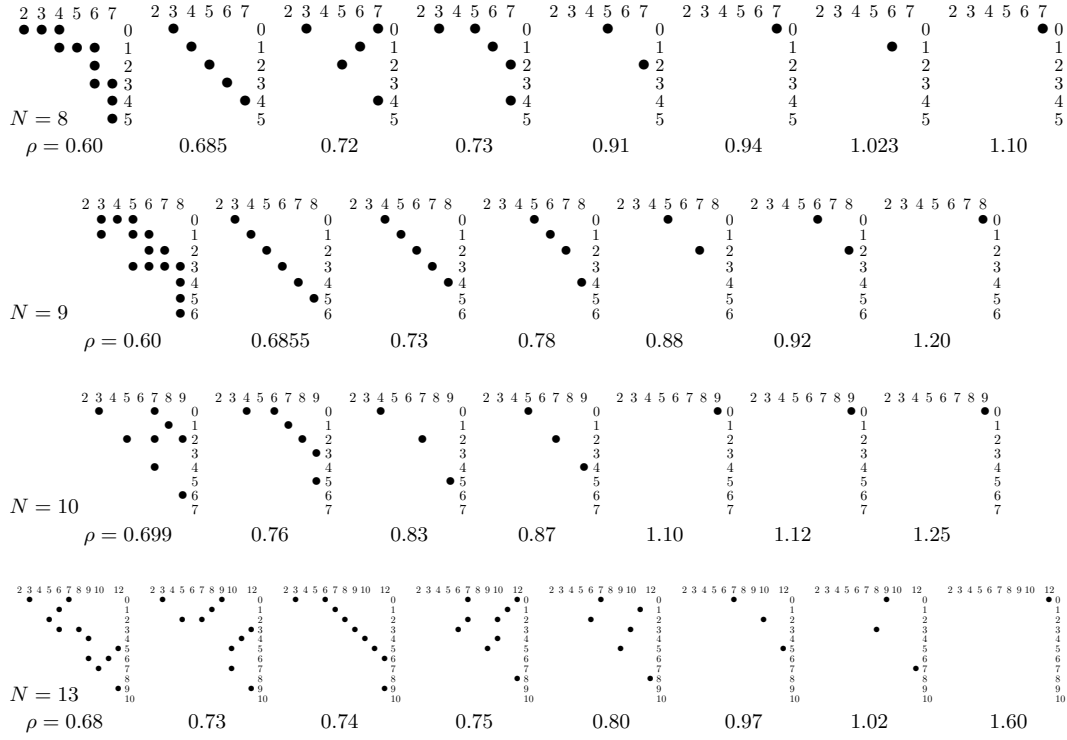
Figure 4.11: Contact maps of the conformations shown in Fig. 4.9. The axes show the monomer numbers i and j, the entries of the matrix are set ($\bullet$), if two monomers i and j are in contact with each other, i.e., if the distance between them in the three-dimensional structure is shorter than a certain threshold value. This value is here slightly larger than the minimum distance of the LJ potential $r_{ij}^{\min}$.

chain, if opposite torsional angles, relative to the middle of the chain, are equal. They are called antisymmetric if the respective angles cancel each other:

$$\tau_{s\mp} = \frac{2}{N_\phi} \sum_{i < N_\phi/2} \phi_i \mp \phi_{N_\phi+1-i} \,, \tag{4.7}$$

where N_ϕ is the number of torsional angles along the chain. Hence, in the case of symmetric conformations, τ_{s-} vanishes and for antisymmetric ones τ_{s+}. For an intuitive understanding, one can say, that antisymmetric conformations are mirror-symmetric, i.e., one finds a mirror-plane through the conformation (see, for example, the conformation with $N = 8$ at $\rho = 0.72$ in Fig. 4.9), whereas for the symmetric case, the ends of the conformations can "only" be rotated onto each other (see, for example, the helical conformations). The observable is finally normalized by $N_\phi/2$. The symmetry is generally not essential for defining or distinguishing different "phases", but it is an interesting property of the theory and facilitate the understanding of ground-state structures. One can imagine, of course, lots of similar
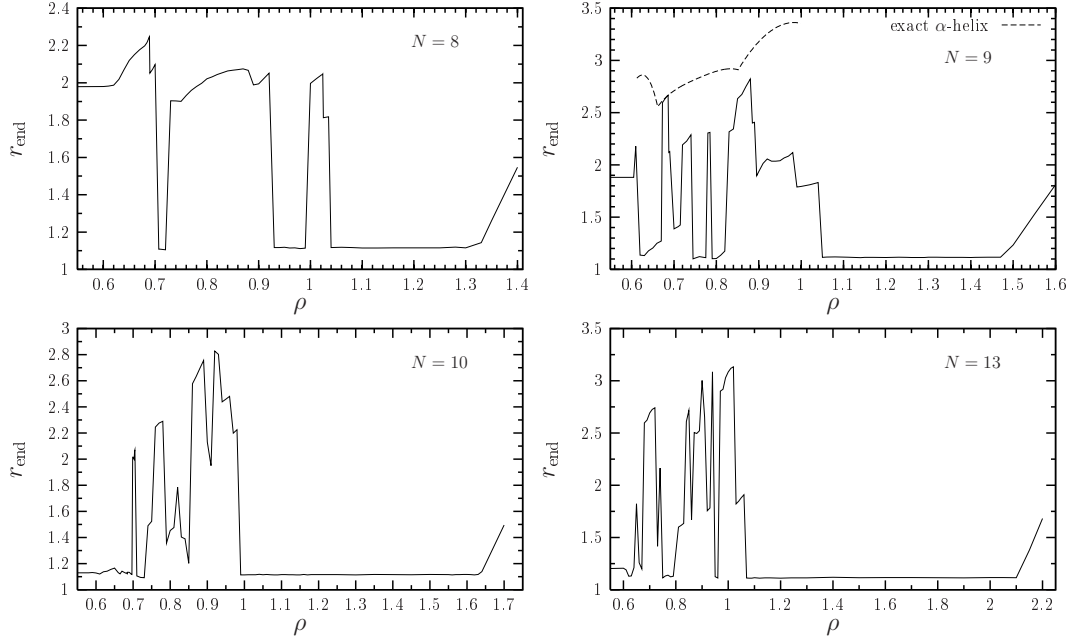
Figure 4.12: End-to-end distances of ground-state conformations depending on the thickness constraint ρ. The *dashed line* for $N = 9$ shows for comparison the end-to-end distance for the exact α-helix.

observables, for example the symmetry of bond angles, i.e. local radii of curvature, κ_s, or the periodicity of local radii curvature κ_p. These observables could give, for example, some interesting insight in the unwinding or deformation of helices. Anyhow, I will confine myself to the previously mentioned observables, the special study of deformed helices may be subject of future work.

4.4.3 Thin Tubes, $0.6 \leq \rho \lesssim 0.9$

The thin-tubes region is dominated by helical and helicallike conformations. I call a conformation "helical", if $\bar{\phi} = \bar{\phi}_{\pi/2}$, where $\bar{x}$ is the arithmetic mean along the chain, $\bar{x} = (1/N) \sum_i x_i$ (cp. Eq. (4.6) and Fig. 4.13). This is equivalent to the condition, that all torsion angles lie in the range $0 \ldots \pm \pi/2$, whereas I do not distinguish between right- and left-handed helices, but the sign must not change within the conformation. Furthermore, the entries in the contact map lie precisely parallel to the diagonal of the matrix in these cases, a clear indication for helix structures (see, for example, $N = 8; \rho = 0.685$ or $N = 9; \rho = 0.73$ in Fig. 4.11). "Helicallike" conformations share some properties with helical structures, e.g., they exhibit a large, slightly increasing end-to-end distance (cp. Fig. 4.12) with increasing thickness, but the torsion-angle criterion above may be violated (typically in a periodical manner) and the contact-map entries do not form an exact parallel, but a line roughly par-
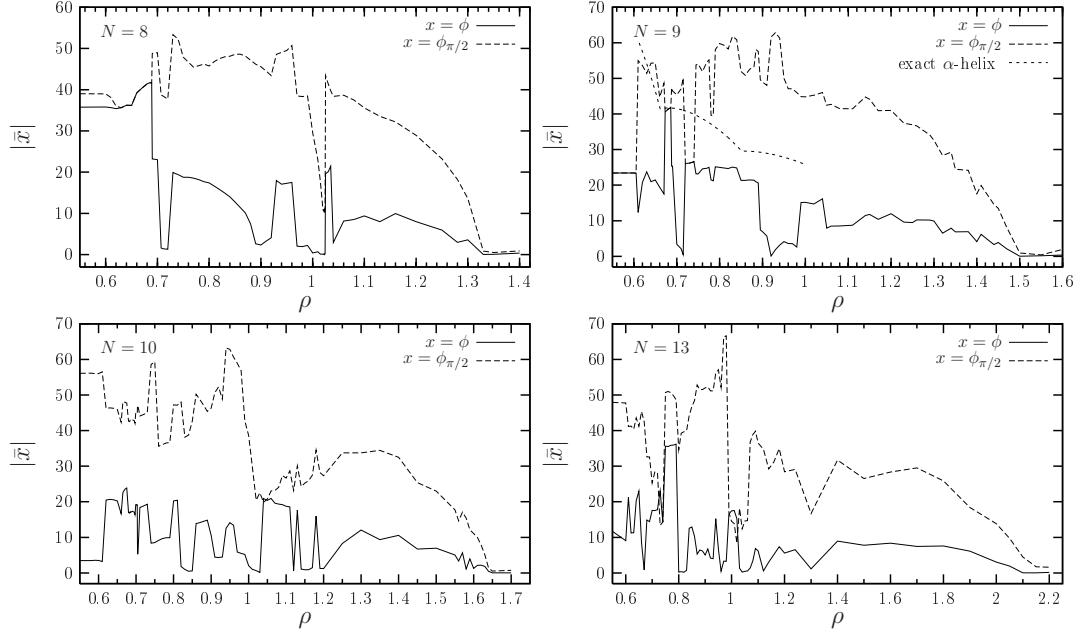
Figure 4.13: Mean torsional angles of ground-state conformations depending on the thickness constraint ρ. Shown are absolute mean values of ϕ and $\phi_{\pi/2} := \min(|\phi|, \pi - |\phi|)$. The *short-dashed line* for $N = 9$ shows the behavior for the exact α-helix.
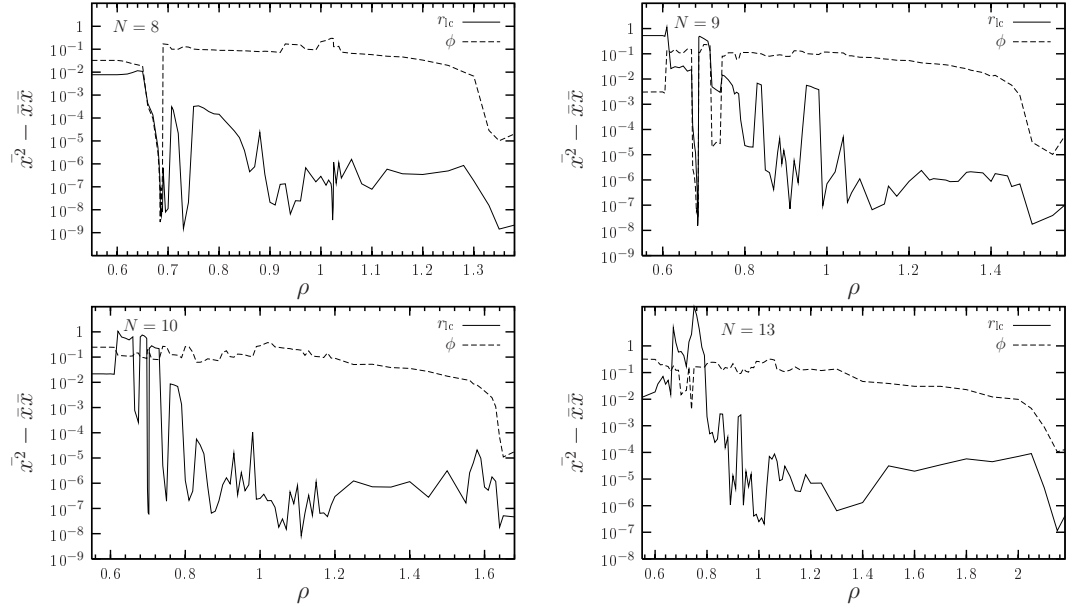
Figure 4.14: Fluctuations of bond- (*solid lines*) and torsion (*dashed lines*) angles within ground-state conformations depending on the thickness constraint ρ. Vanishing fluctuations correspond to conformations of constant curvature (κ_0) or torsion angles (τ_0), respectively.
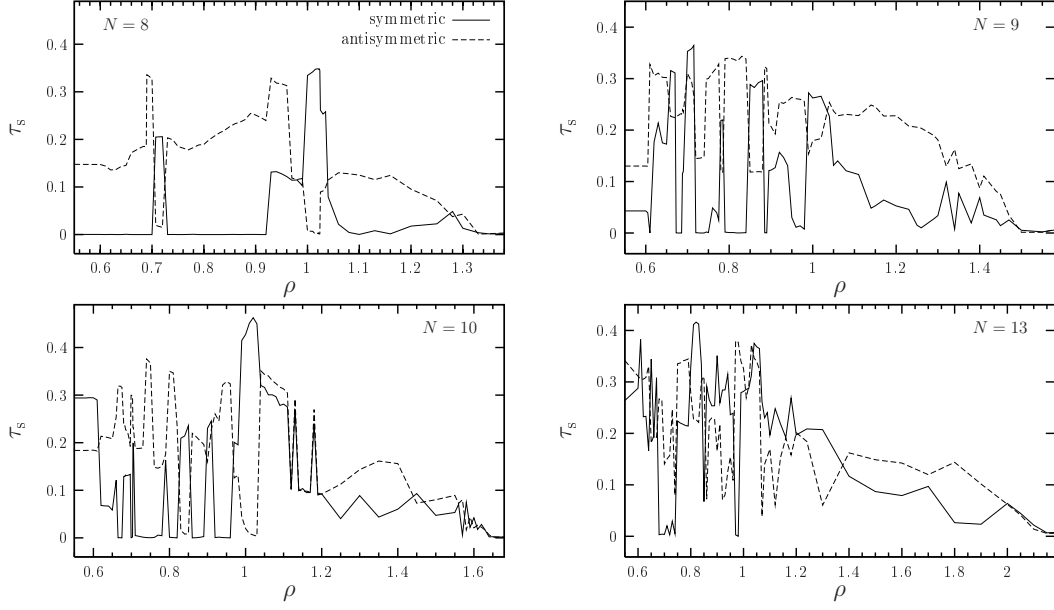
Figure 4.15: The symmetry parameter as defined in Eq. (4.7) for ground-state conformations depending on the thickness constraint ρ. Zero values indicates torsional symmetry of the conformation relative to the middle of the chain.

allel to the diagonal (for example, at $N = 8; \rho = 0.6$ or $N = 9; \rho = 0.78$). Generally, one finds three interesting effects looking at the contact maps in Fig. 4.11, which have been mentioned above or will be discussed later again: First one sees, that polymer chains without thickness constraint (see the maps for $N = 8$ and $N = 9$ with $\rho = 0.6$) do not have a pronounced structure. Just by increasing the thickness a bit, clear helical structures emerge, indicated by straight "lines" parallel to the diagonal of the map (cp. $N = 8$ and $N = 9$ with $\rho = 0.685(5)$). Secondly, by increasing the thickness further, one sees, for example for $N = 9$, that this parallel "lines" moves away from the diagonal, i.e., the helical conformations are "untwisting". Finally, looking at the contact maps for $N = 13$, one sees that tertiary effects come into play, indicated by "disrupting" vertical "lines", which is typically an indication for sheetlike structures.

Remarkably, within certain intervals ($N = 8$: $0.63 \leq \rho \leq 0.688$; $N = 9$: $0.673 \leq \rho \leq 0.6855$), the ground-state conformations expand with increasing thickness to a perfect space-filling helix with κ_0- and τ_0-property, i.e., an α-helix with constant bond- and torsion angles ($\bar{\phi^2} - \bar{\phi}\,\bar{\phi}$ and $\bar{r^2}_{lc} - \bar{r}_{lc}\bar{r}_{lc}$ vanish[5]). The comparison of measured observables with the data for the exact α-helix is emphasized in the insets of Fig. 4.7 and furthermore exemplarily

---

[5]A remark on the precision of the simulation: The values of $\bar{\phi^2} - \bar{\phi}\,\bar{\phi}$ and $\bar{r^2}_{lc} - \bar{r}_{lc}\bar{r}_{lc}$ become even with the stochastic methods smaller than 10^{-8} at this point (see Fig. 4.14), i.e., the difference between any two torsion angles, for example, in the chain is already less than $1.5 \times 10^{-4}\pi$.

shown in Figs. 4.12 and 4.13. I will resume the discussion on this fact in Sec. 4.5.3 ("The α-Helix Region") below.

As a remark: What is the motivation to call these conformations α-helical in imitation of the real biological α-helix? In natural proteins, α-helices possess about 3.6 amino acids per helix turn [5] and have mainly constant bond and torsion angles. If one constructs a perfect space filling helix with exactly 3.6 monomers per turn, one finds that it has a global radius of curvature of $r_{gc} \approx 0.69$. Or, the other way around in the region $0.6845 \leq \rho \leq 0.688$ (example for $N = 8$), one counts $3.576 \ldots 3.596$ monomers per turn, which is in perfect agreement with natural α-helices. I thus see the first biological relevant structure realized by the simplest model with just Lennard-Jones interaction and thickness but without any conformational assumptions or additional input. This observation is indeed one of the key results, and among the most impressive ones, in this study. I would like to repeat, that the α-helical structure arose "just" due to the incipient influence of the thickness parameter added to a linelike homopolymer model with pairwise Lennard-Jones interaction.

A singular point of further particular interest is located in the vicinity of the perfect helices at $\rho \approx 1/\sqrt{2} \approx 0.71$, where ground states "attempt" to crystallize in a regular simple cubic (sc) lattice structure. I find for example for $N = 8$ at $\rho = 0.73$ a κ_0-conformation[6] almost fitting the sc lattice (elsewhere called "simple cubic lattice helix" [182]), which then untwists with increasing thickness. One sees the same tendency for longer chains as well, see Fig. 4.9 for visualizations and Sec. 4.5.3 ("The α-Helix Region") for further discussion. Note that a perfect cube will not be a ground state at any thickness, as long as the Lennard-Jones interaction length scale is larger than, or generally unequal to, the bond length. If the potential is reconfigured such that its minimum value equals the bond length, i.e. set $r_{ij}^{min} = 1$, one finds indeed that the ground-state conformations fit exactly into the simple cubic lattice (i.e. are exact cubes for adequate monomer numbers) up to lengths of ≈ 36 [180]. A very detailed analysis of special parameter set can also be found in [180]. Further general remarks on the crystallization on regular lattices will be given in Sec. 4.5.2 ("The Crystallization on Regular Lattices").

At larger thickness one observes, see Fig. 4.9, extended helicallike conformations, which may overlap due to the shortness of the chains only at the end bonds.

4.4.4   Intermediate Tubes, $0.9 \lesssim \rho \lesssim 1.1$

In the interval $0.9 \lesssim \rho \lesssim 1.0$, an abrupt switch to almost flat (cp. Fig. 4.13) and mostly closed (cp. Fig. 4.12) conformations can be observed. One finds bended double-rings, hairpins, and even conformations that are "crystallized" on a two-dimensional honeycomb lattice (cp. Fig. 4.9, $N = 8$, 13, $\rho \approx 1.02$). These curves are, of course, κ_0-curves as well and have apparent similarities to β-sheets known from secondary structures of biopolymers.

---

[6]The fluctuation of the local radii of curvature along the cahin $\bar{r}^2_{lc} - \bar{r}_{lc}\bar{r}_{lc}$ is about 10^{-9} at this point, see Fig. 4.14.

See Sec. 4.5.2 ("The Crystallization on Regular Lattices") for general remarks and further discussion on this crystallization and Sec. 4.7 ("The Hydrophobic-Polar Tube Model") for another example. In some small regions, one finds competitions between mesomeric structures, i.e. structures with the same monomer positions but different bond distributions (see, for example, Fig. 4.9, $N = 10$, $\rho \approx 1.1$).

It is particularly remarkable, that just the increasing of the thickness constraint can drive the system from perfect α-helical conformations to planar crystallized conformations like β-sheets without any further changes, a fact constituting a further major outcome of the present work.

4.4.5 Thick Tubes, $\rho \gtrsim 1.1$

At $\rho \approx 1.1$, the ground-state conformation becomes (again) "closed" for all chain lengths. Here begins the region of the twisted circles of constant curvature ("windschiefe Kreise") [197, 198]. Nice illustrations of two examples of this class of structures with $N = 32$ monomers consisting of four half-circles or helix segments can be found in [180]. With increasing thickness, the rings become more and more flat until they reach the two-dimensional ring at $\rho \approx N/2\pi$, which is again a κ_0- and τ_0-curve. A further increasing of the thickness just pushes apart the ends of the ring, what can clearly be seen in the end-to-end distance and the torsion angles (see Figs. 4.12 and 4.13). For the somehow pathological case of $\rho \to \infty$ one would reach the limit of stiff rods [7].

4.4.6 General Remarks

It is not surprising, that the situation becomes more complex with increasing chain length. At least some of the described "nice-looking phases" above are artificial in the sense, that they occur at exactly one short length, or are favored just by that very short length, respectively. One sees, for example, for $N = 10$ and $N = 13$ no exact (α-)helices anymore, it rather seems that at these lengths "tertiary" effects already play a role in the sense, that two small secondary structures are formed which are then arranged "side by side". An indication for this trend may be that conformations with low thickness are often symmetric[8], i.e., the conformations get buckled and turn back at some point (generally in the middle). See for example the helical region for $N = 13$ in Fig. 4.9. Anyhow, the helical structures being present for shorter chains indeed exist as excited states "very close" to the ground states, i.e., with a slightly higher energy. Two of these conformations, which appeared during the

---

[7]These stiff (random) rods will be later observed in the study of the thermodynamic behavior at finite thickness $\rho \approx 1$ for $T > 0$ and are separated from the ringlike conformations by a structural transition with first-order-like behavior. See Sec. 4.6 ("Thermodynamic Behavior of Tubelike Homopolymers").

[8]With "symmetric" I refer to the symmetry of torsion angles as defined in Eq. (4.7) on p. 68. It is generally not essential for defining or distinguishing different conformational phases, but it is an interesting property and helps the understanding. Corresponding symmetry observables are shown in Fig. 4.15.

Figure 4.16: Snapshots of two $N = 13$ conformations from the simulation with $\rho = 0.73$ (*left*) and $\rho = 0.74$ (*right*), which are not the ground-state conformations but have a just slightly higher energy than these. The conformations correspond to distinguished ground-state structures at shorter chain lengths (helical and crystallized on the sc lattice, cp. Fig. 4.9). For reasons of better visibility, the thickness is not shown on scale.

ground-state search and are most likely located in local minima close to the global minimum, are depicted in Fig. 4.16.

There will be further convincing arguments for this classification scheme when I will investigate in Sec. 4.6 ("Thermodynamic Behavior of Tubelike Homopolymers") the thermodynamic behavior of these polymers in the aforementioned general structural phases. The transition lines between the phases then depend indeed on both thickness and temperature. For low temperatures, the helical phase corresponds to polymers with low thickness, the sheet phase to a little higher thickness and the ring phase to the very thick polymers. See also [179, 181].

4.5   Deeper Analysis and Remarks

In the above section (4.4, "Ground State Analysis, $\sigma = 1$"), I analyzed ground states and ground-state regions of the tube model with σ set to 1 (cp. Eq. 4.1) for polymers with chain lengths $8 \leq N \leq 10$ and $N = 13$.

In this part I address selected interesting questions arisen there witch may open the door to a wide new field of things to investigate. I will comment on the effect of crystallization on regular lattices and investigate parts of the $(\rho - \sigma)$-parameter space by varying both, the thickness constraint and the Lennard-Jones potential (i.e., the σ-parameter). I will look especially at the α-helical region for $N = 8$.

4.5.1   Ground-State Description in Detail

Beforehand, I would like to describe ground-state conformations again, but in more detail and in a maybe somehow prosaic way. The reader may skip this section without loosing essential information. The descriptions here will furthermore overlap in parts with those in Sec. 4.4 ("Ground State Analysis, $\sigma = 1$"). Finally, I will not refer to this section elswhere, either.

$N = 8$

helical ($0.63 \leq \rho \leq 0.688$) The first notable region is a helical one, which follows a pre-helical region $0 \leq \rho \leq 0.62$. The region is characterized by a monotonous increase of the mean torsional angle, followed by a monotonous increase of the end-to-end distance r_{end}. Remarkably, the conformations expand with increasing thickness to a perfect spacefilling helix, i.e. a helix with constant bond- and torsion angles (κ_0 and τ_0, $\bar{\theta}^2 - \bar{\theta}\,\bar{\theta}$ and $\bar{r}_{\mathrm{lc}}^2 - \bar{r}_{\mathrm{lc}}\bar{r}_{\mathrm{lc}}$ become smaller than 10^{-8} (cp. Fig. 4.14), θ in units of π). I will call this the perfect α-helix. It is realized in the range $0.6845 \leq \rho \leq 0.688$.

tilted cubes ($0.707 \leq \rho \lesssim 0.8$) After passing a small transition region, ground-state conformation reach cubelike states. Below $\rho \leq 0.72$ they have parallel end bonds (i.e., are "closed") and are antisymmetric ($\tau_{\mathrm{s}+} \approx 0$), at $\rho = 73$ a κ_0-conformation ($\bar{r}_{\mathrm{lc}}^2 - \bar{r}_{\mathrm{lc}}\bar{r}_{\mathrm{lc}} \approx 10^{-9}$) with non-parallel ends is formed (which is now symmetric: $\tau_{\mathrm{s}-} = 0$) which untwists with increasing thickness. This somehow artificial transition between the two types of cubes is best seen in the end-to-end distance and in the symmetry of the conformations, see Figs. 4.12 and 4.15. See also the notes on perfect cubes in Sec. 4.4.3 ("Thin Tubes, $0.6 \leq \rho \lesssim 0.9$").

keyring ($0.89 \leq \rho \leq 0.92$) Here, the former cube has cranked up to a ring with two ends lying on top of each other. The region is a κ_0-region, too.

bended double-ring ($0.93 \leq \rho \leq 0.99$) At $\rho \leq 0.93$, there is an abrupt switch to "closed" conformations. The region has κ_0 curves and is a transition region to the next, remarkable region.

hairpin ($1.0 \leq \rho \leq 1.023$) This is the first region, where the ground-state conformation becomes almost "flat". (See the sharp dip in the plot in Fig. 4.13 at $\rho \approx 1.02$. The configuration would become exactly 2-dimensional, if $\bar{\phi}_{\pi/2}$ would approach zero.). The boundaries of this region can be clearly seen in the end-to-end distance, where it starts with a jump from "closed" to $r_{\mathrm{end}} \approx 2$. r_{end} increases slightly and jumps at the end of the region to some lower value. At the end of this region, the ground-state conformation becomes a κ_0-curve.

Windschiefe Kreise ($1.04 \leq \rho \leq 1.33$) After an intermediate step (seven-ring with tail), the ground-state conformation becomes again "closed" at $\rho \geq 1.04$. This is the region of the so-called "windschiefe Kreise", i.e., bended rings (of constant curvature). With increasing thickness, the rings become more and more flat until they reach the planar 2-dimensional ring at $\rho \approx 1.33$, which now is a κ_0 and τ_0-curve as well. From here on, increasing thickness just pushes apart the ring, what can clearly be seen by the end-to-end distance and the torsion angles.

$N = 9$

At $N = 9$ one sees even three not connected helical regions and several pre-helical regions. Besides some regions, where the ground state structure falls into non-natural or non-biological conformations, one observes here very nicely the "evolution" from the (α-)helix through some intermediate states ("key rings") to rings ("windschiefe Kreise"). This "process" agrees well with the naive idea of untwisting a helix or a spring. I tried to visualize it in the respectice lines in Fig. 4.9.

helical 1 ($0 \leq \rho \leq 0.605$)   The first helical region begins already with the ground state at zero-thickness, i.e. in the model without thickness constraint, in contrast to the helical region at $N = 8$. The conformations are neither κ_0 nor τ_0, but the torsional angles shows a notable symmetry. One may say, the helix is compressed from a horizontal and the vertical direction.

helical 2 ($0.673 \leq \rho \leq 0.6855$)   The second helical region is comparable in its behavior with that one of the $N = 8$-chain. It also contains the α-helix at its upper end, with the same characteristics as the α-helix at $N = 8$, namely κ_0 and τ_0.

helical 3 ($0.72 \leq \rho \leq 0.74$)   The third helical region finally is again neither κ_0 nor exactly τ_0, but the torsion angles are symmetrically distributed and almost constant and the local radii of curvatures are periodically constant and symmetrically distributed as well.

pre-helical ($\rho \approx 0.78$ and $0.85 \leq \rho \leq 0.88$)   The conformations here are not helical by definition but share some properties with helical structures, e.g. they show a big, slightly increasing end-to-end distance. At the end of this region the end-to-end distance reaches its global maximum for the $N = 9$ chain.

key ring ($0.92 \leq \rho \leq 0.98$)   Again, the key rings are circles with two parallel overlapping end-bonds with a mainly constant end-to-end distance. The curves are generally no κ_0-curves.

rings ($\rho > 1.05$)   This region have the same properties in all observables as the "windschiefen Kreise" at $N = 8$. Especially they are "closed", a property not seen so far for this chain length, except for the non-natural transition regions at lower thickness.

$N = 10$

At $N = 10$ one finds no τ_0-curves (except for the planar circles), in particular one finds no helical region anymore. In fact, it seems, that at this length already "tertiary" effects

become relevant at low thicknesses. An indication therefor may be, that conformations with low thickness are often symmetric.

At higher thickness values, there are no symmetric structures anymore and one encounters familiar structures like bended double-rings or "windschiefe Kreise".

Ω-region (0.699 ≤ ρ ≤ 0.703) At the beginning of the region there is a discrete jump in the end-to-end distance from "closed" to an almost constant value of about 2. The bond angles are almost constant (κ_0) and the torsion angles are symmetric. Leaving the region, this symmetry breaks down abruptly.

anti-parallel planar five-rings (0.76 ≤ ρ ≤ 0.78) After some intermediate states, which possess exactly symmetric torsion angle distributions at $\rho \geq 0.71$ and may be "closed" $0.71 \leq \rho \leq 0.73$ or become κ_0 (at $0.75 \lesssim \rho < 0.76$), this next stable region is reached. It still has symmetric torsion angles distribution and is characterised by an almost constant end-to-end distance plateau.

parallel bended five-rings (0.83 ≤ ρ ≤ 0.85) In comparison to the former region, the five rings are not planar anymore but bended such, that a football-like pentagon-hexagon surface is formed. For larger system sizes, this may lead to quasicrystalline structures, but this is highly speculative.

pre-helical (0.86 ≤ ρ ≤ 0.89) This region shares the same properties as the pre-helical region at $N = 9$. Parts of this region tends to be κ_0-curves.

bended double six-ring (0.99 ≤ ρ ≤ 1.2) In this region one finds a "competition" between mesomerismic structures, i.e. the monomer distribution is (except for the perturbation due to the inequality of potential minimum and bond length) the same but the distribution of the bonds differs. Two of them are shown in the corresponding line in Fig. 4.9, whereas one may call the first a β-hairpin. All conformations are "closed" and, at least almost, κ_0.

windschiefe Kreise (1.25 ≤ ρ ≤ 1.63) These structures do not differ in their general behavior from that ones at $N = 8$ and $N = 9$.

$N = 13$

For this length, the general statements given for $N = 10$ hold as well. Without going into much detail I present shortly some interesting regions.

$0.68 \leq \rho \leq 0.74$ The first noticeable region lies in the range $0.68 \leq \rho \leq 0.74$. It is characterized by the symmetry of bond and torsion angles and a high, slightly increasing end-to-end distance, both indications of a (pre)helical region. There were a lot of helices in this thickness range at lower chain lengths, including the α-helix as well as simple cubic-like conformations.

The corresponding structures are indeed recovered during the ground-state search, see Fig. 4.16, but although they are quite close to them in energy, they are not the ground-states conformations anymore. In fact, ground states already show some "tertiary" structure, as already mentioned above.

$0.75 \leq \rho \lesssim 0.79$ Directly following, there is a region of locally distorted sc-like ground-states. Locally means, that there is one single monomer not sitting on a corresponding sc-lattice site.

$0.80 \lesssim \rho \lesssim 0.85$ The distorted sc-like region defects smoothly to the extension of the *bended double-ring* (cp. $N = 8$), composed of the $N = 8$-ground state with an additional attached ring (cp. also $N = 10$, $0.83 \leq \rho \leq 0.85$).

$0.97 \leq \rho \leq 0.98$ This region is very similar to that one finds for $N = 9$, $0.92 \leq \rho \leq 0.98$ (*key ring*), with four bonds overlapping.

$0.99 \leq \rho \leq 1.06$ The above groundstate "flips" into the almost planar six-ring region, which can be seen in some sense as the "extension" of the regions found at $N = 8$ and $N = 10$ and similar thickness. Within this phase, there is again a mesomeric flip between "both end outside" and "one end inside".

$1.07 \leq \rho$ Like for all chain lengths considered so far, one finds again the rings, which become for $\rho \geq 1.4$ "real" convex bended rings ("windschiefe Kreise").

4.5.2 The Crystallization on Regular Lattices

In Sec. 4.4.3 ("Thin Tubes, $0.6 \leq \rho \lesssim 0.9$") I showed an example for a special, isolated point in the (ρ, σ)-parameter space, at which the ground-state structure crystallizes on a regular lattice, namely the simple cubic lattice in three dimensions at $\rho = 1/\sqrt{2}$.[9] This can of course be explained by the fact, that conformations at the simple cubic lattice would have local (and hence global) curvatures of $r_{\mathrm{lc}} = 1/\sqrt{2}$ (or ∞), see Fig. 4.17, left. The crystallization of ground-states on the sc-lattice could be observed for chains with lengths up to $N = 36$ [180] and it was argued, that these crystal structures are likely existing the thermodynamic limit

---

[9]And even if this, in fact, seems to be somehow unnatural in the context of secondary structure formation of proteins for example, it is an interesting feature of the theory.
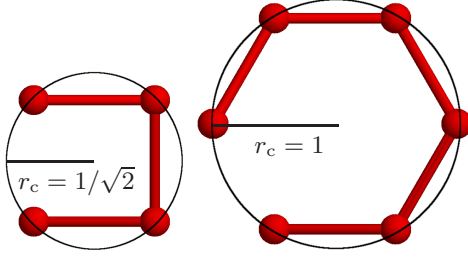
Figure 4.17: Radii of curvature on the simple cubic (*left*) and the honeycomb (*right*) lattice.

$(N \to \infty)$ as well. I will later show (Sec. 4.6.2, "The Cuboid Region in Phase α"), that these structures not only occur as ground states for lengths which are able to fill a complete cube or cuboid, but are representatives of thermodynamic pseudophases at finite temperatures also for other chain lengths. See also Fig. 4.16, right.

There are, of course, other regular lattices, which correspond, for example in two dimensions, to $r_{lc} = 1/\sqrt{3} \approx 0.577$ (triangular lattice) and $r_{lc} = 1$ (honeycomb lattice), see Fig. 4.17, right. The curvature on the triangulat lattice is smaller than the natural thickness d of about 0.6 (see Sec. 4.4.2, "Preliminary Remarks, Overview"). The crystallization on that lattice should be visible therefore in simulations without explicit thickness constraint and was indeed found, for example, in simulations in the original work by Stillinger and Head-Gordon [65] or for groundstates of polymers on strongly attractive substrates [98]. The onset of the crystallization on the honeycomb lattice in three dimensions can bee seen in the conformations at $\rho \approx 1$ in Fig. 4.9. The crystallization in planar honeycomb structures in three dimensions is in any case surprising, but not at least due to the formation of tertiary structure it is very unlikely, that these crystalline conformations would persist in the thermodynamic limit. By contrast, one would expect this persistence for simulations in two dimensions, which has, however, not been studied so far.

4.5.3 The α-Helix Region

For the $N = 8$ and 9 polymer, I found a thickness region, where the α-helix is the ground-state conformation (see Sec. 4.4.3, "Thin Tubes, $0.6 \leq \rho \lesssim 0.9$"). Remember that I used the Lennard-Jones potential with $\sigma = 1$ there, which sets the interaction length scale. There is nothing special with it, except that the potential just vanishes at the bond length, a fact that plays just a secondary role, as I am not counting energy contribution from consecutive monomers at all.

Because of the special role of the α-helix in nature (besides its geometrical elegance), I will here try to track the α-helix not only in the thickness but also in the σ-direction of the parameter space, i.e. ρ and σ will be varied independently in the vicinity of the assumed "α-region". The results are displayed, exemplarily for $N = 8$, in Fig. 4.18. One sees, that the α-helix occurs as ground-state conformation in a small, bounded thickness interval ($0.66 < \rho < 0.75$) right "before" an abrupt conformational change (depicted by
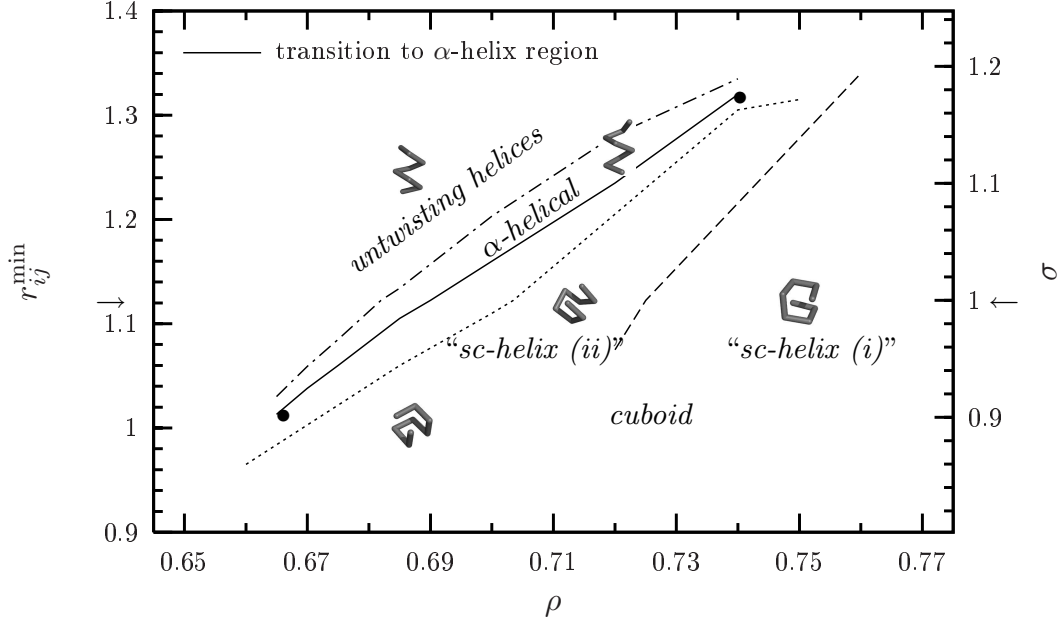
Figure 4.18: $N = 8$: The σ–ρ plane and ground-state conformations near the α-helix. The left and right coordinates are connected just via $r_{ij}^{\min} = 2^{1/6}\sigma$. See text for details.

the *solid line*) to cubelike structures. The transition line increases approximately linearly in the interaction-length–thickness plane, a dependence, which seems to hold generally for structural transitions in the vicinity. Following a perpendicular path, i.e., with increasing interaction lengths and decreasing thickness, the helices untwist smoothly. The *dashed-dotted* line together with the *solid line* define the region, where the α-helix is the ground state of the system (cp. insets in Fig. 4.7 on p. 66). Note that for $\rho < 0.66$ and $\rho > 0.75$, α-helices are no ground states at all.

   A further interesting transition is marked by the *dashed line* in Fig. 4.18. This line indicates the transition between the so-called simple cubic "lattice helices (ii)" and "(i)" [182], i.e., cuboidlike structures with parallel and antiparallel tails (remember that for $r_{ij}^{\min} = 1$ and $\rho = 1/\sqrt{2}$, one observes the "crystallization" exactly at the simple cubic lattice, cp. Sects. 4.4.3, "Thin Tubes, $0.6 \le \rho \lesssim 0.9$" and 4.5.2, "The Crystallization on Regular Lattices").

   For the sake of completeness, the *dotted line* indicates a conformational change to some intermediate structure "between" α- and lattice helices and the *arrows* on the y-axes mark the line $\sigma = 1$ investigated so far in this study.

4.6 Thermodynamic Behavior
of Tubelike Homopolymers

4.6.1 General Observations and Description

After having studied the low-temperature regime, i.e., ground states, so far, I here concentrate on the conformational phase behavior at finite temperatures. As common, the specific heat is calculated and the peak regions of this observable are considered as indicators of relevant thermodynamic activity. Figure 4.19 shows these specific-heat landscapes for the $N = 8$ and $N = 9$ polymer. The points (+) plotted in the top-view representation of Figs. 4.19 c and d indicate the positions of the crest lines in this landscape, i.e., the lines signaling structural changes. One notices four major pseudophases, which I denote by α, β, γ, and δ. In Fig. 4.20, I show the corresponding canonical energy histograms at temperature $T = 0.1$ for different thickness constraints ρ. The histograms at the transition values of ρ are
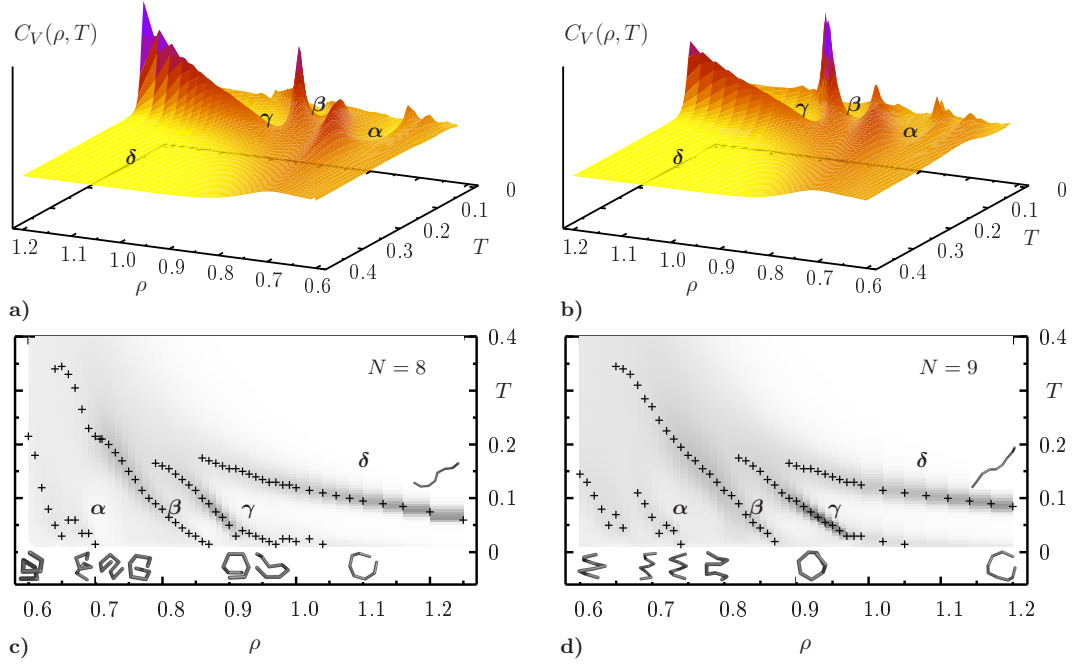
Figure 4.19: Phase diagrams of the homopolymers with $N = 8$ (left) and $N = 9$ (right). The labels α, β, γ, and δ indicate the different pseudophases at finite temperature. Figures **a** and **b** show the perspective views of the specific-heat landscapes, and in **c** and **d**, the top-views are plotted with marked peak positions for various parameters ρ. The specific-heat values are encoded in gray scale. The pictures in the insets in **c** and **d** correspond to the ground-state conformations presented in Fig. 4.9, the pictures in the δ regions show relevant conformations there.
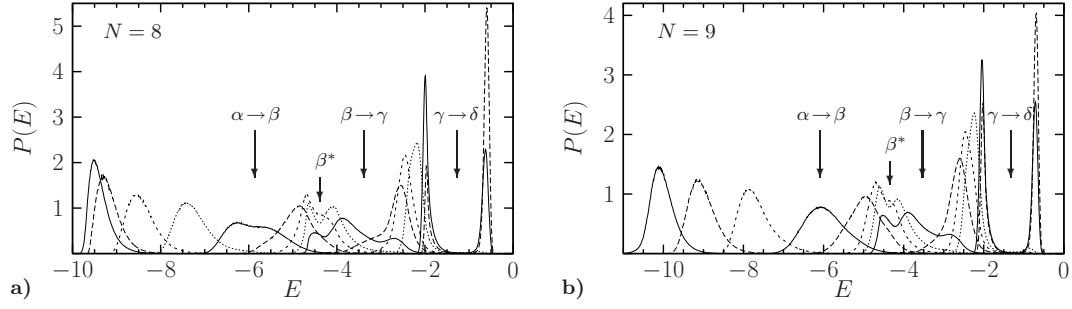
Figure 4.20: Energy histograms for various thickness constraints ρ at $T = 0.1$. Histograms corresponding to specific-heat maxima are marked with arrows. **a** $N = 8$ polymer. Histograms correspond to the following thickness parameters: $\rho = 0.7$ (solid line), 0.72, 0.74, 0.76, 0.78 (solid line, $\alpha \to \beta$), 0.8, 0.82, 0.84, 0.86 (solid line, $\beta \to \gamma$), 0.88, 0.9, 0.95, 1.08 (solid line, $\gamma \to \delta$), 1.13. **b** $N = 9$ polymer. Histograms correspond to $\rho = 0.72$ (solid line), 0.75, 0.78, 0.81 (solid line, $\alpha \to \beta$), 0.83, 0.85, 0.87, 0.89 (solid line, $\beta \to \gamma$), 0.92, 0.95, 1.11 (solid line, $\gamma \to \delta$), 1.14. The histograms were obtained by reweighting the density of states and are consistent with histograms obtained from independent canonical simulations at this temperature. These histograms contain about 10^{10} entries. Statistical errors are less than 1% and, almost everywhere, smaller than the line width.

marked by arrows. Both plots, for $N = 8$ and $N = 9$, do not differ qualitatively, i.e., have all interesting features in common. The phase structure will be discussed in the subsequent analysis of the pseudophase diagrams.

In the insets of Figs. 4.19 c and d, ground-state conformations at positions according to their thickness, are shown. They provide a first indication for the population of the respective pseudophase at finite temperatures. Deeper analyses will strengthen the expectation that the ground-state conformations are the relevant conformations in the corresponding pseudophases at finite temperatures as well. This includes, for example, the analyses of distributions of structural observables like end-to-end distance, radius of gyration, radial distribution of monomers, bond angles, torsion angles and so on. A further possibility would be the comparisons with reference structures, e.g., by using pattern recognition [199], or counting structural components (as for example in [182]) during separate canonical simulations at fixed temperatures. This has been done experimentally but was not that effective and meaningful in first attempts compared to the methods mentioned before. Let me remember, that I neglect data for $\rho \lesssim 0.6$, which corresponds to the pure Lennard-Jones volume exclusion, as the thickness constraint does not influence the system at all below this "natural thickness" (see Sec. 4.4.2, "Preliminary Remarks, Overview").

4.6.2 Analysis of Structural Phases of Short Polymers

The Phases γ and δ

I begin the detailed discussion of the different structural phases with the high-thickness region, i.e., with the phase γ and the transition to δ. Based on the knowledge of the ground states and the general structural behavior of polymers, I assume in γ a population of bended rings, which undergo a structural change to sprawled random coils in δ, which become more and more rodlike with increasing thickness. This assumption can be illustrated and strengthened by an example in little more detail. For $N = 8$ monomers, let me consider the geometrical objects "octagon" and "straight line" as limiting prototypes of these regions. Based on the calculation of the geometrical properties of these prototypes, one expects for the end-to-end distance distributions a sharp peak at the position of the LJ potential minimum, i.e., at $r_{\mathrm{end}} \approx 1.12$, for the rings and a diffuse peak at $r < 7$ for the rodlike structures. For the radius of gyration distribution a sharp peak at $r_{\mathrm{gyr}} \approx 1.3$ (rings) and a diffuse peak at $r < 2.34$ (rods), and for the radial distribution function sharp peaks at $r \approx 1.1$, 1.8, 2.4, and 2.6 (see Fig. 4.21 c) and smooth peaks below integer values for the respective conformations. In Figs. 4.21 a and b, the respective distributions are shown, measured in canonical simulations at the transition temperature and within both phases. In Fig. 4.21 a, the end-to-end distance and radius of gyration histogram are plotted, Fig. 4.21 b shows the radial distribution function. These quantities exhibit exactly the assumed behavior, i.e., the peaks of the measured distributions appear exactly at the calculated values given above for the anticipated "prototypes". Additionally, the bimodal shapes of the distributions in Fig. 4.20 at the transition $\gamma \rightarrow \delta$ indicate a first-order-like character of the transition with coexisting conformational phases. The energy histograms near the transition point exhibit two distinct peaks separated by broad energy gaps. During simulations at the transition point ($T = 0.1$, $\rho = 1.08$), both structures appear equally, as can be seen in Fig. 4.21 a.

The Phase β

Reducing the thickness parameter ρ, the sheet phase β is reached. Figure 4.22 shows the results of simulations at $\rho = 0.82$ and $T = 0.1$ for the $N = 8$ polymer, which belongs to the histogram labeled β^* in Fig. 4.20 a. There are mainly three structures dominating this phase, amongst them the two ground-state conformations in the range $0.89 \leq \rho \leq 0.99$ (cp. Figs. 4.9 and 4.19). As shown in Fig. 4.22 a, they can be well distinguished by their end-to-end distance, where three distinct peaks in the distribution appear, whereas they are not resolved by specific heat. The plot in Fig. 4.22 b shows the overall energy distribution as well as the contributions from the three regions corresponding to the peaks in the end-to-end distribution. As illustrated in Fig. 4.22 d, the actual peak in the energy distribution is associated with ring-like conformations and their excitations, whereas the shoulder is caused by the hairpin-like conformations. In Fig. 4.22 c, the distribution of torsion angles is plotted.

a)

b)

c)

$r_{\text{end}} = r_0 \approx 1.1$

$r_{\text{gyr}} \approx r_3/2 \approx 1.3$

$r_0 = r_{ij}^{\text{opt}} \approx 1.1$

$r_1 \approx 1.8$

$r_2 \approx 2.4$

$r_3 \approx 2.6$
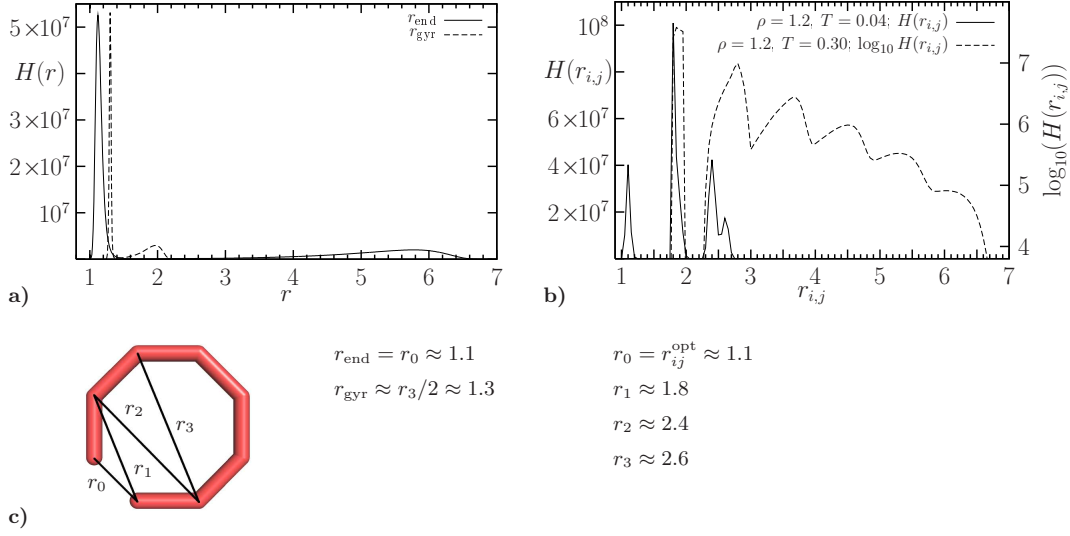
Figure 4.21: Measured histograms from simulations at fixed temperatures for the $N = 8$ polymer **a** at the transition from the bended-ring phase γ to the sprawled-coil phase δ and **b** deep inside these two phases. **a** End-to-end distance (solid line) and radius of gyration (dashed line) at the $\gamma \leftrightarrow \delta$ transition ($\rho = 1.08$ and $T = 0.1$). **b** Radial distribution ($\rho = 1.2$) in the bended-ring phase γ (solid line, $T = 0.04$) and in the sprawled-coil phase δ (dashed line, $T = 0.3$). The histograms are differently scaled for better visibility, each contains more than 10^9 entries. Statistical errors are less than 1% and smaller than the line width. In **c**, the limiting prototype for phase γ, the octagon, is shown with its respective observables. Sharp peaks in **a** and **b** are located very close to the calculated values.

The contributions of the different structural classes can be distinguished very well again. One notes for example an accumulation of torsion angles around $\phi = 0$ in the contribution of the hairpin-like conformations (dashed line), an indication for the planar structure of the conformations. At β^*, the conformations extend into the third dimension, i.e., bonds within the conformations begin to overlap. An analogous behavior is found for $N = 9$, see Fig. 4.20 b.

The Cuboid Region in Phase α

The region of lowest thickness, α, is the helical phase. This phase can be further separated into subphases, where in one of them the exact α-helix resides as a ground state for $N = 8$ and $N = 9$ (see Sec. 4.4.3, "Thin Tubes, $0.6 \leq \rho \lesssim 0.9$"). In a further region, simple-cubic helical structures [182], or cuboids for $N = 8$, corresponding to the ground-state conformations in
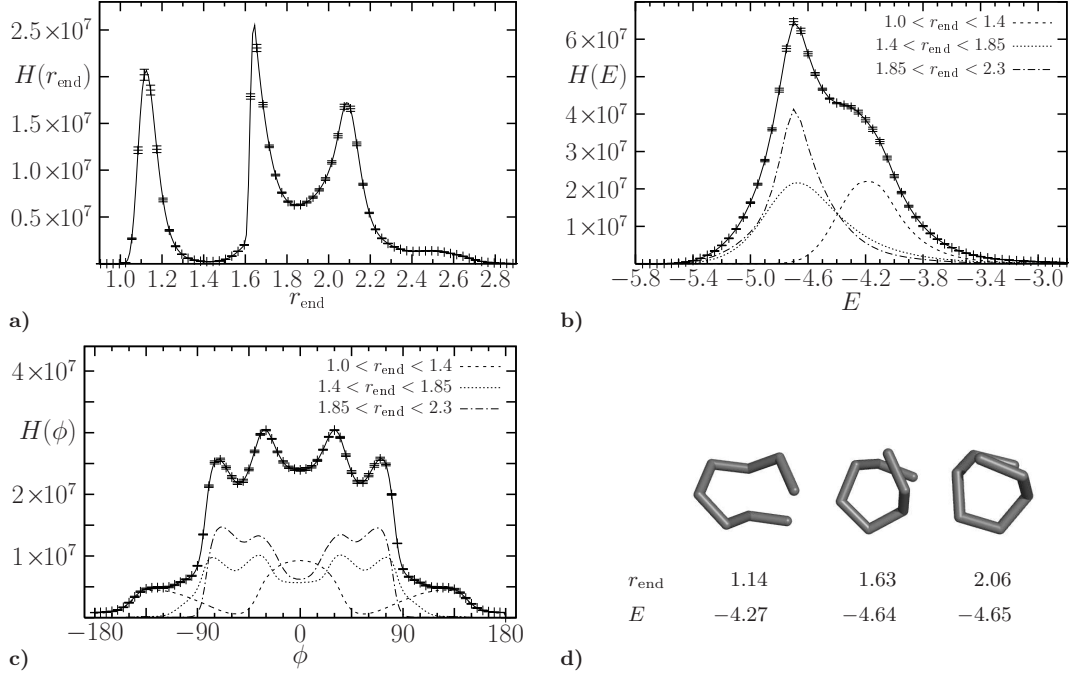
Figure 4.22: Measured histograms in phase β for $\rho = 0.82$ and $T = 0.1$ for the $N = 8$ polymer. **a** The end-to-end distance histogram exhibiting three separate peaks indicating three different major contributing groups of conformations. **b** The energy histogram and **c** the histogram of torsional angles. Error bars were obtained from independent simulations and are shown exemplarily. In **b** and **c**, the histograms for each group of conformations, distinguished by its end-to-end distance, are shown in addition. Each histogram contains at least 10^9 entries. **d** Representatives of each group of this energetic pseudophase and their corresponding properties.

the range $1/\sqrt{2} \approx 0.707 \leq \rho \lesssim 0.8$, respectively, dominate.[10] These regions are separated by noticeable, but in the context of the whole phase diagram less important, transition lines. For illustration, I show in Fig. 4.23 the distribution of torsional angles in the cuboid region for $N = 8$, $\rho = 0.7$ and $N = 9$, $\rho = 0.72$ at temperature $T = 0.1$. For the $N = 8$ polymer, it can clearly be seen that only conformations with torsional angles of 0 and $\pm\pi/2$, i.e., cuboids, occur. For the $N = 9$ polymer, these angles are still dominant, although not occurring exclusively. In any case, the existence of that region is insofar worth mentioning as the corresponding conformations do not appear as ground states for this length and as it shows that it is a characteristic feature and not only a length-dependent artefact.

---

[10]The occurrence of these structures as ground states for certain system sizes, e.g., the crystallization on regular lattices as singular solutions of the theory, has been analyzed and discussed in detail in Ref. [180].

Figure 4.23: Torsion angle distributions at $T = 0.1$ for the **a** $N = 8$ and **b** $N = 9$ polymers in phase α at $\rho = 0.7$ and $\rho = 0.72$, respectively (cuboid or sc-helical region). Each histogram contains about 10^{10} entries. For visualizations of corresponding conformations see, e.g., Fig. 4.19 c.

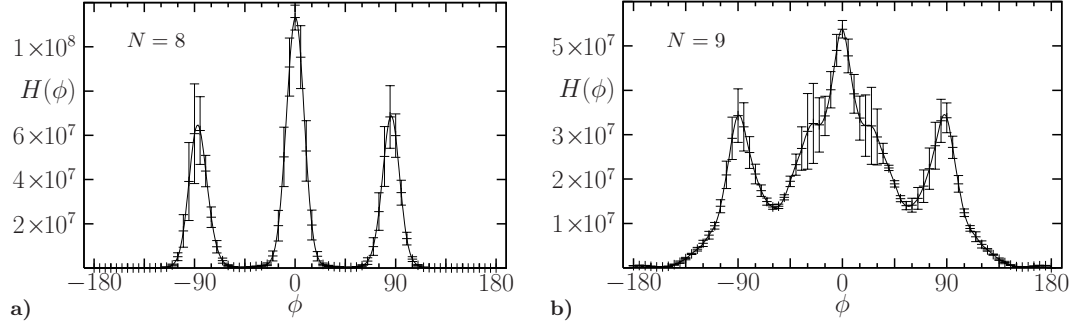### 4.6.3   Analysis of and Remarks on Longer Tubes

Figure 4.24 shows the phase diagrams for the longer tubes consisting of $N = 10$ and $N = 13$ monomers analogously to Fig. 4.19. In general, beside the short-length artefacts near $T = 0$, the phase diagrams at different lengths do not differ qualitatively much from each other. The general thermodynamic behavior is quite similar for all system sizes, especially one finds again the four major phases discussed above. Also, the characteristics of the sprawled-coil and bended-ring regions do not depend, beside an obvious shift of the thickness parameter, on the polymer length. One notes, however, the onset of the formation of tertiary structures, as also discussed in Sec. 4.4.6 ("General Remarks"). Particularly the helical phase α becomes internally more complex. Furthermore, the relevant thermodynamic activity shifts to lower temperatures.

The ground-state conformations for these systems, plotted again in the insets of Fig. 4.24 c and d, support the interpretation of the phases given above. Especially the motivation for denoting β the sheet phase becomes clearer, as I found almost planar, "two-dimensional" ground states seeming to crystallize on a honeycomb lattice. These conformations are the dominant conformations in β at finite temperatures as well and form, in the case of the $N = 13$ polymer, three LJ contacts, in the sense of a contact map, cp. Fig. 4.11 on p. 68. One finds a further interesting detail here, which occurs only for these longer chains. The 13mer is long enough, that an intermediate phase β' emerges between β and γ. This phase is populated, as indicated by the ground-state conformation shown in Fig. 4.24 d, by conformations consisting of two small bended circles such that two LJ contacts are formed. The transition between β and β' also exhibits some characteristics of first order transition, namely two separated peaks in the energy distribution with a gap in between, i.e., dominating conformations of both phases coexist in the transition region. See Fig. 4.25.
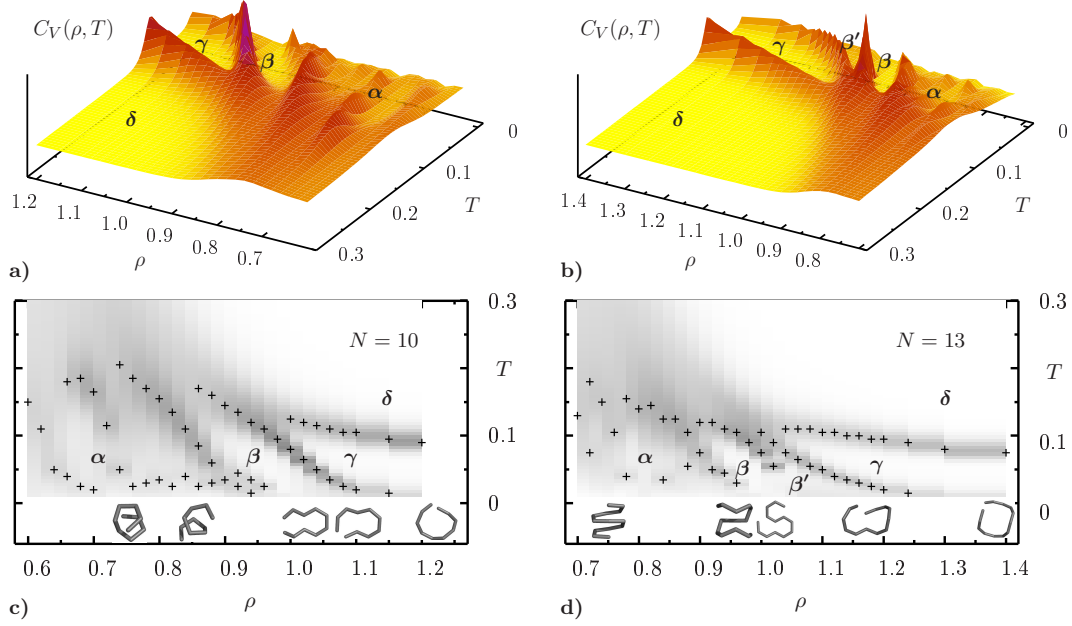
Figure 4.24: Phase diagrams of the $N = 10$ (left) and $N = 13$ (right) polymers analogously to Fig. 4.19.

4.7   The Hydrophobic-Polar Tube Model

The central goal of this study is, of course, to make a contribution to the understanding of structure formation like it occurs in nature. As mentioned in the introductory part to this chapter, one of the main question is: What do one have to put into a model necessarily, to see secondary-structure formation? I have shown above how the sole introduction of a thickness constraint leads to the formation of different structural classes, including helix and sheet conformations, for classes of homopolymers.

What if one upgrades the model in a specific manner? As presented in Sec. 4.1 ("Related Studies, Alternative Approaches"), there are several studies, where the here used tube model or an intentionally similar model have been used in different environments or with additional potentials influencing, facilitating or potentiating structure formation. These include for example the formation of hydrogen bonds or the introduction of stiffness, see again for example [188, 189, 191–193].[11]

I here modify the homopolymer tube model, following the basic ideas of the HP- and AB-model, by introducing two species of monomers: hydrophobic (A) and hydrophilic or polar (B) ones [42, 43]. The nonbonded Lennard-Jones interaction between pairs of monomers

---

[11]I would like to emphasize again, that the tube model used in [192, 193] differs significantly from the version used here. See the discussion in the mentioned section and also in [179].

Figure 4.25: Energy histograms for the $N = 13$ homopolymer with thickness $\rho = 1.0$ at various temperatures near the $\beta \to \beta'$ transition. A clear double-peak structure with energy gap can be observed.

depends now on their types:

$$V_{\text{LJ}}^{\text{AB}}(r_{i,j}) = 4 \left(\frac{1}{r_{i,j}^{12}} - \frac{C(i,j)}{r_{i,j}^6} \right) , \qquad (4.8)$$

where

$$C(i,j) = \begin{cases} +1 & \text{for AA contacts}, \\ +1/2 & \text{for BB contacts}, \\ -1/2 & \text{for AB contacts}. \end{cases}$$

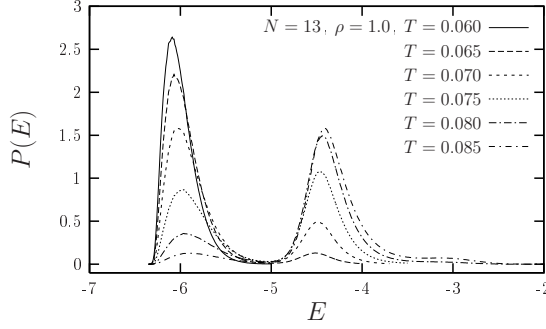Hence, besides the strong attraction of A-type monomers, there is a weak attraction between B-type monomers and a weak repulsion between monomers of different type, favoring hydrophobic core formation of A monomers. To enable a direct comparison with the literature on the standard linelike AB model introduced by Stillinger et al. [64, 65], an additional bending term is introduced and the total energy is then

$$E_{\text{AB}}(\mathbf{X}) = \frac{1}{4} \sum_k (1 - \cos \vartheta_k) + \sum_{i,j=i+2} V_{\text{LJ}}^{\text{AB}}(r_{i,j}), \qquad (4.9)$$

where the ϑ_k are the bending angles of adjacent bond vectors. See for a general introduction and remarks also Sec. 1 ("The HP Model" and "The AB Model").

Just to acquire a taste for the effects of these changes, I show as an example results for the 13mer Fibonacci sequence $AB_2AB_2ABAB_2AB$,[12] which has been studied in the linelike AB model, i.e., with $\rho = 0$, in three dimensions some time ago [65, 67, 68] [13]. Figure 4.26

---

[12]The usage of Fibonacci sequences in the context of heteropolymer models goes, to my knowledge, also back to Stillinger and Head-Gordon [65]. They used them because of some advantageous features like "All As are isolated and flanked on both sides by Bs", "Bs appear isolated or in pairs", the special ratio of A and B monomers, etc. On the other hand, the Fibonacci sequence appears in nature, for example, in the context of quasicrystals or quasiperiodic ordering [200–202], or, mathematically spoken, play a role in the tiling problem (see, for example, Figs. 7.12 or 7.21 in [202]). As a very nice example, the Fibonacci sequence was found in the row separation of a ultrathin Cu film on the surface of an icosahedral quasicrystal [200]. However, a correlation between the importance and role of the Fibonacci sequence in the solid state physics and within this model is by no means obvious.

[13]There are much more works investigating these AB-Fibonacci sequences, but mainly focusing on special algorithmical developments and using the formerly published data "only" as benchmarks. See for some examples Table 4.2.
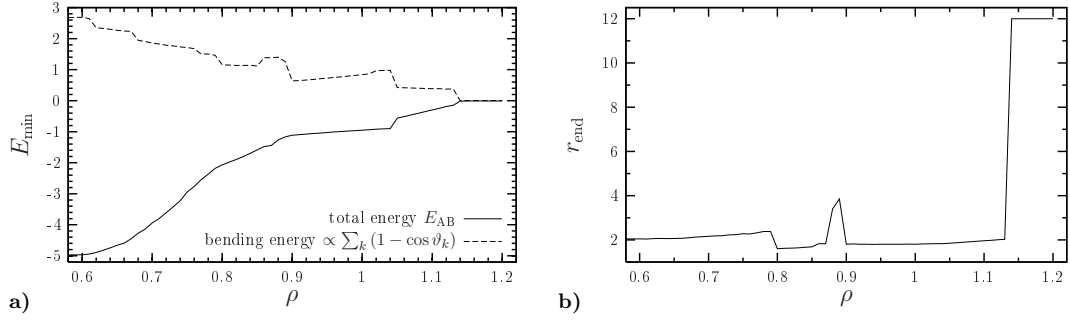
Figure 4.26: Ground-state energy (**a**) and end-to-end distance (**b**) of ground-states of the $N = 13$ Fibonacci AB heteropolymer depending on thickness. In **a**, the contribution of the bending energy to the total energy is shown by the *dashed line*.

shows the energies and end-to-end distances of the ground-state conformations.[14] Figure 4.27 then shows the phase diagram analogously to Figs. 4.19 and 4.24, as well as visualizations of selected ground-state conformations. The general structure including several separated structural subphases is similar to that for the presented homopolymers. The most prominent finding, anyhow, is definitely the very stable β-sheet region in the interval $0.90 \leq \rho \leq 1.01$, at $T \to 0$. The conformations there are neither of κ_0- nor τ_0-type, i.e., they have neither constant bond nor torsion angles (cp. Sec. 4.4.1, "Nomenclature and Methodology"), but they are indeed "planar" (see Fig. 4.27 for visualization). These qualitative properties do not change over the entire region.[15] A quantitatively remarkable fact is the variation of the intra-monomer distances within the conformations. One notes, that the interaction length between the opposite hydrophobic A monomers $1 - 12$ ($r_{1,12} = 1.13$, see Fig. 4.27c for monomer numbering) and $4 - 9$ ($r_{4,9} = 1.15$) in this sheet conformation does not change in the whole thickness region at all. On the other hand, the distances between the B monomers $2-11$ and $3-10$ increase ($\Delta r_{2,9} = \Delta r_{3,10} = 0.27$) and decrease between the A monomers $1-4$ and $9 - 12$ ($\Delta r_{1,4} = \Delta r_{9,12} = -0.10$, differences respecting the conformations at $\rho = 0.9$ and $\rho = 1.0$). The van-der-Waals attraction between the A monomers is thus the dominant factor that stabilizes the β-sheet. Remarkably, as becomes clear by the listed geometrical quantities above (and can also be observed in Fig. 4.26a), the bending energy is even increasing with increasing thickness in this region, contrarily to the general overall trend, that the bending energy decreases with increasing thickness (I will continue to discuss the influence of the

---

[14]Showing other observables depending, for example, on torsional angles or symmetries does not make that much sense like in the study of the homopolymers. Torsional angles are not well defined for three consecutive parallel bonds, a conformation which occurs here not only for the very thick rods, and possible symmetries in the secondary structure are mainly already suppressed by the unsymmertric primary structure, i.e., the monomer sequence.

[15]Remember, that planar sheetlike structures of homopolymers have been found more or less at singular points or at least within a comparativly small thickness region.

a)

b)

c) $\rho = 0.7$ 0.8   0.9   1.0   1.1   1.2
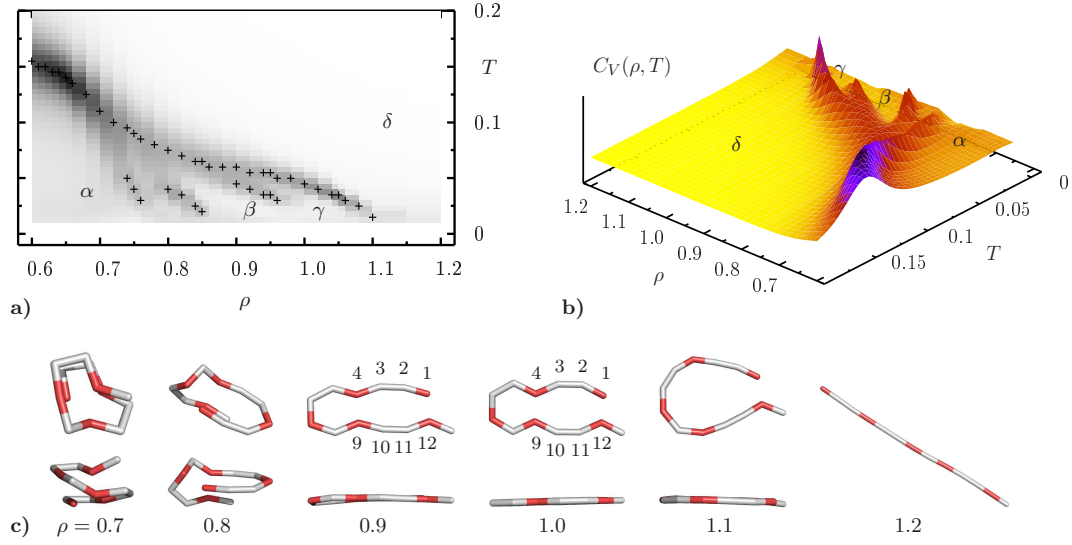
Figure 4.27: Pseudophase diagram of the $N = 13$ Fibonacci AB heteropolymer. **a** The plot shows the top-view with marked peak positions of the heat capacity for various parameters ρ, **b** the qualitative view on the heat-capacity landscape. Gray scales encode the value of the specific heat. The pictures in **c** illustrate selected ground-state conformations. Conformations are shown from different viewpoints, A monomers are marked by red color (dark gray), B monomers are white.

bending term further below). To summarize this point, recall that there are planar six-ring conformations at comparable thicknesses for the $N = 8$, $N = 10$, and $N = 13$ homopolymer ground states, cp. Sec. 4.4.4 ("Intermediate Tubes, $0.9 \lesssim \rho \lesssim 1.1$"). These structures are now *stabilized* by the specific monomer sequence, whereas the tube thickness of course remains the "driving force" of the structure formation.[16] This observation, that specific monomer sequences can stabilize general secondary structures, is a further central results of the here presented work.

At lower thickness parameters one finds structures with helical properties governed by the actual monomer sequence. One notes here a very pronounced conformational transition from random coils to native conformations at $0.1 \lesssim T \lesssim 0.15$, which is in detail discussed for the linelike limit "$\rho \lesssim 0.6$" in [68]. With increasing thickness the ground-state conformation becomes a ring and finally switches to a stretched rod, which, contrarily to the homopolymers discussed above, appears as ground-state conformation because of the changes in the potential. This is a qualitative difference to the results in Sec. 4.6 ("Thermodynamic Behavior of Tubelike Homopolymers").

---

[16] Just simulating the given sequence in a two-dimensional space without thickness leads to completely different conformations consisting of a hydrophobic core and a polar shell [65].

a) $\rho = 0.0$

b) $\rho = 0.95$

c)   w/o bending A_{13} with bending   **d)**   w/o bending A_{13} with bending
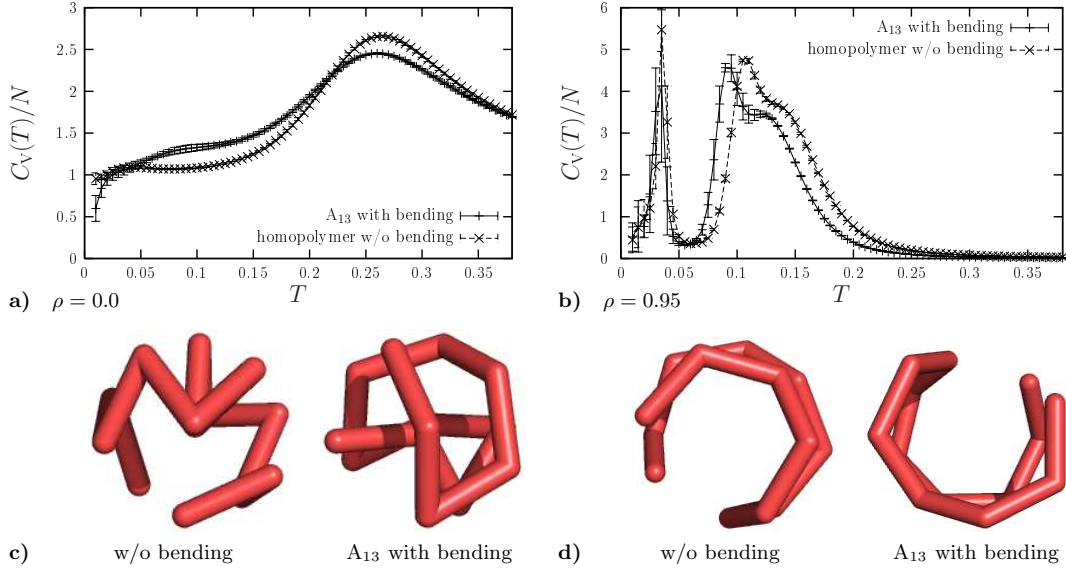
Figure 4.28: Comparison of homopolymers with and without bending energy at $\rho = 0.0$ (*left*) and $\rho = 0.95$ (*right*). In **a** and **b**, specific heats of the respective homopolymers are shown, **c** shows ground-state conformations.

Finally two remarks are in order. Firstly, using the described model, two independent changes compared to the homopolymer model used before were made. I introduced on the one hand different kinds of monomers with different interactions and on the other hand a bending stiffness. To evaluate the influence of each of the two changes, I simulated the 13mer with a sequence consisting of just hydrophobic A monomers (A_{13}), which is equal to the homopolymer studied without bending stiffness in Sec. 4.6[17], for the two exemplified thickness values $\rho = 0.0$ and $\rho = 0.95$. Figure 4.28 illustrates, that the influence of the bending stiffness is marginal for both, ground-state structures and thermodynamic behavior. The ground-state energies change by 1% to 5% for the presented conformations, the structures themselves remain qualitatively the same. This can be quantified, for example, by measuring the root mean square deviation (rmsd) D_{rms} of the respecive conformations $\mathbf{X}^{\mathrm{homo}}$ and $\mathbf{X}^{A_{13}}$

$$D_{\mathrm{rms}} = \sqrt{\frac{1}{N} \sum_{i=1}^{N} \left| \tilde{\mathbf{x}}_i^{A_{13}} - \tilde{\mathbf{x}}_i^{\mathrm{homo}} \right|^2}, \tag{4.10}$$

where the $\tilde{\mathbf{x}}_i$ denote the ith monomer positions relative to the center of mass and with the implicit assumption that the two conformations are already globally rotated against each other in order to find the best match.

_____

[17]Note that choosing a B homopolymer (B_{13}) would correspond to $\sigma = 2^{1/6}$ and $\epsilon = 1/4$ in Eq. (4.1), with $r_{i,j}^{\mathrm{opt}} = 2^{1/3}$ and $V_{\mathrm{LJ}}(r_{i,j}^{\mathrm{opt}}) = -1/4$. Absorbing the energy scale in the definition of temperature (i.e., $\epsilon = 1/4 \to \epsilon_B = 1$), one would work with $T_B = T_A/4$.

For equal conformations, this value is of course zero and becomes the larger, the less the two conformations coincide. The deviation of the conformation at $\rho = 0$ is $D_{\mathrm{rms}} = 0.045$, which can be considered as a quite good match of the conformations. For $\rho = 0.95$ the deviation is $D_{\mathrm{rms}} = 0.098$. To calculate D_{rms}, I used the same algorithm as applied and described in [68, 196]. I have to state, that for this measurement of the deviation D_{rms} only the monomer locations in space and not their position in the sequence were considered, i.e., the path of the conformation through fixed monomer locations has been changed if necessary. Of course, there are several paths through a given "lattice", i.e., configuration, of monomers with almost the same Lennard-Jones energy. Taking the actual sequence of monomers into account when measuring the rmsd, it would be of the same order as for arbitrary conformations with similar radii of gyration, i.e., of similar compactness, as in Eq. (4.10) monomers at equal positions in the sequence are compared with each other, which generally occupy different locations in different paths. As illustrated in Fig. 4.28 c, the A_{13} sequence at $\rho = 0$ chooses a path with as much as possible obtuse angles to reduce the gain of bending energy, whereas in the homopolymer ground-state conformation without bending stiffness, acute angles dominate. At the thickness $\rho = 0.95$ (see Fig. 4.28 d), both ground states are helical conformations changing the direction of winding within the conformation, what is natural, taking into account that the model does not favor a certain winding direction, i.e., left-handed and right-handed helices have the same energy (cp. also the respective conformation illustrated in Fig. 4.9). Roughly spoken, it turns out, that the strong Lennard-Jones interaction is responsible for the arrangement of the monomers and the bending stiffness then potentially "optimizes" the path through these monomers. Particularly, it becomes clear, that for a given AB sequence and hence a given AB monomer "lattice", the choice of a path through it is determined, or at least drastically limited, by the fixed AB sequence itself.

Furthermore, it is shown in Fig. 4.28 a and b, where the specific heats of the homo13mer without bending and the A_{13} sequence with bending are compared at $\rho = 0.0$ and $\rho = 0.95$, that the effect of the bending potential on the thermodynamic behavior is marginal, too. In particular peak positions in the specific heat are not influenced at all, or just slightly shifted to lower temperatures for the case of bending energies, what may be explained by the fact, that collapsed chains have a higher bending energy and will therefore "un-collapse" to random rods more easily, i.e. need less thermal activity to unfold. However, it can be concluded, that the described behavior of the $N = 13$ AB Fibonacci sequence is predominantly based on the influence of different monomer types and not by the bending stiffness. Remember also the above discussion of the stable β-sheet structure with respect to this statement.

Secondly, as a methodological remark, and as already mentioned: It turns out that ground states of one-dimensional linelike models do intrinsically have some measurable "natural thickness" $d(\mathbf{X})$ in the meaning of the interpretation of the global radius of curvature (see Eq. 4.4). Below this value, the thickness does not influence the thermodynamic behavior of the polymer at all, which is shown exemplarily in Fig. 4.29. I there compare the specific heats
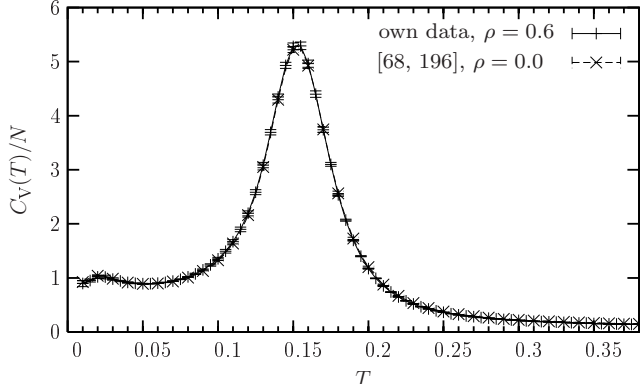
Figure 4.29: Comparison of specific heat of the $N = 13$ Fibonacci AB heteropolymer at $\rho = 0.6$ (*solid line*, and $+$) with data obtained in independent previous studies [68, 196] by multicanonical simulations without thickness constraint, i.e., at $\rho = 0.0$ (*dashed line* and $\times$, mainly covered by solid line and hence not visible). The curves are clearly identical, which confirms the observation, that the thickness does not influence the thermodynamic behavior of the system at $\rho \lesssim 0.6$. They correspond to the data shown in Fig. 4.27 a and b at $\rho = 0.6$. Error bars are plotted on both curves.

of the $N = 13$ Fibonacci AB heteropolymer at $\rho = 0.6$ and $\rho = 0.0$, which are indeed equal.[18] It may be therefore favorable to search for ground states by simulating the polymer with a thickness constraint slightly below its natural thickness. One restricts the conformational space significantly and may travel much faster through the remaining phase space. As a first test of this idea, ground-state energies and -conformations for the Fibonacci 13mer and other widely-used AB polymers with $N \leq 21$ monomers presented over the past years [68, 203–205] could be confirmed. See Table 4.2 for details.

4.8   Summary

In this chapter I presented an analysis of tubelike polymers. The tube picture is, in the first instance, a simplification of the volume extension of polymers due to steric constraints of their backbone or the presence of side chains. Using sophisticated simulation techniques, I have analyzed in the first part of this work systematically and in detail ground-state structures for the described model with fixed interaction length. As a key result, I have shown that basic secondary structures like helices and sheets, including the perfect α-helix and planar sheets "crystallized" on the honeycomb lattice, form solely driven by the variation of the thickness constraint. This statement is, due to the simplicity of the model, valid for various

---

[18]The data for $\rho = 0.0$ were obtained in an independent previous study [68, 196]. Hence, the correctness of the used methods and results obtained in the present study is additionally confirmed (cp. Sec. 4.2.1).

	[68]		[203]	[204]	[205]	this work		
	MUCA	ELP	CSA	DM	HA[b]	ELP+[b]	WL[c]	WL[c]+
13[a]	4.967	4.967	4.975	4.975	4.975	4.975	4.974	4.975
21	12.296	12.316	12.327	12.327	12.327	12.327	12.324	12.327
20.1	33.766	33.810			33.843	33.843	33.840	33.843
20.2	33.920	33.926			33.945	33.945	33.938	33.945
20.3	33.582	33.578			33.609	33.605	33.603	33.610
20.4	34.496	34.498			34.526	34.526	34.522	34.526
20.5	19.653	19.653			19.661	19.661	19.658	19.661
20.6	19.322	19.326			19.347	19.347	19.343	19.347

[a] Sequences 13 and 21 are the Fibonacci sequences used in [65],

   Sequences 20.x introduced in [66]

[b] using ELP results from [68] as input

[c] with thickness constrint $\rho = 0.55$

Table 4.2: Comparison of (negative) energies of native conformation of various AB sequences presented over the last years. "+"-sign indicates the application of a (subsequent) determinsistic optimization (conjugate gradient method [139]). Data of some otimization runs can be found in Appendix B.

classes of polymers. I investigated furthermore in detail the neighborhood of the α-helix in the parameter space by varying both, thickness and interaction length. It turned out that the α-helix exists as ground state in a small, bounded area in the (σ–ρ) space, and is surrounded by other helical and helicallike conformations.

The analysis of ground states was, of course, just a first step to an understanding of the model. In the subsequent step, based on the knowledge of the ground-state conformations, I focused on the thermodynamic behavior and conformational phases at finite temperatures. I identified dominant structural pseudophases at finite temperatures, whereas the specific-heat landscapes depending on the thickness parameter and temperature represents the conformational phase diagram. Independently of the polymer length, I found four major structural phases. These include helices, sheetlike planar structures, bended rings and sprawled random coils. These different secondary structure phases can be assigned to different ranges of the tube thickness. The thickness parameter is therefore suitable for a classification of the structural behavior of classes of polymers.

Finally, I introduced the AB tube model for hydrophobic-polar heteropolymers with different interactions for the different kinds of monomers and an additional explicit stiffness potential similar to that in wormlike chain models. I discussed results for a specific sequence of monomers, which has extensively been studied before without thickness in a linelike model. These previous results are contained in my data as special cases for which the thickness

contraint is smaller than the natural thickness of the system. In particular, I found a very pronounced region of a β-sheet structure stabilized by the special sequence of A and B monomers. Hence, I showed in this additional part, that special sequences of amino acids, i.e., different intramolecular interactions, can stabilize general secondary structures. Regarding the introduced bending stiffness, I assured myself that it plays a minor role for both, the ground-state formation and the thermodynamic behavior. For the scientific placement of the model and remarks on the two-letter alphabet, see also Appendix A ("The HP-Transcription Problem").

Summary

In this work, I presented results on the phase behavior of different coarse-grained models of polymers, which have been obtained by means of computer simulations. Polymers are macromolecules consisting of a large number of (equal) small molecules, the monomers, connected such, that they form a monomer chain. At high temperatures, these chains are in the swollen random coil state. Cooling them down, they collapse at the so-called Θ-temperature into much more compact globules. At very low temperatures, they freeze into glassy or crystalline solids. In the case of proteins, a special and very important class of biopolymers, one speaks also of the "folding" transition.

In the first part of this work, I study lattice polymers using the interacting self-avoiding walk model. Special attention has been paid to the collapse and the freezing transition and the scaling of both. The interesting question is, if the intermediate amorphous phase is stable or vanishes in the thermodynamic limit. In the second part, I study an off-lattice tube model for polymers with the emphasis on the different low-temperature pseudo-phases depending on the thickness of the tube and the folded secondary structures therein.

Simulational Methods For the study of the lattice polymers, in particular for the low temperature freezing regime, I applied sophisticated chain growth algorithms based on the Pruned Enriched Rosenbluth Method (PERM) [29], which are able to perform a quite good random walk through the energy space and system size [104, 105] and can hence estimate the entire density of states of the system within one single simulation. These methods can of course be used for the simulation of the Θ regime as well. But as they sample, in principle, the whole temperature space in parallel, they become relatively demanding with respect to the computational effort. Although the methods can be tuned to sample special temperature ranges as well, I applied for very large system sizes ($N > 4000$ on the simple-cubic lattice) an improved "canonical" version of PERM, which has been shown to be very efficient [159]. For the simulation of the off-lattice systems, I used mainly generalized ensemble Monte Carlo methods, like the Wang–Landau algorithm or the multicanonical recursion. The Wang–Landau algorithm is relatively easy to implement and works well for a variety of problems, but has in its original formulation some intrinsic "defect" as it violates the detailed-balance condition during the simulation. This can be fixed by a subsequent simulation run with fixed

algorithmic parameters, which corresponds then, in fact, to a multicanonical simulation. For reliability reasons, cross-checks have been made for some results using parallel tempering simulations and independent data from previous multicanonical studies. Ground states have been refined using deterministic minimization techniques.

Lattice Polymers   In the study of lattice polymers, I considered homopolymers on the simple cubic (sc) and the face centered cubic (fcc) lattice. I studied conformational transitions of these systems, namely the collapse (or coil–globule transition) at the so-called Θ-temperature and the freezing transition at very low temperatures, i.e., well below the Θ-temperature. A question of particular interest deals with the coincidence of these transitions, i.e., with the instability of intermediate phases between the random coil (vapor) phase and the frozen (solid) phase, in the thermodynamic limit, as found for colloidal systems with short range interaction [167]. Both scenarios, the disappearance and the stability of the liquid phase in the thermodynamic limit, have been found later for polymeric systems as well and were explained in a similar way by different interaction ranges [63, 127]. In general, this behavior can be attributed to the range of the (attractive) interaction between the single monomers or particles. It can be qualitatively described introducing an interaction range parameter R. In colloidal systems, for R smaller than some threshold value, different solid phases can coexist and for R larger than *another* threshold, there is a stable liquid phase [169]. As I used in the first part of my work a potential leading to $R \to 0$, i.e., R is smaller than any finite threshold, one would expect a two-stage collapse from random-coil conformations at high temperatures to the ground states of the system. [19]

I studied the thermodynamic behavior of the polymer systems considering peaks in the specific heat as indicators of structural activity. In contrast to similar studies for different polymer models [127], these peaks seem not to behave in any regular way at first view. Unraveling the non-uniform peak structure, it became rather clear, that the general behavior of the finite size freezing temperature is strongly superposed by systematic lattice effects. Due to the high precision of my simulations, it was also possible to explain this behavior. The freezing temperature fluctuates systematically between almost fixed boundaries. In particular, there are "magic" lengths where the ground states fit into compact cuboid shapes and where the transition temperature jumps between these boundaries. Even though for polymers on the fcc lattice, the situation is more complex, polymers behave similar on both lattices with respect to the general behavior of the freezing transition.

To estimate the scaling of the finite size collapse transition temperature, I had to simulate much longer polymers with lengths up to $N = 32\,000$ monomers for the sc lattice. This task is by far not trivial, as the upper critical dimension is just $d_\mathrm{c} = 3$ and hence logarithmic corrections to the leading order scaling $T_\mathrm{c}(N) - T_\Theta \sim 1/\sqrt{N}$ are expected. By fitting my data to various scaling functions motivated by field-theoretic studies, it was not possible

---

[19]With the implicit understanding that the theory is applicable analogously to polymeric systems as well.

to uniquely identify the nature of these corrections. It rather turned out that even these apparently large systems are still to short to determine the type of corrections and hence verify theoretical predictions. This remains a major task for future work on this field. Anyhow, the value of the infinite length Θ temperature seems not to be affected seriously by the explicit type of scaling corrections, as they can mimic each other effectively to a certain degree. Beside a very well agreement of my estimates on the sc lattice with the most precise estimates from the literature, my data confirm, to my best knowledge, the only numerical value existing so far for the fcc lattice.

However, concerning the question of the stability of the structural phases, it can be concluded from my results, that both transitions, the collapse and the freezing remain well separated also in the extrapolation towards the thermodynamic limit. This may be explained by the expected stable "solid" pseudo phase due to the very short attractive interaction in the model. Hence, the separate pseudo phases identified in this study can be understood qualitatively using the analogy to the behavior of colloids. The low-temperature transition can be interpreted as the "freezing" of compact globular shapes into polymer crystals. Even though, a general, qualitative agreement between the behavior or polymers and colloids has been found (see, for example, also [63]), a precise analysis the phase behavior of polymers with different interaction ranges and of the analogy to colloidal systems is left for future work.

The Tube Model In the presented analysis of the tube model, I concentrated on the formation of secondary structures of short systems. The polymer is modelled as an off-lattice chain consisting of monomers, which interact between each other by means of a Lennard–Jones potential. The chain itself is coated by a tube, mimicking the three-dimensional extension of polymers due to steric constraints introduced, for example, by amino-acid side chains in the case of proteins. The diameter of a mesoscopic tube can be considered as a single steric parameter that induces cooperative effects and permits the discrimination of polymers. It was introduced using the concept of the radius of curvature which is indeed, in the first instance, a mathematical concept. In fact, it has been proven that "[it] is connected to various physically appealing properties of a curve. In particular, [it] provides a concise characterization of the thickness of a curve, [...] as have been investigated within the context of DNA" [178], it was further successfully used in more complex models for proteins [79, 80, 82] and it was finally shown, that this concept is effectively equal to a volume exclusion using two-point functions for polymers in good solvents [177].

The main task of this work was, to take this simple coarse-grained model and to show, to which degree secondary structure formation as observed in nature can be understood even with this approach. The other way around one may ask: What are the essential ingredients to a model, i.e., which level of coarse graining is necessary, to observe secondary structure formation including helices, sheets, etc. Therefore, I first studied systematically the ground-

state structures depending on the thickness parameter and the system size. It turned out that, driven by the variation of the thickness parameter, several different conformations occur as ground states. In particular, I could show that the exact α-helix and planar β-sheets are amongst them. This is remarkable as the model consist of nothing but Lennard–Jones interaction and an additional length scale, the tube diameter. It should be stated though, that special ground-state structures are generally not very stable against variations of the thickness, but this was not expected either. Anyhow, the thickness can be considered as the "driving force" of the process of structure formation in this system. Doubtlessly, secondary structures can be stabilized by further interactions, for example due to special primary structures (see below).

It was of course known for a long time, that helices and sheets form within coarse-grained models including a somehow defined volume exclusion. One of the first basic studies was done by Banavar and Maritan et al. using the tube model and a square well potential for the interaction between the monomers. They showed, that in principle in this model secondary structures like helices and sheets occur [80–82]. Further studies on that topic mainly used dedicated or less simple and not that general models. In some interesting works, for example, explicit hydrogen bonds [191, 193] or solvent particles [188–190] play a role, which indeed support structure formation. It is a common ansatz to investigate and understand protein folding, stressing that I do not speak only of proteins but of a general class of polymers including proteins, at different abstraction (coarse grained) levels. It can be concluded so far that at least parts of the general secondary structure formation can be attributed to simplest generic models for thick polymers.

This was of course just a first step in the understanding of the model. Subsequently, in detailed and elaborate studies I could develop the full conformational phase diagrams depending on the thickness constraint and temperature for short polymers. In contrast to an earlier study of a similar model, where rough sketches of the folding- and collapse-transition line are presented [82], I could unravel the internal structure of the pseudo phases of folded conformations. Independently of the polymer length, I identified four major structural phases, where helices, sheetlike planar structures, bended rings and sprawled random coils are the dominant conformations. These dominant conformations correspond generally to the ground states in the respective regions. Furthermore I found special regions in the parameter space, where conformations crystallized on regular lattices dominate. After introducing then the AB tube model for heteropolymers, I studied a special AB protein in this tube model, which has been subject of several preceding works without thickness. As a key result, I showed that special sequences of different monomers, involving different intramolecular interactions, can stabilize the secondary structures of tube polymers. In particular, I found a broad and stable ground-state region of a β-sheet structure for that protein. On the other hand, the general qualitative structure of the pseudo-phase diagram keeps unchanged.

To conclude, I could resolve in this work the complete (pseudo)phase behavior of the Lennard–Jones tube model for polymers with respect to the thickness constraint and temperature, including the formation of the native states for $T \to 0$. This allowed, for example, for the classification of thermodynamic conformational phases. Hence, I have identified the generic structure of the conformational phase space for classes of polymers, parameterized by their thickness. Although a mesoscopic model for flexible polymers was employed, I found that the thickness constraint is an intrinsic source of an effective stiffness and enhances the capability of a polymer to form secondary structures which are stable against thermal fluctuations. It is therefore suitable for a classification of the structural behavior of classes of polymers.

Of course, the here studied tube model may be employed in other contexts as well, for example, for simulations of a tube model for entangled networks of polymers, where the hypothetical tube around a polymer models the suppression of transverse undulation by the network [2, 206]. As another example one could imagine, that the tube picture also may be applicable for the the diffusion of knots in knotted DNA [207]. Finally, the model may be applied in the context of branched or bottle-brushed polymers, a field which is very popular not only in computational physics. Such a bottle-brush polymer consists of an, in principle, flexible main chain or backbone, where many short side chains are attached. The resulting polymer is a cylindrical brush, which becomes rodlike for long enough attached side chains [208–210]. However, the problem is still not completely understood. One question for example, and the work here and subsequent studies of tube polymers may contribute to the answer, is that dealing with the structural behavior depending on control parameters like the length of the side chains [210], i.e., in a sense, the tube thickness. In order to follow this idea, one should firstly find an appropriate mapping between the main characteristics of both models, as for example persistence lengths of the brush polymers and bond lengths of the coarse-grained tube model and mean radii of gyration of the side chains and tube diameter. Then one should, for example, be able to reproduce data like the mean square radius of the backbone depending on the (adequately scaled) monomer number for different perpendicular extensions, as presented in [211]. These considerations may be the starting point of further future work on the tube model.

Acknowledgements

of polymers, and Andreas Nußbaumer and Elmar Bittner for the sacrificial and devoted maintenance of our computer facilities.

Needless to say, that this work has been accompanied by numerous further discussions on the actual topic of this work and on general related fields. I wish to thank here, in an arbitrary order:

- Thomas Strauch, Wolfgang Paul and Kurt Binder for comments, suggestions and explications of their work on the bond-fluctuation model with different interaction ranges,

- Frank Dressel for ideas for statistical analyses of large protein data bases,

- Hsiao-Ping Hsu for numerous discussions for example on chain-growth algorithms, lattice polymers or bottle-brush polymers and her general interest in my work,

- Handan Arkin for comments on AB polymers and provision of data of her previous studies,

- Peter Grassberger for his comments and ideas on the freezing transition in the bond-fluctuation model,

- Michael Schreiber and Michael Schmiedeberg for new insights and explications regarding Fibonacci sequences and quasi-crystalline structures,

- and Klaus Kroy for discussions and insights on wormlike chains and colloidal systems.

I acknowledge the following concrete participation regarding the results presented in this work of Thomas Neuhaus, providing source code for the calculation of a perfect helix with given winding number and for parallel, exemplified independent simulations for cross checks, and of Stefan Schnabel, providing low-temperature conformations of FENE polymers and Lennard-Jones clusters for the study of minimization techniques.

Finally, I am deeply grateful to my wife and my daughters for the private help, encouragement and cheering up during all that time!

Appendix A

The HP-Transcription Problem

I will here comment on the general difficulty to translate sequences of potentially twenty amino acids in real polymers into a two-letter code, what has been attempted occasionally [48, 49]. Indeed, one of the main properties of amino acids is the hydrophobicity, which is either positive or negative. But, on the one hand, the dispersive strength of this property is neglected completely, on the other hand it seems not to be trivial to determine the hydrophobicity in a standardized manner. This difficulty led to different hydrophobicity scales, as shown in Table A.1.

Take, for example, the Trp-cage miniprotein with code 1RIJ from the Protein Data Bank [176] (this is one of the small proteins studied in [87]). It has the amino-acid sequence:

<div align="center">ALQEL LGQWL KDGGP SSGRP PPS .</div>

Using now the data given in Table A.1, one notes that for several amino acids in 1RIJ it is not obvious, whether they should be translated into hydrophobic (H) or polar (P) ones in the HP- or AB-model. In Fig. A.1, this dilemma is visualized.

Apart from the above mentioned difficulty, I tried to simulate 1RIJ in the AB model with thickness anyhow by translating the above given sequence as follows:

<div align="center">AABBA A0BAA BB00A BB0BA AAB ,</div>

where "0" monomers (the "G"s in the original sequence) does not interact at all with any other monomer. Furthermore, I measured the global radius of curvature of 1RIJ and used that value as the thickness constraint ρ for my simulation (cp. Sects. 4.2.2, "The Global Radius of Curvature", 4.2.3, "The Tube Thickness" and 4.7, "The Hydrophobic-Polar Tube Model"). To make it short, this naive procedure could not reproduce structural properties of the real protein. (Data and results on the study of 1RIJ and a further miniprotein (2EQV) designed to fold into a sheet are not shown.)

It remains unclear, how to translate real proteins into two-letter coarse grained models reliably. It is, furthermore, doubtful, if it makes sense to study specific proteins within these

Amino acid	Abbrev./		Hydrophobicity[a]							1RIJ	
	Symbol		[212]	[213]				[214]			
			a[b]	b	c	d	OONS	Consensus			
Isoleucin	Ile	I	+	+	+	+	+	+	+	✓	
Valin	Val	V	+	+	+	+	+	+	+	✓	
Leucin	Leu	L	+	+	+	+	+	+	+	✓	•
Phenylalanin	Phe	F	+	+	+	+	+	−	+	!	
Cystein	Cys	C	+	+	+	+	+	−	+	!	
Methionine	Met	M	+	+	+	+	+	+	+	✓	
Alanin	Ala	A	+	+	+	+	+	+	+	✓	•
Glycin	Gly	G	−	0	0	0	0	0	+	!	•
Threonin	Thr	T	−	−	+	+	−	−	−	!	
Tryptophan	Trp	W	−	+	+	+	+	+	+	!	•
Serin	Ser	S	−	−	−	−	−	−	−	✓	•
Tyrosin	Tyr	Y	−	−	+	+	+	−	+	!	
Prolin	Pro	P	−	nv	+	+	+	+	−	!	•
Histidin	His	H	−	−	+	+	−	−	−	!	
Glutamat	Glu	E	−	−	−	−	−	−	−	✓	•
Glutamin	Gln	Q	−	−	−	−	−	−	−	✓	•
Aspartat	Asp	D	−	−	−	−	−	−	−	✓	•
Asparagin	Asn	N	−	−	−	−	−	−	−	✓	
Lysin	Lys	K	−	−	−	−	−	−	−	✓	•
Arginin	Arg	R	−	−	−	−	−	−	−	✓	•

[a] Only sign is given. For precise numbers, see the given references.

[b] The scale is adjusted such that the value is zero for glycin.

Table A.1: The twenty standard amino acids occurring in real proteins with their hydrophobicity according to different scales from literature [212–214]. Negative values correspond to hydrophilic amino acids, positive values to hydrophobic ones. The "✓" in the second last row indicates, that all scales are in agreement for the respective amino acids, whilst "!" indicates disagreement. Amino acids marked by "•" in the last row occur in the protein 1RIJ (see text). Horizontal lines are inserted only for clarity. "nv" means "no value given".

models at all. Rather, the results obtained using these two-letter models should represent a general frame and lead to a more general understanding of the hydrophobic core formation in proteins and protein systems and, in particular the results for the AB tube model, of possible conformational phases of secondary structures and their stabilization for thick polymers and proteins. Hence, they are the basis of further analysis of pseudo phases of models designed for specific polymers or proteins.
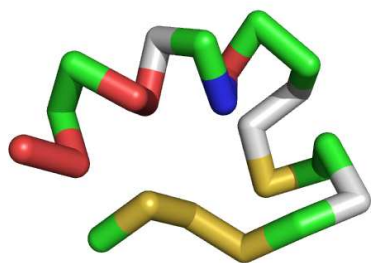
Figure A.1: Backbone of 1RIJ. Color code: **green** – clearly hydrophilic, "−" in all scales in Tab. A.1, → "B" monomer. **red** – clearly hydrophobic, "+" in all scales, → "A" monomer. **white** – Glycin, depending on scale "+", "−" or "0" (adjustment). **blue** – Tryptophan, depending on scale "+" oder "−". **yellow** – Prolin, depending on scale "+", "−" or undefined ("nv").

Appendix B

Non-Stochastic Minimization − Examples

I show in this appendix some examples of the application of the deterministic conjugate gradient optimization [139] to different systems studied during this work and the work on FENE polymers [76]. I will comment on different (technical) aspects shortly. The introduction of the method an some general remarks can be found in Sec. 2.2.6 ("Conjugate Gradient Optimization").
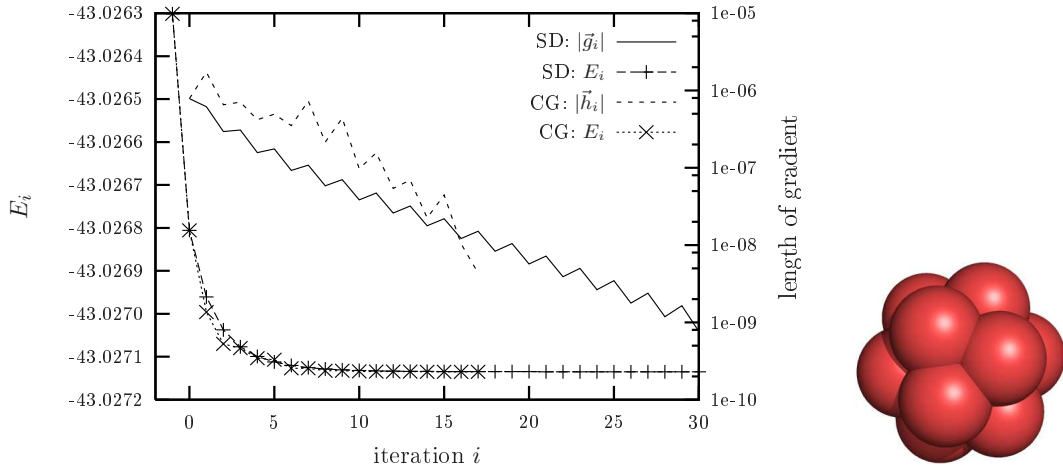

Figure B.1: Conjugate gradient optimization of a $N = 13$ FENE polymer. Left: Energy and lengths of gradients during the iterations, right: Visualization of the ground-state conformation.

FENE Polymers

As FENE Polymers have flexible bonds, every monomers has three independent degrees of freedom. Hence, one optimizes in a $3N$-dimensional phase space. In Fig. B.1 the results of such an optimization for $N = 13$ is shown. The pure lines show the length of the gradients (solid line: Steepest Descent (SD) method, dashed line: Conjugate Gradient (CG) method, note the logarithmic scale), $+$ (SD) and $\times$ (CG) mark the energy of the system at every iteration step of the optimization. The iteration converges after a few steps, both methods (SD and CG) do not differ significantly. The picture shows the ground-state conformation in a specific representation (spheres at monomer positions, bonds are not shown explicitly).
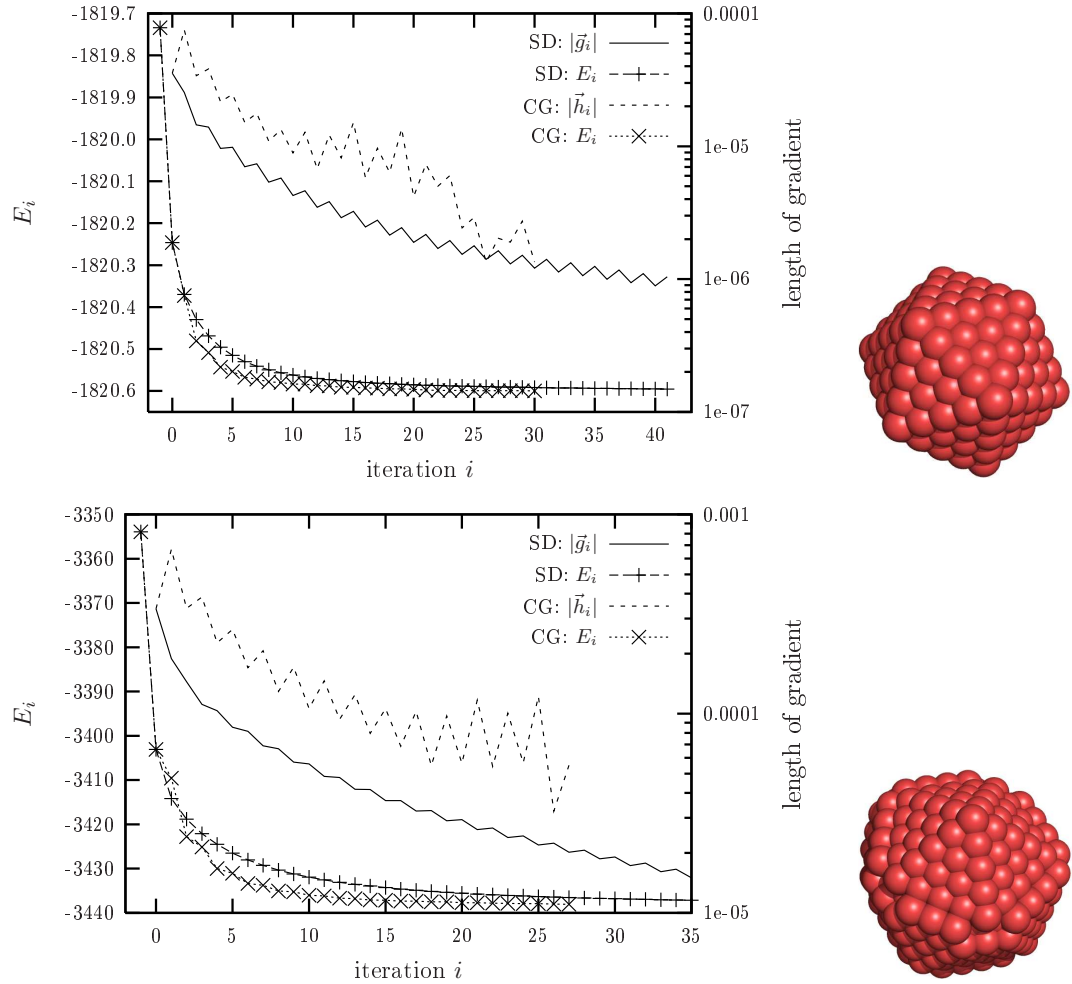

Figure B.2: Conjugate gradient optimization of FENE polymers with $N = 309$ (top) and $N = 561$ (bottom).

Results for more interesting systems with $N = 309$ and $N = 561$ are shown in Fig. B.2. The dimensions of the phase spaces are 927 and 1683, respectively. The shown data is the same as for the example above. Here it can be seen, that the conjugate gradient method performs better than the steepest descent method. Anyhow, the absolute times both methods required for the optimization are in the range of some seconds on a single standard processor. The input conformations were obtained during exhaustive multicanonical simulations [132], the energy is lowered by the deterministic optimization in the range of $\lesssim 1\%$.

Lennard-Jones Cluster

Figure B.3 shows the result of a conjugate gradient optimization of a Lennard-Jones cluster consisting of $N = 102$ particles. The input state was obtained by a multicanonical simulation [132]. Its energy was still higher than the actual accepted minimum of that system $E_{\min} = -569.363652$ [215], but the particles were already in the correct qualitative positions with respect to each other. With the conjugate gradient method, it took a few seconds and about 10 iterations to bring the system into a state with $E = -569.3636525$.

There are much similarities between ground states of FENE polymers and Lennard-Jones clusters [76, 77]. Hence, it might make sense to search ground states of FENE polymers, what has some technical advantages compared to simulations of Lennard-Jones clusters, optimize them, remove the bonds to get ground state estimates for Lennard-Jones cluster and optimize again. A naive experiment following that protocol with $N = 561$ particles led to a ground-state energy of $E_{\mathrm{LJ}} \approx -3826$, which corresponds to a FENE energy of $E_{\mathrm{FENE}} \approx -3437$. The at the moment accepted minimum energy is $E_{\mathrm{LJ,min}} \approx 3842$ [215],
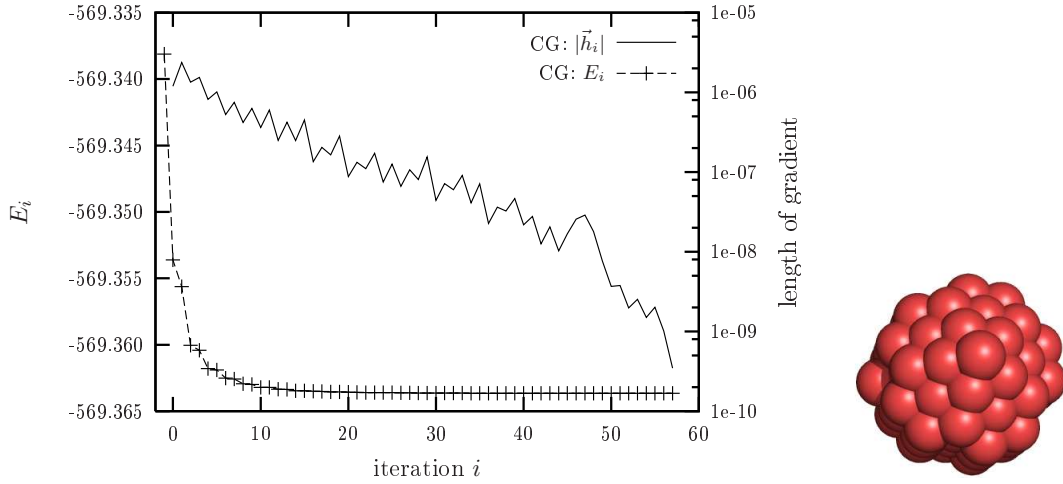

Figure B.3: Conjugate gradient optimization of a Lennard-Jones cluster consisting of $N = 102$ particles. The minimum energy is the same as given in the Cambridge Cluster Database [215].

so just a few ($E_{\text{LJ,diff}} \approx 16$) monomers were still located at "wrong" positions (without figure).

Thick Polymers

The optimization becomes more difficult and less efficient when considering thick polymers, where the energy landscape is, in practice, arbitrarily restricted by "hidden walls" due the thickness constraint. This effect is worsen by the fixed bond length of the system. In the first instance, I forget the conjugate gradient method, otherwise I would "hit" the walls permanently, and use the naive steepest descent method instead. Furthermore, non-differentiable points at the walls has to be treated separately using several case differentiations.

Figure B.4 shows the results of two steepest descent runs (starting with different input states) for a thick polymer with $N = 10$ monomers at $\rho = 0.6$. One sees, that both input states result in the same ground state. Very interesting here is, that the structure of the energy landscape seems to be non-trivial, as indicated by the local and global fluctuations of the lengths of the gradients. [1]
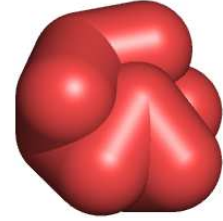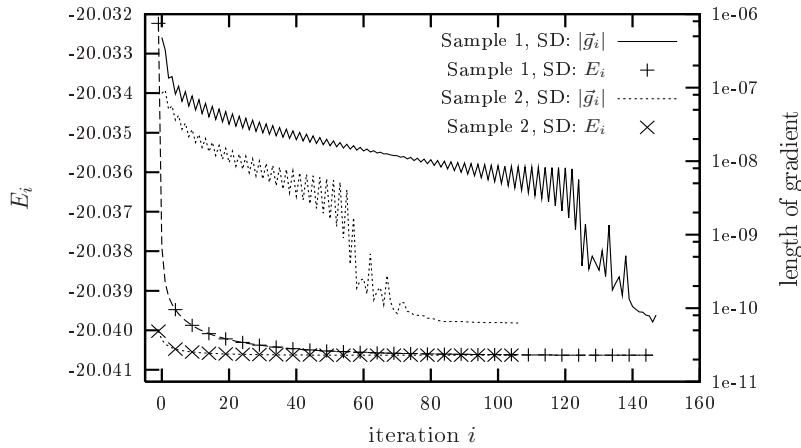

Figure B.4: Conjugate gradient optimization of a thick polymer with $N = 10$ monomers and thickness $\rho = 0.6$. Shown are results of two independent samples, i.e., optimizations of two different input states. Both result in the same ground state.

As shown in Chap. 4 ("Tubelike Flexible Polymers"), the thickness constraint does not influence the ground state below $\rho \lesssim 0.6$. An optimization with $\rho = 0.0$ should lead therefore to the same ground state energy. This is indeed the case, see Fig. B.5, where the characteristics of such an optimization are shown.

It was above mentioned, that several difficulties may arise while optimizing thick polymers. A probably misbehaving optimization (it might of course be, that the input state

---

[1] I have honestly to admit, that I can not provide a clear picture of the correspondence between the observed behavior of the gradients and the structure of the energy landscape.
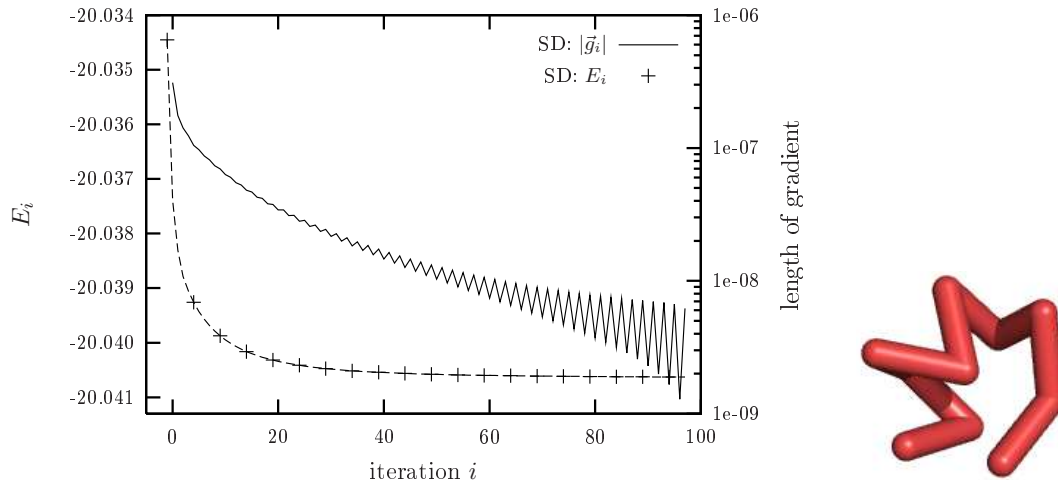
Figure B.5: Conjugate gradient optimization of a thin polymer with $N = 10$ monomers and thickness $\rho = 0.0$. Compare results with Fig. B.4.
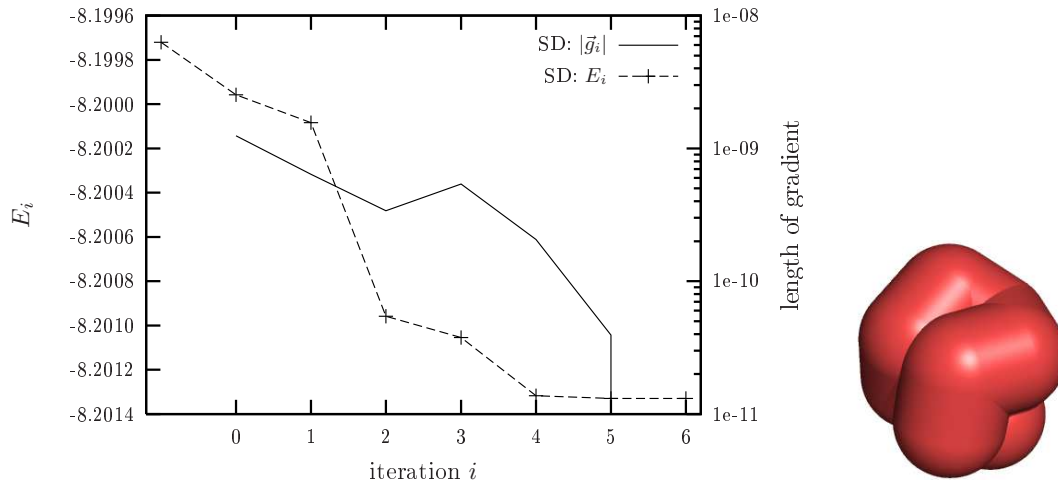
Figure B.6: Conjugate gradient optimization of a thick polymer with $N = 9$ monomers and thickness $\rho = 0.8$.

already was extremely close to the ground state and the minimum was found by chance directly) is shown in Fig. B.6. The optimization stops already after five iterations, supposably because it got trapped due to the thickness constraint.

AB-Polymers

Figure B.7 shows characteristics of some optimization runs for ground-state conformations of linelike AB proteins from [68] presented in Table 4.2 (Sec. 4.7, "The Hydrophobic-Polar Tube
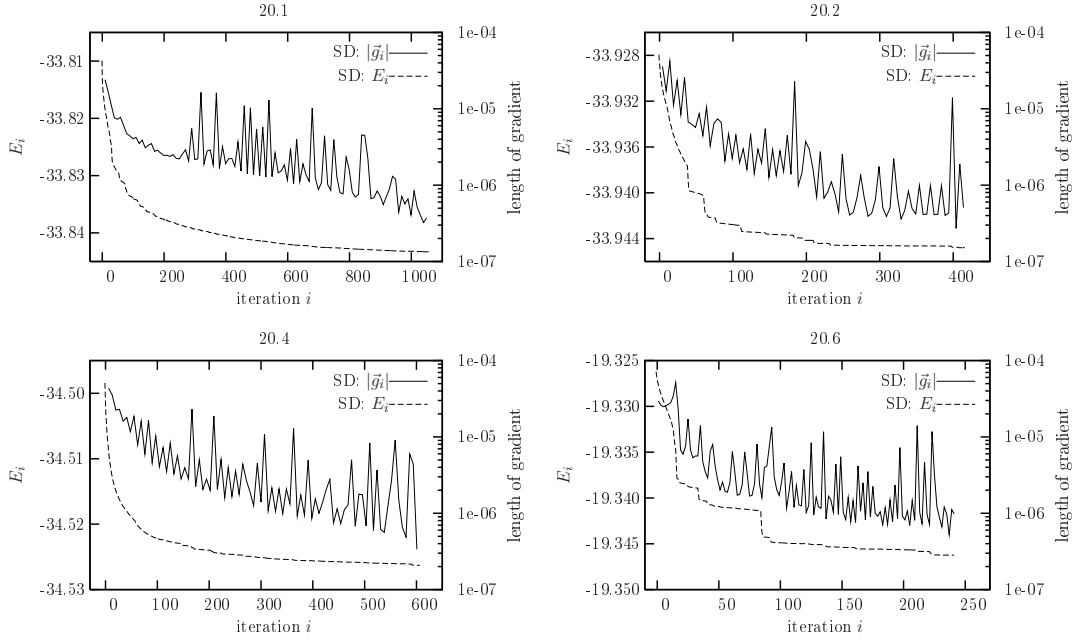
Figure B.7: Conjugate gradient optimization of ground-states of AB proteins from [68]. For clarity, only values for every nth iteration are shown in the curves for the gradient length (solid lines, $n = 10\,(20.1)$, $5\,(20.2)$, $7\,(20.4)$, $2\,(20.6)$).

Model", p. 94). The fact, that the energies after the optimization process are lower or equal to that presented in the meantime [203–205] indicates, that the ground-state conformations in [68] are in fact the same ones, besides some marginal fluctuations in the positions of single monomers.

Note that the optimization proceeds not always equally smooth, or smooth at all, respectively. Compare, for example, the energies for the 20.4 and the 20.6 polymer during the optimization or check the peculiar fluctuations of the gradient lengths against those for some homopolymer optimization runs shown earlier. This might be some additional indication of the complexity of the energy landscape.

Bibliography

[1] P. J. FLORY, *Principles of Polymer Chemistry* (Cornell University Press, Ithaca, 1953)

[2] P.-G. DE GENNES, *Scaling Concepts in Polymer Physics* (Cornell University Press, Ithaca, 1979)

[3] L. MANDELKERN, *Crystallization of Polymers* (Cambridge University Press, Cambridge, 2002), 2nd edn.

[4] G. REITER AND J.-U. SOMMER (eds.) *Polymer Crystallization, Lecture Notes in Physics*, vol. 606 (Springer, Berlin, 2003)

[5] A. L. LEHNINGER, D. L. NELSON, AND M. M. COX, *Principios de Bioquimica*

[6] C. BUSTAMANTE, S. B. SMITH, J. LIPHARDT, AND D. SMITH, *Single-molecule studies of DNA mechanics.* Curr. Opin. Struct. Biol. **10**(3), 279 (2000)

[7] U. F. KEYSER, B. N. KOELEMAN, S. VAN DORP, D. KRAPF, R. M. M. SMEETS, S. G. LEMAY, N. H. DEKKER, AND C. DEKKER, *Direct force measurements on DNA in a solid-state nanopore.* Nat. Phys. **2**, 473 (2006)

[8] S. L. LEVY, J. T. MANNION, J. CHENG, C. H. RECCIUS, AND H. G. CRAIGHEAD, *Entropic Unfolding of DNA Molecules in Nanofluidic Channels.* Nano Lett. **8**(11), 3839 (2008)

[9] M. E. J. NEWMAN AND G. T. BARKEMA, *Monte Carlo Methods in Statistical Physics* (Clarendon Press, Oxford University Press, 1999)

[10] D. P. LANDAU AND K. BINDER, *A Guide to Monte Carlo Simulations in Statistical Physics* (Cambridge University Press, 2009), 3rd edn.

[11] M. BACHMANN AND W. JANKE, *Thermodynamics of Protein Folding from Coarse-Grained Models' Perspectives*, in: W. JANKE (ed.) *Rugged Free Energy Landscapes, Lecture Notes in Physics*, vol. 736, pp. 203–246 (Springer, Berlin, 2008)

[12] W. KUHN, *Über die Gestalt fadenförmiger Moleküle in Lösungen.* Kolloid Z. (Colloid & Polymer Sci.) **68**(1), 2 (1934)

[13] F. T. Wall, L. A. Hiller Jr., and D. J. Wheeler, *Statistical Computation of Mean Dimensions of Macromolecules.* J. Chem. Phys. **22**, 1036 (1954)

[14] M. N. Rosenbluth and A. W. Rosenbluth, *Monte Carlo Calculation of the Average Extension of Molecular Chains.* J. Chem. Phys. **23**, 356 (1955)

[15] F. T. Wall, L. A. Hiller Jr., and W. F. Atchison, *Statistical Computation of Mean Dimensions of Macromolecules. II, III, IV.* J. Chem. Phys. **23**, 913 (1955), **23**, 2314 (1955), **26**, 1742 (1957)

[16] W. J. C. Orr The Late, *Statistical Treatment of Polymer Solutions at Infinite Dilution.* Trans. Faraday Soc. **43**, 12 (1947)

[17] M. E. Fisher and M. F. Sykes, *Excluded-Volume Problem and the Ising Model of Ferromagnetism.* Phys. Rev. **114**(1), 45 (1959)

[18] J. M. Hammersley, *Limiting Properties of Numbers of Self-Avoiding Walks.* Phys. Rev. **118**(3), 656 (1960)

[19] M. E. Fisher and B. J. Hiley, *Configuration and Free Energy of a Polymer Molecule with Solvent Interaction.* J. Chem. Phys. **34**, 1253 (1961)

[20] M. E. Fisher, *Effect of Excluded Volume on Phase Transitions in Biopolymers.* J. Chem. Phys. **45**, 1469 (1966)

[21] A. J. Guttmann, *On the Critical Behaviour of Self-Avoiding Walks.* J. Phys. A: Math. Gen. **20**(7), 1839 (1987)

[22] V. Blavatska and W. Janke, *Scaling Behavior of Self-Avoiding Walks on Percolation Clusters.* Europhys. Lett. **82**(6), 66006 (2008)

[23] M. F. Sykes, A. J. Guttmann, M. G. Watts, and P. D. Roberts, *The Asymptotic Behaviour of Selfavoiding Walks and Returns on a Lattice.* J. Phys. A: Gen. Phys. **5**(5), 653 (1972)

[24] A. J. Guttmann, *Bounds on Connective Constants for Self-Avoiding Walks.* J. Phys. A: Math. Gen. **16**(10), 2233 (1983)

[25] D. MacDonald, D. L. Hunter, K. Kelly, and N. Jan, *Self-Avoiding Walks in Two to Five Dimensions: Exact Enumerations and Series Study.* J. Phys. A: Math. Gen. **25**(6), 1429 (1992)

[26] J. F. Douglas and T. Ishinabe, *Self-Avoiding-Walk Contacts and Random-Walk Self-Intersections in Variable Dimensionality.* Phys. Rev. E **51**(3), 1791 (1995)

[27] D. MacDonald, S. Joseph, D. L. Hunter, L. L. Moseley, N. Jan, and A. J. Guttmann, *Self-Avoiding Walks on the Simple Cubic Lattice*. J. Phys. A: Math. Gen. **33**(34), 5973 (2000)

[28] P. Grassberger and R. Hegger, *Simulations of Three-dimensional θ Polymers*. J. Chem. Phys. **102**, 6881 (1995)

[29] P. Grassberger, *Pruned-Enriched Rosenbluth Method: Simulations of θ Polymers of Chain Length up to 1 000 000*. Phys. Rev. E **56**, 3682 (1997)

[30] T. Vogel, M. Bachmann, and W. Janke, *Freezing and Collapse of Flexible Polymers on Regular Lattices in Three Dimensions*. Phys. Rev. E **76**, 061803 (2007)

[31] H.-P. Hsu and P. Grassberger, *A Single Polymer Grafted to a Porous Membrane*. Europhys. Lett. **77**(1), 18003 (2007)

[32] H.-P. Hsu, W. Paul, and K. Binder, *One- and Two-Component Bottle-Brush Polymers: Simulations Compared to Theoretical Predictions*. Macromol. Theory Simul. **16**(7), 660 (2007)

[33] L. I. Klushin, A. M. Skvortsov, H.-P. Hsu, and K. Binder, *Dragging a Polymer Chain into a Nanotube and Subsequent Release*. Macromolecules **41**(15), 5890 (2008)

[34] J. Krawczyk, A. L. Owczarek, and T. Prellberg, *Polymers with Self-Attraction and Stiffness: A Generic Phase Structure*. EPL (Europhys. Lett.) (2009), (submitted)

[35] S. Kumar and D. Giri, *Force-Induced Conformational Transition in a System of Interacting Stiff Polymers: Application to Unfolding*. Phys. Rev. E **72**, 052901 (2005)

[36] H. Zhou, J. Zhou, Z.-C. Ou-Yang, and S. Kumar, *Collapse Transition of Two-Dimensional Flexible and Semiflexible Polymers*. Phys. Rev. Lett. **97**, 158302 (2006)

[37] S. Kumar, I. Jensen, J. L. Jacobsen, and A. J. Guttmann, *Role of Conformational Entropy in Force-Induced Biopolymer Unfolding*. Phys. Rev. Lett. **98**, 128101 (2007), see also: J. Math. Chem. (published online: 17 May 2008)

[38] D. Giri and S. Kumar, *Effects of the Eye Phase in DNA Unzipping*. Phys. Rev. E **73**, 050903(R) (2006)

[39] S. Kumar and D. Giri, *Does Changing the Pulling Direction Give Better Insight into Biomolecules?* Phys. Rev. Lett. **98**, 048101 (2007)

[40] M. S. Causo, B. Coluzzi, and P. Grassberger, *Simple Model for the DNA Denaturation Transition*. Phys. Rev. E **62**, 3958 (2000)

[41] R. Everaers, S. Kumar, and C. Simm, *Unified Description of Poly- and Oligonucleotide DNA Melting: Nearest-Neighbor, Poland–Sheraga, and Lattice Models.* Phys. Rev. E **75**, 041918 (2007)

[42] K. A. Dill, *Theory for the Folding and Stability of Globular Proteins.* Biochemistry **24**(6), 1501 (1985)

[43] K. F. Lau and K. A. Dill, *A Lattice Statistical Mechanics Model of the Conformational and Sequence Spaces of Proteins.* Macromolecules **22**(10), 3986 (1989)

[44] A. Irbäck and E. Sandelin, *Local Interactions and Protein Folding: A Model Study on the Square and Triangular Lattices.* J. Chem. Phys. **108**, 2245 (1998)

[45] A. Irbäck, C. Peterson, F. Potthast, and E. Sandelin, *Design of Sequences with Good Folding Properties in Coarse-Grained Protein Models.* Structure **7**(3), 347 (1999)

[46] A. Irbäck and C. Troein, *Enumerating Designing Sequences in the HP Model.* J. Biol. Phys. **28**, 1 (2002)

[47] R. Schiemann, M. Bachmann, and W. Janke, *Exact Sequence Analysis for Three-Dimensional Hydrophobic-Polar Lattice Proteins.* J. Chem. Phys. **122**(11) (2005)

[48] K. A. Dill, K. M. Fiebig, and H. S. Chan, *Cooperativity in Protein-Folding Kinetics.* Proc. Natl. Acad. Sci. USA **90**(5), 1942 (1993)

[49] E. E. Lattman, K. M. Fiebig, and K. A. Dill, *Modeling Compact Denatured States of Proteins.* Biochemistry **33**(20), 6158 (1994)

[50] K. Yue, K. M. Fiebig, P. D. Thomas, H. S. Chan, E. I. Shakhnovich, and K. A. Dill, *A Test of Lattice Protein Folding Algorithms.* Proc. Natl. Acad. Sci. USA **92**(1), 325 (1995)

[51] T. C. Beutler and K. A. Dill, *A Fast Conformational Search Strategy for Finding Low Energy Structures of Model Proteins.* Protein Sci **5**(10), 2037 (1996)

[52] R. Ramakrishnan, B. Ramachandran, and J. F. Pekny, *A Dynamic Monte Carlo Algorithm for Exploration of Dense Conformational Spaces in Heteropolymers.* J. Chem. Phys. **106**(6), 2418 (1997)

[53] G. Chikenji, M. Kikuchi, and Y. Iba, *Multi-Self-Overlap Ensemble for Protein Folding: Ground State Search and Thermodynamics.* Phys. Rev. Lett. **83**(9), 1886 (1999)

[54] F. Liang and W. H. Wong, *Evolutionary Monte Carlo for Protein Folding Simulations.* J. Chem. Phys. **115**(7), 3374 (2001)

[55] M. Bachmann and W. Janke, *Thermodynamics of Lattice Heteropolymers.* J. Chem. Phys. **120**(14), 6779 (2004)

[56] T. Vogel, *HP Proteine auf verallgemeinerten Gittern und Homopolymerkollaps*, Master's thesis, University Leipzig (2004)

[57] R. Schiemann, M. Bachmann, and W. Janke, *Exact Enumeration of Three-Dimensional Lattice Proteins.* Comput. Phys. Commun. **166**, 8 (2005)

[58] M. Bachmann and W. Janke, *Substrate Specificity of Peptide Adsorption: A Model Study.* Phys. Rev. E **73**(2), 020901 (2006)

[59] H.-P. Hsu, V. Mehra, W. Nadler, and P. Grassberger, *Growth Algorithms for Lattice Heteropolymers at Low Temperatures.* J. Chem. Phys. **118**, 444 (2002)

[60] I. Carmesin and K. Kremer, *The Bond Fluctuation Method: A New Effective Algorithm for the Dynamics of Polymers in All Spatial Dimensions.* Macromolecules **21**(9), 2819 (1988)

[61] K. Kremer and K. Binder, *Monte Carlo Simulation of Lattice Models for Macromolecules.* Comp. Phys. Rep. **7**(6), 259 (1988)

[62] Q. Yan and J. J. de Pablo, *Critical Behavior of Lattice Polymers Studied by Monte Carlo Simulations.* J. Chem. Phys. **113**(14), 5954 (2000)

[63] W. Paul, T. Strauch, F. Rampf, and K. Binder, *Unexpectedly Normal Phase Behavior of Single Homopolymer Chains.* Phys. Rev. E **75**(6), 060801(R) (2007), and references therein

[64] F. H. Stillinger, T. Head-Gordon, and C. L. Hirshfeld, *Toy Model for Protein Folding.* Phys. Rev. E **48**, 1469 (1993)

[65] F. H. Stillinger and T. Head-Gordon, *Collective Aspects of Protein Folding Illustrated by a Toy Model.* Phys. Rev. E **52**, 2872 (1995)

[66] A. Irbäck, C. Peterson, F. Potthast, and O. Sommelius, *Local Interactions and Protein Folding: A Three-dimensional Off-lattice Approach.* J. Chem. Phys. **107**(1), 273 (1997)

[67] H.-P. Hsu, V. Mehra, and P. Grassberger, *Structure Optimization in an Off-lattice Protein Model.* Phys. Rev. E **68**(3), 037703 (2003)

[68] M. Bachmann, H. Arkin, and W. Janke, *Multicanonical Study of Coarse-Grained Off-lattice Models for Folding Heteropolymers.* Phys. Rev. E **71**, 031906 (2005)

[69] S. Schnabel, M. Bachmann, and W. Janke, *Identification of Characteristic Protein Folding Channels in a Coarse-Grained Hydrophobic-Polar Peptide Model.* J. Chem. Phys. **126**(10), 105102 (2007)

[70] G. Iori, E. Marinari, and G. Parisi, *Random Self-Interacting Chains: A Mechanism for Protein Folding.* J. Phys. A: Math. Gen. **24**(22), 5349 (1991)

[71] A. Irbäck and H. Schwarze, *Sequence Dependence of Self-Interacting Random Chains.* J. Phys. A: Math. Gen. **28**(8), 2121 (1995)

[72] H. R. W. Jr., *Kinetic Theory and Rheology of Dilute Suspensions of Finitely Extendible Dumbbells.* Ind. Eng. Chem. Fundam. **11**(3), 379 (1972)

[73] R. C. Armstrong, *Kinetic Theory and Rheology of Dilute Solutions of Flexible Macromolecules. I. Steady State Behavior.* J. Chem. Phys. **60**(3), 724 (1974)

[74] M. Bishop, M. H. Kalos, and H. L. Frisch, *Molecular Dynamics of Polymeric Systems.* J. Chem. Phys. **70**(3), 1299 (1979)

[75] A. Milchev, A. Bhattacharya, and K. Binder, *Formation of Block Copolymer Micelles in Solution: A Monte Carlo Study of Chain Length Dependence.* Macromolecules **34**(6), 1881 (2001)

[76] S. Schnabel, T. Vogel, M. Bachmann, and W. Janke, *Surface Effects in the Crystallization Process of Elastic Flexible Polymers.* Chem. Phys. Lett. (2009), in press. doi:10.1016/j.cplett.2009.05.052

[77] S. Schnabel, M. Bachmann, and W. Janke, *Elastic Lennard-Jones Polymers Meet Clusters – Differences and Similarities* (2009), preprint

[78] J. R. Banavar, A. Maritan, C. Micheletti, and A. Trovato, *Geometry and Physics of Proteins.* Proteins **47**(3), 315 (2002)

[79] J. R. Banavar, O. Gonzalez, J. H. Maddocks, and A. Maritan, *Self-Interactions of Strands and Sheets.* J. Stat. Phys. **110**(1–2), 35 (2003)

[80] J. R. Banavar and A. Maritan, *Colloquium: Geometrical Approach to Protein Folding: A Tube Picture.* Rev. Mod. Phys. **75**(1), 23 (2003)

[81] J. R. Banavar, A. Flammini, D. Marenduzzo, A. Maritan, and A. Trovato, *Geometry of Compact Tubes and Protein Structures.* ComPlexUs **1**(1), 4 (2003)

[82] J. R. Banavar, A. Flammini, D. Marenduzzo, A. Maritan, and A. Trovato, *Tubes Near the Edge of Compactness and Folded Protein Structures.* J. Phys. Cond. Mat. **15**(18), S1787 (2003)

[83] O. Kratky and G. Porod, *Röntgenuntersuchung gelöster Fadenmoleküle.* Recl. Trav. Chim. Pays-Bas. **68**, 1106 (1949)

[84] C. Bustamante, Z. Bryant, and S. B. Smith, *Ten Years of Tension: Single-Molecule DNA Mechanics.* Nature **421**, 423 (2003)

[85] G. Maret and G. Weill, *Magnetic Birefringence Study of the Electrostatic and Intrinsic Persistence Length of DNA.* Biopolymers **22**(12), 2727 (1983)

[86] G. Lattanzi, T. Munk, and E. Frey, *Transverse Fluctuations of Grafted Polymers.* Phys. Rev. E **69**(2), 021801 (2004)

[87] S. Mohanty and U. H. E. Hansmann, *Folding of Proteins with Diverse Folds.* Biophys. J. **91**(10), 3573 (2006)

[88] A. Irbäck and S. Mitternacht, *Spontaneous β-barrel Formation: An All-Atom Monte Carlo Study of $A\beta_{16-22}$ Oligomerization.* Proteins **71**, 207 (2008)

[89] S. Gnanakaran, H. Nymeyer, J. Portman, K. Y. Sanbonmatsu, and A. E. Garcia, *Peptide Folding Simulations.* Curr. Opin. Struct. Biol. **13**(2), 168 (2003)

[90] N. A. Alves, Y. Peng, and U. H. E. Hansmann, *All-Atom Protein-Folding Simulations in Generalized-Ensembles.* Braz. J. Phys. **34**(2A), 363 (2004), special Issue: III Brazilian Meeting on Simulational Physics

[91] T. Yoda, Y. Sugita, and Y. Okamoto, *Comparisons of Force Fields for Proteins by Generalized-Ensemble Simulations.* Chem. Phys. Lett. **386**, 460 (2004)

[92] A. Irbäck and S. Mohanty, *PROFASI: A Monte Carlo Simulation Package for Protein Folding and Aggregation.* J. Comput. Chem. **27**(13), 1548 (2006)

[93] A. Irbäck, *Protein Folding, Unfolding and Aggregation Studied Using an All-Atom Model with a Simplified Interaction Potential,* in: W. Janke (ed.) *Rugged Free Energy Landscapes, Lecture Notes in Physics,* vol. 736, pp. 269–291 (Springer, Berlin, 2008)

[94] U. H. E. Hansmann, *All-Atom Simulations of Proteins,* in: W. Janke (ed.) *Rugged Free Energy Landscapes, Lecture Notes in Physics,* vol. 736, pp. 293–313 (Springer, Berlin, 2008)

[95] A. Irbäck, S. Mitternacht, and S. Mohanty, *An Effective All-Atom Potential for Proteins.* PMC Biophys. **2**, 2 (2009)

[96] R. Hegger and P. Grassberger, *Chain Polymers near an Adsorbing Surface.* J. Phys. A: Math. Gen. **27**(12), 4069 (1994)

[97] M. Bachmann and W. Janke, *Substrate Adhesion of a Nongrafted Flexible Polymer in a Cavity.* Phys. Rev. E **73**(4), 041802 (2006)

[98] M. Möddel, M. Bachmann, and W. Janke, *Conformational Mechanics of Polymer Adsorption Transitions at Attractive Substrates.* J. Phys. Chem. B **113**(11), 3314 (2009)

[99] H.-P. Hsu, K. Binder, L. I. Klushin, and A. M. Skvortsov, *Escape Transition of a Polymer Chain from a Nanotube: How to Avoid Spurious Results by Use of the Force-Biased Pruned-Enriched Rosenbluth Algorithm.* Phys. Rev. E **78**(4), 041803 (2008)

[100] M. C. Tesi, E. J. J. Rensburg, E. Orlandini, and S. G. Whittington, *Monte Carlo Study of the Interacting Self-Avoiding Walk Model in Three Dimensions.* J. Stat. Phys. **82**(1–2), 155 (1996)

[101] M. Lal, *'Monte Carlo' Computer Simulation of Chain Molecules. I.* Mol. Phys. **17**(1), 57 (1969)

[102] N. Madras and A. D. Sokal, *The Pivot Algorithm: A Highly Efficient Monte Carlo Method for the Self-Avoiding Walk.* J. Stat. Phys. **50**(1–2), 109 (1988)

[103] F. T. Wall and J. J. Erpenbeck, *New Method for the Statistical Computation of Polymer Dimensions.* J. Chem. Phys. **30**(3), 634 (1959)

[104] M. Bachmann and W. Janke, *Multicanonical Chain-Growth Algorithm.* Phys. Rev. Lett. **91**, 208105 (2003)

[105] T. Prellberg and J. Krawczyk, *Flat Histogram Version of the Pruned and Enriched Rosenbluth Method.* Phys. Rev. Lett. **92**, 120602 (2004)

[106] N. Metropolis, A. W. Rosenbluth, M. N. Rosenbluth, A. H. Teller, and E. Teller, *Equation of State Calculations by Fast Computing Machines.* J. Chem. Phys. **21**(6), 1087 (1953)

[107] K. Hukushima and K. Nemoto, *Exchange Monte Carlo Method and Application to Spin Glass Simulations.* J. Phys. Soc. Jpn. **65**, 1604 (1996)

[108] C. J. Geyer, in: E. M. Keramidas (ed.) *Computing Science and Statistics*, Proceedings of the 23rd Symposium on the Interface, p. 156 (Interface Foundation, Fairfax Station, 1991)

[109] H. G. Katzgraber, S. Trebst, D. A. Huse, and M. Troyer, *Feedback-Optimized Parallel Tempering Monte Carlo.* J. Stat. Mech.: Theory Exp. **2006**(03), P03018 (2006)

[110] N. Rathore, M. Chopra, and J. J. de Pablo, *Optimal Allocation of Replicas in Parallel Tempering Simulations.* J. Chem. Phys. **122**(2), 024111 (2005)

[111] A. Kone and D. A. Kofke, *Selection of Temperature Intervals for Parallel-Tempering Simulations.* J. Chem. Phys. **122**(20), 206101 (2005)

[112] E. BITTNER, A. NUSSBAUMER, AND W. JANKE, *Make Life Simple: Unleash the Full Power of the Parallel Tempering Algorithm.* Phys. Rev. Lett. **101**, 130603 (2008), and references therein

[113] A. M. FERRENBERG AND R. H. SWENDSEN, *Optimized Monte Carlo Data Analysis.* Phys. Rev. Lett. **63**(12), 1195 (1989)

[114] W. JANKE, *Histograms and All That*, in: B. DÜNWEG, D. P. LANDAU, AND A. I. MILCHEV (eds.) *Computer Simulations of Surfaces and Interfaces*, *NATO Science Series, II. Mathematics, Physics and Chemistry*, vol. 114, pp. 137–157, NATO Advanced Study Institute (Kluwer, Dordrecht, 2003)

[115] B. A. BERG AND T. NEUHAUS, *Multicanonical Algorithms for First Order Phase Transitions.* Phys. Lett. B **267**(2), 249 (1991)

[116] B. A. BERG AND T. NEUHAUS, *Multicanonical Ensemble: A New Approach to Simulate First-Order Phase Transitions.* Phys. Rev. Lett. **68**, 9 (1992)

[117] W. JANKE, *Multicanonical Monte Carlo Simulations.* Physica A: Stat. Theor. Phys. **254**(1–2), 164 (1998)

[118] B. A. BERG, *Multicanonical Recursions.* J. Stat. Phys. **82**(1–2), 323 (1996)

[119] F. WANG AND D. P. LANDAU, *Efficient, Multiple-Range Random Walk Algorithm to Calculate the Density of States.* Phys. Rev. Lett. **86**, 2050 (2001)

[120] C. ZHOU AND R. N. BHATT, *Understanding and Improving the Wang–Landau Algorithm.* Phys. Rev. E **72**, 025701(R) (2005)

[121] E. BITTNER AND W. JANKE, *Comparative Study of General Ensemble Algorithms* (2009), in preparation

[122] F. WANG AND D. P. LANDAU, *Determining the Density of States for Classical Statistical Models: A Random Walk Algorithm to Produce a Flat Histogram.* Phys. Rev. E **64**(5), 056101 (2001)

[123] C. YAMAGUCHI AND Y. OKABE, *Three-Dimensional Antiferromagnetic q-state Potts Models: Application of the Wang–Landau Algorithm.* J. Phys. A: Math. Gen. **34**, 8781 (2001)

[124] M. TROYER, S. WESSEL, AND F. ALET, *Flat Histogram Methods for Quantum Systems: Algorithms to Overcome Tunneling Problems and Calculate the Free Energy.* Phys. Rev. Lett. **90**(12), 120201 (2003)

[125] C. JUNGHANS AND U. H. E. HANSMANN, *Numerical Comparison of Wang Landau Sampling and Parallel Tempering for Met-enkephalin.* Int. J. Mod. Phy. C **17**, 817 (2006)

[126] N. Rathore and J. J. de Pablo, *Monte Carlo Simulation of Proteins through a Random Walk in Energy Space.* J Chem Phys **116**(16), 7225 (2002)

[127] F. Rampf, W. Paul, and K. Binder, *On the First-Order Collapse Transition of a Three-Dimensional, Flexible Homopolymer Chain Model.* Europhys. Lett. **70**, 628 (2005)

[128] F. Rampf, K. Binder, and W. Paul, *The Phase Diagram of a Single Polymer Chain: New Insights from a New Simulation Method.* J. Polym. Sci. B: Polym. Phys. **44**(18), 2542 (2006)

[129] B. J. Schulz, K. Binder, M. Müller, and D. P. Landau, *Avoiding Boundary Effects in Wang–Landau Sampling.* Phys. Rev. E **67**(6), 067102 (2003)

[130] D. F. Parsons and D. R. M. Williams, *An Off-lattice Wang–Landau Study of the Coil-Globule and Melting Transitions of a Flexible Homopolymer.* J. Chem. Phys. **124**, 221103 (2006)

[131] D. F. Parsons and D. R. M. Williams, *Globule Transitions of a Single Homopolymer: A Wang–Landau Monte Carlo Study.* Phys. Rev. E **74**(4), 041804 (2006)

[132] S. Schnabel, private communication

[133] D. T. Seaton, S. J. Mitchell, and D. P. Landau, *Developments in Wang–Landau Simulations of a Simple Continuous Homopolymer.* Braz. J. Phys. **38**(1), 48 (2008)

[134] D. T. Seaton, T. Wüst, and D. P. Landau, *A Wang–Landau Study of the Phase Transitions in a Flexible Homopolymer.* Comp. Phys. Commun. **180**(4), 587 (2009)

[135] U. H. E. Hansmann and L. T. Wille, *Global Optimization by Energy Landscape Paving.* Phys. Rev. Lett. **88**(6), 068105 (2002)

[136] H. Arkin and T. Çelik, *Comparison of the ELP and Multicanonical Methods in Simulation of the Heptapeptide Deltorphin.* Eur. Phys. J. B **30**(4), 577 (2002)

[137] A. Schug, W. Wenzel, and U. H. E. Hansmann, *Energy Landscape Paving Simulations of the trp-cage Protein.* J. Chem. Phys. **122**(19), 194711 (2005)

[138] C. Junghans, M. Bachmann, and W. Janke, *Thermodynamics of Peptide Aggregation Processes. An Analysis from Perspectives of Three Statistical Ensembles.* J. Chem. Phys. **128**, 085103 (2008)

[139] W. H. Press, S. A. Teukolsky, W. T. Vetterling, and B. P. Flannery, *Numerical Recipes: The Art of Scientific Computing*, chap. Conjugate Gradient Methods in Multidimensions, p. 515 (Cambridge University Press, Cambridge, 2007), 3rd edn.

[140] I. M. LIFSHITZ, A. Y. GROSBERG, AND A. R. KHOKHLOV, *Some Problems of the Statistical Physics of Polymer Chains with Volume Interaction.* Rev. Mod. Phys. **50**(3), 683 (1978)

[141] A. R. KHOKHLOV, *Theory of the Polymer Chain Collapse for the d-dimensional Case.* Physica A **105**(1–2), 357 (1981)

[142] A. Y. GROSBERG AND A. R. KHOKHLOV, *Statistical Theory of Polymeric Lyotropic Liquid Crystals.* Adv. Polym. Sci. **41**, 53 (1981)

[143] B. DUPLANTIER, *Lagrangian Tricritical Theory of Polymer Chain Solutions near the Θ-point.* J. Phys. (France) **43**(7), 991 (1982)

[144] B. DUPLANTIER, *Geometry of Polymer Chains near the Theta-Point and Dimensional Regularization.* J. Chem. Phys. **86**(7), 4233 (1987)

[145] B. DUPLANTIER, *Tricritical Polymer Chains in or below Three Dimensions.* Europhys. Lett. **1**, 491 (1986)

[146] J. HAGER AND L. SCHÄFER, *Θ-point Behavior of Diluted Polymer Solutions: Can one Observe the Universal Logarithmic Corrections Predicted by Field Theory?* Phys. Rev. E **60**(2), 2071 (1999)

[147] M. C. TESI, E. J. J. RENSBURG, E. ORLANDINI, AND S. G. WHITTINGTON, *Interacting Self-Avoiding Walks and Polygons in Three Dimensions.* J. Phys. A: Math. Gen. **29**(10), 2451 (1996)

[148] N. B. WILDING, M.MÜLLER, AND K. BINDER, *Chain Length Dependence of the Polymer–Solvent Critical Point Parameters.* J. Chem. Phys. **105**(2), 802 (1996)

[149] H. FRAUENKRON AND P. GRASSBERGER, *Critical Unmixing of Polymer Solutions.* J. Chem. Phys. **107**(22), 9599 (1997)

[150] A. Z. PANAGIOTOPOULOS, V. WONG, AND M. A. FLORIANO, *Phase Equilibria of Lattice Polymers from Histogram Reweighting Monte Carlo Simulations.* Macromol. **31**(3), 912 (1998)

[151] M. A. ANISIMOV AND J. V. SENGERS, *Scaling, Tricriticality, and Crossover in Polymer Solutions.* Mol. Phys. **103**(21–23), 3061 (2005)

[152] F. L. MCCRACKIN, J. MAZUR, AND C. M. GUTTMAN, *Monte Carlo Studies of Self-Interacting Polymer Chains with Excluded Volume. I. Squared Radii of Gyration and Mean-Square End-to-End Distances and Their Moments.* Macromol. **6**, 859 (1973)

[153] W. BRUNS, *The Ideal and the Pseudoideal State of Macromolecules: A Comparison.* Macromol. **17**(12), 2826 (1984)

[154] J. BATOULIS AND K. KREMER, *Residual 3-Body Interactions of a Θ-Polymer: Star Polymers.* Europhys. Lett. **7**(8), 683 (1988)

[155] H. MEIROVITCH AND H. A. LIM, *Computer Simulation Study of the θ-point in Three Dimensions. I. Self-Avoiding Walks on a Simple Cubic Lattice.* J. Chem. Phys. **92**, 5144 (1990)

[156] K. KREMER, *Computer Simulation Methods for Polymer Physics*, in: K. BINDER AND G. CICOTTI (eds.) *Monte Carlo and Molecular Dynamics of Condensed Matter Systems*, p. 669 (Editrice Compositori, Bologna, 1996)

[157] M. P. TAYLOR AND J. E. G. LIPSON, *A Born–Green–Yvon Integral Equation Theory for Self-Interacting Lattice Polymers.* J. Chem. Phys. **109**, 7583 (1998)

[158] A. L. OWCZAREK AND T. PRELLBERG, *First-Order Scaling near a Second-Order Phase Transition: Tricritical Polymer Collapse.* Europhys. Lett. **51**(6), 602 (2000)

[159] H.-P. HSU, V. MEHRA, W. NADLER, AND P. GRASSBERGER, *Growth-Based Optimization Algorithm for Lattice Heteropolymers.* Phys. Rev. E **68**(2), 021113 (2003)

[160] S. CARACCIOLO, M. S. CAUSO, AND A. PELISSETTO, *High-Precision Determination of the Critical Exponent γ for Self-Avoiding Walks.* Phys. Rev. E **57**(2), R1215 (1998)

[161] R. GUIDA AND J. ZINN-JUSTIN, *Critical Exponents of the N-vector Model.* J. Phys. A: Math. Gen. **31**, 8103 (1998)

[162] M. CHEN AND K. Y. LIN, *Universal Amplitude Ratios for Three-Dimensional Self-Avoiding Walks.* J. Phys. A: Math. Gen. **35**, 1501 (2002)

[163] R. SCHIEMANN, M. BACHMANN, AND W. JANKE, *Exact Sequence Analysis for Three-Dimensional Hydrophobic-Polar Lattice Proteins.* J. Chem. Phys. **122**(11), 114705 (2005)

[164] M. BACHMANN AND W. JANKE, *Conformational Transitions of Nongrafted Polymers near an Absorbing Substrate.* Phys. Rev. Lett. **95**(5), 058102 (2005)

[165] T. P. J. KRAWCZYK, A. L. OWCZAREK AND A. RECHNITZER, *Layering Transitions for Adsorbing Polymers in Poor Solvents.* Europhys. Lett. **70**, 726 (2005)

[166] I. CARMESIN AND K. KREMER, *The Bond Fluctuation Method: A New Effective Algorithm for the Dynamics of Polymers in all Spatial Dimensions.* Macromolecules **21**(9), 2819 (1988)

[167] M. G. NORO AND D. FRENKEL, *Extended Corresponding-States Behavior for Particles with Variable Range Attractions.* J. Chem. Phys. **113**(8), 2941 (2000)

[168] G. A. Vliegenthart, J. F. M. Lodge, and H. N. W. Lekkerkerker, *Strong Weak and Metastable Liquids Structural and Dynamical Aspects of the Liquid State.* Physica A **263**(1–4), 378 (1999)

[169] A. Daanoun, C. F. Tejero, and M. Baus, *Van der Waals Theory for Solids.* Phys. Rev. E **50**(4), 2913 (1994)

[170] D. H. E. Gross, *Microcanonical Thermodynamics* (World Scientific, Singapore, 2001)

[171] C. Junghans, M. Bachmann, and W. Janke, *Microcanonical Analyses of Peptide Aggregation Processes.* Phys. Rev. Lett. **97**(21), 218103 (2006)

[172] R. G. Miller, *The Jackknife – A Review.* Biometrika **61**, 1 (1974)

[173] B. Efron, *The Jackknife, the Bootstrap, and Other Resampling Plans* (SIAM, Philadelphia, 1982)

[174] W. Janke, *Logarithmic Corrections in the Two-Dimensional XY Model.* Phys. Rev. B **55**(6), 3580 (1997)

[175] T. Vogel, M. Bachmann, and W. Janke, *Freezing and Collapse of Flexible Polymers*, in: U. H. E. H. et al. (ed.) *From Computational Biophysics to System Biology (CBSB08), Proceedings, NIC Series*, vol. 40 (John von Neumann Institute for Computing (NIC), Jülich, 2008)

[176] Protein Data Bank: `www.rcsb.org/pdb/explore/explore.do?structureId=1RIJ`

[177] T. Neuhaus, O. Zimmermann, and U. H. E. Hansmann, *Ring Polymer Simulations with Global Radius of Curvature.* Phys. Rev. E **75**(5), 051803 (2007)

[178] O. Gonzalez and J. H. Maddocks, *Global Curvature, Thickness, and the Ideal Shapes of Knots.* Proc. Natl. Acad. Sci. USA **96**(9), 4769 (1999)

[179] T. Vogel, M. Bachmann, and W. Janke, *Thickness-Dependent Secondary Structure Formation of Tubelike Polymers.* EPL (Europhys. Lett.) **85**, 10003 (2009)

[180] T. Vogel, T. Neuhaus, M. Bachmann, and W. Janke, *Ground-State Properties of Thick Flexible Polymers* (2009), preprint

[181] T. Vogel, T. Neuhaus, M. Bachmann, and W. Janke, *Thermodynamics of Tubelike Flexible Polymers* (2009), submitted to Phys. Rev. E

[182] H. S. Chan and K. A. Dill, *The Effects of Internal Constraints on the Configurations of Chain Molecules.* J. Chem. Phys. **92**(5), 3118 (1990)

[183] H. Noguchi and K. Yoshikawa, *Morphological Variation in a Collapsed Single Homopolymer Chain.* J. Chem. Phys. **109**, 5070 (1998)

[184] J. P. Kemp and Z. Y. Chen, *Formation of Helical States in Wormlike Polymer Chains.* Phys. Rev. Lett. **81**(18), 3880 (1998)

[185] D. C. Rapaport, *Molecular Dynamics Simulation of Polymer Helix Formation Using Rigid-Link Methods.* Phys. Rev. E **66**(1), 011906 (2002)

[186] S. A. Sabeur, F. Hamdache, and F. Schmid, *Kinetically Driven Helix Formation during the Homopolymer Collapse Process.* Phys. Rev. E **77**, 020802(R) (2008)

[187] A. Maritan, C. Micheletti, A. Trovato, and J. R. Banavar, *Optimal Shapes of Compact Strings.* Nature **406**, 287 (2000)

[188] Y. Snir and R. D. Kamien, *Entropically Driven Helix Formation.* Science **307**, 1067(Brevia) (2005)

[189] Y. Snir and R. D. Kamien, *Helical Tubes in Crowded Environments.* Phys. Rev. E **75**, 051114 (2007)

[190] H. Hansen-Goos, R. Roth, K. Mecke, and S. Dietrich, *Solvation of Proteins: Linking Thermodynamics to Geometry.* Phys. Rev. Lett. **99**(12), 128101 (2007)

[191] T. X. Hoang, A. Trovato, F. Seno, J. R. Banavar, and A. Maritan, *Geometry and Symmetry Presculpt the Free-Energy Landscape of Proteins.* Proc. Natl. Acad. Sci. USA **101**(21), 7960 (2004)

[192] S. Auer, M. A. Miller, S. V. Krivov, C. M. Dobson, M. Karplus, and M. Vendruscolo, *Importance of Metastable States in the Free Energy Landscapes of Polypeptide Chains.* Phys. Rev. Lett. **99**(17), 178104 (2007)

[193] K. Wolff, M. Vendruscolo, and M. Porto, *A Stochastic Method for the Reconstruction of Protein Structures from One-Dimensional Structural Profiles.* Gene **422**(1–2), 47 (2008)

[194] K. Wolff, private communication

[195] T. Neuhaus, private communication

[196] M. Bachmann, private communication

[197] R. Koch and C. Engelhardt, *Closed Space Curves of Constant Curvature Consisting of Arcs of Circular Helices.* J. Geom. Graph. **2**(1), 17 (1998)

[198] E. Cesàro, *Vorlesungen über natürliche Geometrie*, p. 182 (Teubner, Leipzig, 1926), 2nd edn., translated by G. Kowalewski

[199] J. B. Tenenbaum, V. de Silva, and J. C. Langford, *A Global Geometric Framework for Nonlinear Dimensionality Reduction.* Science **290**, 2319 (2000)

[200] J. Ledieu, J. T. Hoeft, D. E. Reid, J. A. Smerdon, R. D. Diehl, T. A. Lograsso, A. R. Ross, and R. McGrath, *Pseudomorphic Growth of a Single Element Quasiperiodic Ultrathin Film on a Quasicrystal Substrate*. Phys. Rev. Lett. **92**(13), 135507 (2004)

[201] M. Engel, S. Sonntag, H. Lipp, and H.-R. Trebin, *Structure Factors of Harmonic and Anharmonic Fibonacci Chains by Molecular Dynamics Simulations*. Phys. Rev. B **75**(14), 144203 (2007)

[202] M. Schmiedeberg, *Colloidal Particles on Quasicrystalline Substrates*, Ph.D. thesis, TU Berlin (2008), available at: `http://opus.kobv.de/tuberlin/volltexte/2008/1945/`

[203] S.-Y. Kim, S. B. Lee, and J. Lee, *Structure Optimization by Conformational Space Annealing in an Off-lattice Protein Model*. Phys. Rev. E **72**, 011916 (2005)

[204] V. Elser and I. Rankenburg, *Deconstructing the Energy Landscape: Constraint-Based Algorithms for Folding Heteropolymers*. Phys. Rev. E **73**, 026702 (2006)

[205] W. Huang, M. Chen, and Z. Lü, *Energy Optimization for Off-lattice Protein Folding*. Phys. Rev. E **74**, 041907 (2006)

[206] H. Hinsch, J. Wilhelm, and E. Frey, *Quantitative Tube Model for Semiflexible Polymer Solutions*. Eur. Phys. J. E **24**(1), 35 (2007)

[207] A. Y. Grosberg and Y. Rabin, *Metastable Tight Knots in a Wormlike Polymer*. Phys. Rev. Lett. **99**(21), 217801 (2007)

[208] M. Wintermantel, M. Schmidt, Y. Tsukahara, K. Kajiwara, and S. Kohjiya, *Rodlike Combs*. Macromol. Rapid Comm. **15**(3), 279 (1994)

[209] M. Zhang and A. H. E. Müller, *Cylindrical Polymer Brushes*. J. Polym. Sci. Part A: Polym. Chem. **43**(16), 3461 (2005)

[210] H.-P. Hsu, W. Paul, and K. Binder, *Structure of Bottle-Brush Polymers in Solution: A Monte Carlo Test of Models for the Scattering Function*. J. Chem. Phys. **129**(20), 204904 (2008)

[211] H.-P. Hsu, W. Paul, and K. Binder, *Monte Carlo Simulations of Bottle-Brush Polymers in a Good Solvent*. 34th Conference of the Middle European Cooperation in Statistical Physics (MECO34), 30 March–01 April, Leipzig, Germany (2009), (still unpublished)

[212] J. Kyte and R. F. Doolittle, *A Simple Method for Displaying the Hydropathic Character of a Protein*. J. Mol. Biol. **157**(1), 105 (1982)

[213] T. E. CREIGHTON, *Proteins: Structures and Molecular Properties*, chap. 4 (W. H. Freeman & Co, New York, 1993), 2nd edn.

[214] N. A. ALVES, V. ALEKSENKO, AND U. H. E. HANSMANN, *A Simple Hydrophobicity-Based Score for Profiling Protein Structures.* J. Phys.: Cond. Mat. **17**(18), S1595 (2005)

[215] The Cambridge Cluster Database: `http://www-wales.ch.cam.ac.uk/CCD.html`

Curriculum Vitae

Personal Details

Name	Thomas Vogel
Date of birth	October 19, 1977
Place of birth	Osterburg/Altmark
Nationality	German
Marital status	Married, two children

Education

09/1992–06/1996	Secondary school "Albert Schweizer Gymnasium" Erfurt
06/1996	Abitur
10/1997–02/2004	Study of Physics at the University of Leipzig
	Thesis title: *HP-Proteine auf verallgemeinerten Gittern und Homopolymerkollaps*
	Supervisor: Prof. Dr. W. Janke
08/2000–04/2001	Stay abroad. Study of Physics at "Universidad Nacional Mayor de San Marcos" Lima/Perú
02/2004	Degree: *Dipl.-Phys.*

Ph.D. Study

since 04/2005	Ph.D. thesis in Theoretical Physics at the University of Leipzig
	Thesis title: *Structural Behavior of Polymers from Monte Carlo Studies of Coarse-Grained Models*
	Supervisor: Prof. Dr. W. Janke